

---

# Macroscopic superposition states and decoherence by quantum telegraph noise

Benjamin Simon Abel

---



München 2008



---

# **Macroscopic superposition states and decoherence by quantum telegraph noise**

**Benjamin Simon Abel**

---

Dissertation  
an der Fakultät für Physik  
der Ludwig–Maximilians–Universität  
München

vorgelegt von  
Benjamin Simon Abel  
aus Bochum

München, den 19. Dezember 2008

Erstgutachter: DR. FLORIAN MARQUARDT

Zweitgutachter: PROF. DR. STEFAN KEHREIN

Tag der mündlichen Prüfung: 13. Februar 2009



# Contents

<b>Summary</b>	<b>xiii</b>
<b>List of publications</b>	<b>xvii</b>
<b>I How fat is Schrödinger's cat?</b>	<b>1</b>
<b>1 The validity of Quantum Mechanics</b>	<b>3</b>
1.1 Introduction . . . . .	3
<b>2 Cattiness for many-body states</b>	<b>7</b>
2.1 Introduction . . . . .	7
2.2 Definition of the measure for many-body states . . . . .	7
2.2.1 Application to generalized GHZ-states . . . . .	9
2.3 General properties of the measure . . . . .	11
2.3.1 Unitary changes of the basis . . . . .	11
2.3.2 Symmetry . . . . .	12
2.4 Summary . . . . .	12
<b>3 How fat is Schrödinger's cat?</b>	<b>13</b>
3.1 Introduction . . . . .	13
3.2 How fat is the cat in the ring? . . . . .	13
3.3 Numerical results and discussion . . . . .	16
3.4 Open questions . . . . .	17
<b>II Decoherence by quantum telegraph noise</b>	<b>19</b>
<b>4 Basics of dephasing</b>	<b>21</b>

4.1	Introduction . . . . .	21
4.2	Dephasing in mesoscopic physics . . . . .	22
4.3	Dephasing of qubits . . . . .	23
4.3.1	Classical noise . . . . .	23
4.4	Quantum noise . . . . .	27
4.5	Harmonic oscillator bath . . . . .	28
4.6	Spin-boson model with longitudinal coupling . . . . .	31
4.6.1	Quantum noise correlator . . . . .	31
4.7	Summary . . . . .	32
<b>5</b>	<b>Charge qubit subject to non-Gaussian noise</b>	<b>33</b>
5.1	Introduction . . . . .	33
5.2	The model: Fluctuating background charges . . . . .	34
5.3	Summary . . . . .	36
<b>6</b>	<b>Decoherence by classical telegraph noise</b>	<b>37</b>
6.1	Introduction . . . . .	37
6.2	Classical telegraph noise . . . . .	37
6.3	Gaussian approximation . . . . .	41
6.4	Probability distribution . . . . .	42
6.5	Time evolution of the visibility for classical telegraph noise . . . . .	46
6.6	Decoherence rate for classical telegraph noise . . . . .	50
6.7	Summary . . . . .	51
<b>7</b>	<b>Decoherence by quantum telegraph noise</b>	<b>53</b>
7.1	Introduction . . . . .	53
7.2	Calculation of the coherence . . . . .	53
7.2.1	Time evolution of the visibility: General exact solution . . . . .	54
7.3	Gaussian approximation . . . . .	58
7.3.1	Results for the visibility according to the Gaussian approximation . . . . .	59
7.4	Exact numerical results and discussion . . . . .	60
7.5	Decoherence rate . . . . .	63
7.6	Phase diagram . . . . .	64
7.6.1	Temperature-dependence of the strong-coupling threshold . . . . .	65
7.6.2	Algorithm . . . . .	66
7.7	Summary . . . . .	67
<b>8</b>	<b>Spin-Echo</b>	<b>69</b>
8.1	Introduction . . . . .	69

---

8.2	Spin-echo for classical telegraph noise . . . . .	73
8.2.1	Time evolution of the echo according to the Gaussian approximation . .	74
8.2.2	Time evolution of the spin-echo signal . . . . .	74
8.3	Quantum spin-echo . . . . .	76
8.3.1	Time evolution of the spin-echo signal: General exact solution . . . . .	77
8.3.2	Time evolution of the echo according to the Gaussian approximation . .	79
8.3.3	Exact numerical results and discussion . . . . .	80
8.3.4	Arbitrary pulse-sequences . . . . .	81
8.4	Summary . . . . .	82
<b>9</b>	<b>Open questions</b>	<b>83</b>
<b>A</b>	<b>Hamiltonian of the three-junction flux qubit</b>	<b>85</b>
A.1	Calculation of the Hamiltonian . . . . .	85
<b>B</b>	<b>Coherence for classical telegraph noise</b>	<b>89</b>
<b>C</b>	<b>Spin-echo signal for classical telegraph noise</b>	<b>93</b>
<b>D</b>	<b>Quantum Telegraph Noise</b>	<b>95</b>
D.1	Coherence . . . . .	95
D.1.1	Calculation of the self-energy part . . . . .	98
D.1.2	Linked Cluster Expansion . . . . .	99
D.2	Spin-echo . . . . .	101
D.2.1	Numerics . . . . .	101
<b>E</b>	<b>Calculation of the Keldysh Green's function</b>	<b>103</b>
E.1	Keldysh Green's function . . . . .	103
E.2	Properties of the Keldysh Green's function . . . . .	105
	<b>Acknowledgement</b>	<b>107</b>





# List of Figures

2.1	Distance between normal persistent current states. . . . .	8
2.2	Properties of the Hilbert-space $\mathcal{H}$ :	
	(a) Generation of states belonging to the Hilbert-spaces $\mathcal{H}_0, \mathcal{H}_1, \dots, \mathcal{H}_N$	
	(b) Shell structure of the Hilbert space $\mathcal{H}$ . . . . .	10
2.3	(a) Distance for generalized GHZ-states.	
	(b) Probability distribution $P_\theta(D = d)$ for the distance $D$ . . . . .	11
3.1	Three-junction flux qubit:	
	(a) Circuit-diagram of the three-junction flux qubit.	
	(b) Three superconducting islands.	
	(c) Energy-diagram as a function of the applied flux $\Phi$ . . . . .	14
3.2	Size of Schrödinger's cat in the ring:	
	(a) Average distance $\bar{D}$ between the clockwise and counterclockwise current states.	
	(b) Probability distribution $P(D = d)$ for $\alpha = 0.8$ .	
	(c) Average current $I$ and average charge fluctuations $\delta N$ . . . . .	15
4.1	Double-slit experiment . . . . .	22
4.2	Quantum interference in mesoscopic physics	
	Weak-Localization: Interference of time-reversed trajectories . . . . .	23
4.3	Bloch sphere representation of the density matrix. . . . .	24
4.4	Separation of the energy levels due to a fluctuating environment. . . . .	25
4.5	Harmonic oscillator bath. . . . .	28
5.1	The model for quantum telegraph noise:	
	(a) Interaction between the qubit and intrinsic background charges.	
	(b) Charge qubit coupled to the fluctuations produced by a single impurity.	
	(c) Classical limit of quantum telegraph noise. . . . .	34

6.1	Two types of stochastic processes with the same noise-power:	
	(a) Gaussian Lorentzian noise.	
	(b) Non-Gaussian telegraph noise.	
	(c) Noise-power $\langle \delta Q \delta Q \rangle_\omega$ . . . . .	38
6.2	Time evolution of possible realizations of $Q(t)$ and the random phase $\varphi(t)$ . . . .	40
6.3	Probability distribution function $p(\varphi, t)$ of the phase for classical telegraph noise.	45
6.4	(a) Time evolution of the observable $\langle \hat{\sigma}_x(t) \rangle$ .	
	(b) Time evolution of the visibility $v(t) =  D(t) $ . . . . .	48
6.5	Effect of the detuning $\Delta\gamma/\gamma$ on the time evolution of the visibility and the phase	49
6.6	Decoherence rate $\Gamma_\varphi(v)$ for classical telegraph noise. . . . .	50
7.1	Schematic representation of the interaction between qubit and heat-bath. . . . .	57
7.2	Noise-spectrum $\langle \delta \hat{Q} \delta \hat{Q} \rangle_\omega$ :	
	(a) Noise-spectrum $\langle \delta \hat{Q} \delta \hat{Q} \rangle_\omega$ for different temperatures $T$ .	
	(b) Noise-spectrum $\langle \delta \hat{Q} \delta \hat{Q} \rangle_\omega$ for different switching-rates $\gamma$ . . . . .	59
7.3	Time evolution of the visibility at $T = 0$ . . . . .	61
7.4	(a) Time evolution of the visibility for different temperatures $T$ .	
	(b) Time evolution of the visibility for different energies of the impurity level $\varepsilon$ .	62
7.5	Decoherence rate $\Gamma_\varphi$ for quantum telegraph noise:	
	(a) Decoherence rate $\Gamma_\varphi(v)$ as a function of the coupling $v$ , $\varepsilon = 0$ .	
	(b) Decoherence rate $\Gamma_\varphi(v)$ as a function of the coupling $v$ , $\varepsilon = 3.0$ .	
	(c) log – log-plot of $\Gamma_\varphi$ as a function of temperature $T$ , $\varepsilon = 0$ .	
	(d) log – log-plot of $\Gamma_\varphi$ as a function of temperature $T$ , $\varepsilon = 3.0$ . . . . .	63
7.6	Shifted energy of the impurity level . . . . .	64
7.7	Density-plot of the coherence $D(t)$ for various couplings $v$ and temperatures $T$ .	65
7.8	“Phase diagram”: Critical coupling strength $v_c^q(T)$ as a function of temperature $T$ .	66
7.9	Schematic picture of the algorithm used to find the critical coupling $v_c^q(T)$ . . . . .	67
8.1	Time evolution of the qubit in a spin-echo experiment. . . . .	70
8.2	Schematic experimental setup of Nakamura’s charge-echo experiment. . . . .	71
8.3	Nakamura’s charge-echo experiment:	
	(a) Sequence of qubit manipulations.	
	(b) Sequence of charge pulses.	
	(c) Experimental results: Decay of the spin-echo signal. . . . .	72
8.4	Spin-echo signal for classical telegraph noise compared to	
	(a) the Gaussian approximation $D_{\text{Echo}}^{\text{Gauss}}(t)$	
	(b) the visibility $v(t)$ . . . . .	75
8.5	Spin-echo signal for different $\Delta\gamma/\gamma$ . . . . .	77
8.6	Spin-echo signal $D_{\text{Echo}}(t)$ for quantum telegraph noise compared to	
	(a) the Gaussian approximation $D_{\text{Echo}}^{\text{Gauss}}(t)$	
	(b) the visibility $v(t)$ . . . . .	78
8.7	Comparison of the spin-echo signal $D_{\text{Echo}}(t)$ with the visibility $v(t)$ for different $v$ .	79
8.8	Time evolution of the spin-echo signal for different temperatures and couplings	80

---

8.9	Time evolution of the echo-signal for a sequence of 10 instantaneous $\pi$ -pulses . . . . .	81
9.1	Disordered Quantum Dot coupled to an electronic reservoir. . . . .	83
A.1	Circuit diagram of the three-junction flux qubit. . . . .	86
D.1	Time dependence of the coupling $v$ along the Keldysh-contour. . . . .	96
D.2	Linked Cluster Expansion . . . . .	99
D.3	Time dependence of the coupling $v$ in a spin-echo experiment. . . . .	101
D.4	Comparison of the results: Trace-formula against Keldysh-technique. . . . .	102
E.1	Keldysh Green's function $G^K(t)$ :	
	(a) Contour of integration.	
	(b) Keldysh Green's function $G^K(t)$ in real-time representation. . . . .	104
E.2	Keldysh Green's function $G^K(t)$ as a function of time for different $\varepsilon$ .	
	(a) real part of $G^K(t)$ .	
	(b) imaginary part of $G^K(t)$ . . . . .	105



*All science is either physics or stamp  
collecting.*

ERNEST RUTHERFORD

## Summary

THE emergence of classical states in quantum systems is of fundamental importance for the foundations of quantum physics as well as for practical purposes in quantum engineering and applications (e.g. quantum computation) therein. One of the paradigms of quantum theory is the superposition principle, which says that a quantum system may be in two distinct states at the same time. In the year 1935 SCHRÖDINGER proposed his famous gedankenexperiment [1] questioning the validity of the superposition principle for “macroscopic” objects. In the original article a rather obscure example of a cat being simultaneously in the state “dead” and “alive” was chosen. Although this example is counterintuitive it doesn’t contradict the laws of quantum mechanics and the question whether it is possible to find superpositions of macroscopically distinct states still deserves its experimental verification. However, recent experiments have been successful in building “Schrödinger cats” superimposing macroscopically distinct states, like clockwise and counterclockwise circulating current states in superconducting flux qubits [2, 3, 4] or  $C_{60}$ -molecules being simultaneously at two different positions in space [5].

In the first part of the present thesis, “*How fat is Schrödinger’s cat?*”, we address the question about the size of superpositions of macroscopically distinct quantum states. We propose a measure for the “size” of a Schrödinger cat state, i.e. a quantum superposition of two many-body states with (supposedly) macroscopically distinct properties, by counting how many single-particle operations are needed to map one state onto the other. This definition gives reasonable results for simple, analytically tractable cases and is consistent with a previous definition restricted to GREENBERGER-HORNE-ZEILINGER (GHZ) like states. We apply our measure to the experimentally relevant, nontrivial example of a superconducting three-junction flux qubit put into a superposition of clockwise and counterclockwise circulating supercurrent states and find this Schrödinger cat to be surprisingly small.

In Chap. 1 we briefly describe the problem and introduce other measures for the size of Schrödinger cat states. A precise definition of our measure is given in Chap. 2 with an application to normal persistent current states and an analytically tractable example for generalized GHZ-states. The application of the measure to the experimental relevant three-junction flux qubit is presented in Chap. 3 with a discussion of our numerical results.

The crossover from quantum to classical states in quantum systems may be induced by their environments. The unavoidable coupling of any quantum system to many environmental degrees

of freedom leads to an irreversible loss of information about an initially prepared superposition of quantum states. This phenomenon, commonly referred to as *decoherence* or *dephasing*, is the subject of the second part of the thesis with the title “*Decoherence by quantum telegraph noise*”. We have studied the time evolution of the reduced density matrix of a two-level system (qubit) subject to *quantum telegraph noise* which is the major source of decoherence in Josephson charge qubits. A thorough understanding of decoherence is important not only for fundamental reasons but it is also important for achieving the long dephasing times in applications of coherent quantum dynamics. A general introduction into decoherence of two-level systems can be found in Chap. 4.

The classical limit of quantum telegraph noise corresponds to a stochastic process where the random variable jumps between two values, e.g. 0 and 1 at the switching rate  $\gamma$ . Quantum telegraph noise is an example of non-Gaussian noise and cannot be modeled by any of the paradigmatic models in this field, e.g. a bath of harmonic oscillators. However, we are able to derive an exact expression for the time evolution of the reduced density matrix which is accessible for numerical evaluation.

The model under consideration is introduced in Chap. 5 with a discussion of the relevant parameters of the system. We consider a single impurity level which is tunnel coupled to a fermionic reservoir. The fluctuating charge on the defect level induces fluctuations of the qubit’s energy levels which causes decoherence. Since the interaction with the environment (fluctuator) randomizes the relative phase of an initially prepared superposition of qubit states, models of this kind are commonly referred to as “*pure dephasing*”.

A review of the classical limit of quantum telegraph noise can be found in Chap. 6. We derive the coherence of a qubit subject to classical telegraph noise from an equation of motion approach and discuss the time evolution of the visibility for different coupling strengths to the fluctuator. As a result of our calculations we observe oscillations in the time evolution of the visibility with complete loss of visibility and coherence revivals in-between. Moreover, we calculate the non-Gaussian probability distribution of the random phase and discuss its crossover to a Gaussian distribution at long times. Finally, we calculate the decoherence rate  $\Gamma_\phi(\nu)$  as a function of the coupling  $\nu$  and compare it against the Gaussian approximation. In agreement with earlier results, we find a non-analytic decoherence rate which has a cusp when the coupling strength is equal to the switching rate. The cusp continue to exist even in the quantum limit at low temperature as our numerical evaluation shows.

Chapter 7 includes a thorough discussion of quantum telegraph noise. We derive an exact quantum mechanical expression for the coherence including all backaction and non-equilibrium effects. Our calculation is based on a trace-formula, well known from the theory of full-counting statistics, and is in principle applicable to other quantum baths of non-interacting fermions. The full time evolution of the visibility is calculated numerically for the entire range of parameters. We observe visibility oscillations to appear beyond a certain temperature dependent coupling of the qubit to the heat-bath with complete loss of visibility and visibility revivals in-between. These zeros in the time evolution of the visibility are a signature of non-Gaussian noise and their appearance is used in order to characterize the strong coupling regime. We develop an algorithm based on the iterative application of two combined bisection procedures in the  $\nu - T$ -plane in order to find the critical coupling strength  $\nu_c^q$  where the first zero-crossing in the time evolution of

the visibility appears at temperature  $T$ . The result is a “phase-diagram” which shows the regimes of strong and weak coupling. Above the critical coupling (strong coupling) one observes zeros in the visibility whereas no zeros occur below (weak coupling).

In Chap. 8 we consider a qubit subject to quantum telegraph noise in a spin-echo experiment. Spin-echo experiments are based on stroboscopic pulsing on the qubit by external fields in order to average out the effect of the heat-bath. The results of spin-echo for classical noise are briefly reviewed: We find that in the strong-coupling regime plateaux in the time evolution of the spin-echo signal occur. We present an exact formula for the quantum spin-echo signal and evaluate its full time evolution numerically for different parameters. The extension of this approach to an arbitrary sequence of pulses is shown and we compare the results for a sequence of 10 equally spaced pulses (CARR-PURCELL-MEIBOOM-GILL-cycle) against an optimized version with varying duration between consecutive pulses recently proposed for an Gaussian heat-bath with an Ohmic noise-spectrum.





## List of publications

1. F. MARQUARDT, B. ABEL, AND J. VON DELFT, Measuring the size of a quantum superposition of many-body states, *Physical Review A* **78**, 12109, 2008.
2. B. ABEL AND F. MARQUARDT, Decoherence by quantum telegraph noise: A numerical evaluation, *Physical Review B* **78**, 201302, 2008.
3. C. NEUENHAHN, B. KUBALA, B. ABEL AND F. MARQUARDT, Recent progress in open quantum systems: Non-Gaussian noise and decoherence in fermionic systems, accepted for publication in *Physica Status Solidii*



## **Part I**

**How fat is Schrödinger's cat?**



*Quantum physics thus reveals a basic  
oneness of the universe.*

ERWIN SCHRÖDINGER

# Chapter 1

## The validity of Quantum Mechanics

### 1.1 Introduction

QUANTUM MECHANICS has been proven to be one of the most successful theories in physics, in particular explaining the phenomena at the atomic scale like the photoelectric effect or the spectrum of the hydrogen atom. Despite its great success, quantum theory has been confusing generations of physicists (including the author) when confronted with some of its fundamental aspects and consequences like the superposition principle or the wave-particle dualism, just to mention two of them. Already at the early stage of quantum mechanics, one of its founding fathers the austrian physicist SCHRÖDINGER proposed a gedankenexperiment, nowadays commonly known as “*Schrödinger’s cat*”, questioning the validity of the superposition principle for “macroscopic” objects [1]. In his 1935 original article, a macroscopic object, (SCHRÖDINGER chose the rather obscure example of a cat), is being prepared (by some quantum mechanical mechanism) in a superposition of obviously macroscopically distinct states of “dead” and “alive”. However, there is no *a priori* reason why the quantum mechanical superposition principle should not be valid when it is extrapolated to “macroscopic” scales and the question whether macroscopic objects can be superimposed still deserves its experimental verification. Indeed, recent experiments claim to produce “macroscopic” Schrödinger cat states. The range of experiments detecting quantum superpositions of states involving a “macroscopic” number of particles widely extends from Rydberg atoms in microwave cavities [6], superconducting circuits [2, 3, 4, 7, 8, 9], optomechanical [10, 11] and nanomechanical [12] systems, molecule interferometer [5], magnetic biomolecules [13], to atom optical systems [14, 15]. The basic feature of those systems, is that their quantum mechanical state can be expressed as a superposition of macroscopically distinct states, i.e.

$$|\psi\rangle = \frac{1}{\sqrt{K}} (|\psi_A\rangle + |\psi_B\rangle), \quad (1.1)$$

where  $|\psi_A\rangle$  and  $|\psi_B\rangle$  are two states which are in some sense “macroscopic” and  $K$  is a normalization constant. Among these experiments the quest for quantum superpositions of macroscopically distinct states has been most advanced in superconducting devices containing one or several Josephson junctions. In the case of superconducting circuits the states  $|\psi_{A,B}\rangle$  represent

clockwise or counterclockwise current states circulating in the superconducting ring involving the collective motion of a macroscopic number of Cooper pairs.

The question which immediately arises is about the “size” of the superposition, commonly referred to as “*How fat is Schrödinger’s cat?*”. Already in the year 1980 LEGGETT [16] raised this question and proposed a measure for the size of Schrödinger cat states. He suggested two quantities, termed as *extensivity*  $\Lambda$  and *disconnectivity*  $D$  for the size (or frequently also referred to as “*cattiness*”) of Schrödinger cats. The extensivity  $\Lambda$  is the maximal expectation value of a characteristic observable in the two branches ( $|\psi_A\rangle$  or  $|\psi_B\rangle$ ) of the superposition  $|\psi\rangle$  measured in units of typical atomic quantities. In the case of a SQUID this might be the magnetic moment in units of Bohr’s magneton  $\mu_B$ . The very basic idea of disconnectivity  $D$  is to count the “effective” number of quantum correlated particles participating in the superposition.

Since LEGGETT’S initial proposal for the search of *Quantum Interference of Macroscopically distinct states (QIMDS)* and successful experiments producing “large” Schrödinger cats, this question has been attracting much interest and was attacked by several authors [16, 17, 18] sometimes restricted to certain special states like generalizations of GREENBERGER-HORNE-ZEILINGER (GHZ)- states.

It is reasonable to begin with a simple example, asking about the size of the generalized many-body GHZ-state,

$$|\psi\rangle = \frac{1}{\sqrt{K}} (|\psi_A\rangle^{\otimes N} + |\psi_B\rangle^{\otimes N}), \quad (1.2)$$

where  $K = 2 + \langle\psi_A|\psi_B\rangle^N + \langle\psi_B|\psi_A\rangle^N$  is a normalization and the overlap between the two individual constituents of the superposition  $|\langle\psi_A|\psi_B\rangle|^2 = 1 - \varepsilon^2$  is assumed to be large, i.e.  $\varepsilon \ll 1$ . The individual constituents may represent the clockwise or counterclockwise current states in a SQUID or a Bose-Einstein condensate (BEC) inside a double-well potential.

One way of assigning an effective size to the Schrödinger cat state  $|\psi\rangle$  has been proposed by DÜR, CIRAC and SIMON (DCS) [17], by comparing it against an ideal GHZ-state of the form  $|GHZ\rangle_n = 1/\sqrt{2}(|0\rangle^{\otimes n} + |1\rangle^{\otimes n})$  as a standard of comparison, where  $|0\rangle$  and  $|1\rangle$  are orthogonal states, and ask for the effective particle number  $n$  such that the state  $|\psi\rangle$  is in some sense equivalent to  $|GHZ\rangle_n$ . The result obtained by DCS for the effective size of the generalized GHZ-state  $|\psi\rangle$  is  $n = N\varepsilon^2$ , which means that the superposition  $|\psi\rangle$  involving  $N$  particles contains (by some precisely defined distillation protocol) the same amount of information as the ideal GHZ-state  $|GHZ\rangle_n$  with  $n$  particles.

Another measure for the size of Schrödinger cat states, in particular for interacting BECs, has been proposed recently by KORSBAKKEN *et al.* This measure is based on counting the number of fundamental subsystems of the superposition that have to be measured in order to collapse the entire state into a single branch corresponding either to  $|\psi_A\rangle$  or  $|\psi_B\rangle$ .

The disadvantage of the measures introduced above is their restricted range of applicability to superpositions of general many-body states. LEGGETT’S disconnectivity measure is quite general but complicated to calculate for specific states. The measures by DÜR, CIRAC AND SIMON or KORSBAKKEN *et al.* are only applicable to some special states.

In the present part of the thesis we present a measure for the size of many-body Schrödinger cat states. This part is based on our publication “Measuring the size of a quantum superposition

of many-body states” in [19]. This measure is in general applicable to a wide range of fermionic as well as bosonic states. We give the general definition of the measure in Chap. 2 and apply it to some simple examples including generalized GHZ-states. In Chap. 3 we apply our measure to superpositions of clockwise and counterclockwise circulating persistent currents in SQUIDS as they have been created experimentally recently. We present the results of the numerical implementation of our measure for the full range of parameters characterizing the superconducting circuit and we find an astonishing result for the size of the Schrödinger cat.



*In mathematics you don't understand things,  
you just get used to them.*

JOHN VON NEUMANN

## Chapter 2

# Cattiness for many-body states

## 2.1 Introduction

WHEN one is dealing with quantum superpositions of macroscopic states the obvious question which immediately emerges is about the “size” (cattiness) of the superposition, i.e. the number of particles which is involved in the quantum superposition. So far this question has not been answered in general and most discussions of this point related to existing experiments often remained qualitative.

For the specific case of the SQUID this means: “What is the number of Cooper pairs that have to change their state in order to turn the clockwise into the counterclockwise current state?”. A large number would suggest that we are indeed dealing with a large Schrödinger cat. In the present chapter we propose a quantitative measure for the size of a Schrödinger cat. This measure is in principle applicable to any superposition of two many-body states (with fixed particle number). It is consistent with previous approaches by other authors, [17], that had been restricted to generalizations of GHZ-states.

## 2.2 Definition of the measure for many-body states

Already in the year 1935 Schrödinger [1] predicted the existence of superpositions of macroscopically distinct quantum states. Recent experiments have been successful producing many-body Schrödinger cat states of the form

$$|\psi\rangle = \frac{1}{\sqrt{K}} (|\psi_A\rangle + |\psi_B\rangle), \quad (2.1)$$

where  $|\psi_A\rangle$  and  $|\psi_B\rangle$  are (by some definition) macroscopically distinct and  $K$  is a normalization constant. These states could be persistent current states of clockwise or counterclockwise circulating current direction in a SQUID [2, 3, 4] or they represent the two constituents (passing the left or right slit) of the wave-function of a  $C_{60}$  molecule in a double-slit experiment [5].

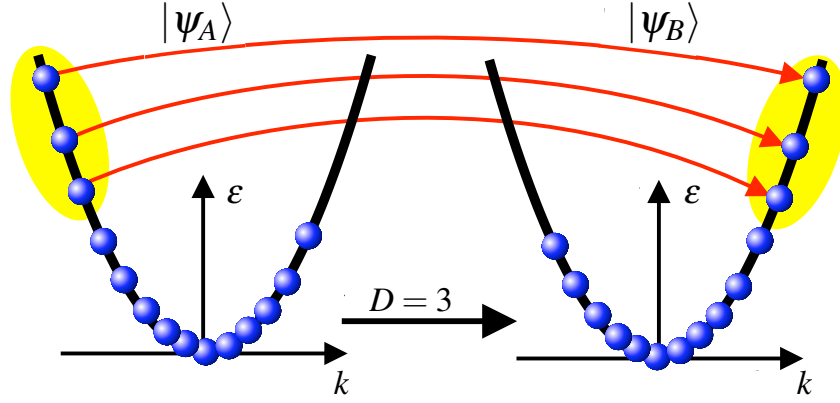


**Figure 2.1:** Example of normal persistent current states, where  $D = 3$  single-particle operations are necessary to convert state  $|\psi_A\rangle$  into  $|\psi_B\rangle$ .

Let us start the general definition of the measure for superpositions of many-body states with a simple example. Consider a clean, ballistic, single channel ring capable of supporting persistent currents of electrons. Suppose it is prepared in a superposition of two Slater determinants  $|\psi_A\rangle$  and  $|\psi_B\rangle$  which differ only in the number of clockwise and counterclockwise moving electrons. The number of particles effectively participating in a coherent superposition is obviously the number of particles that have to be converted from right- to left-movers in order to turn one of these many-body states into the other. The procedure is schematically depicted in Fig. 2.1: In the present example one has to convert exactly three left-movers (left branch) into right-movers (right branch). This is identical to the number  $D$  of single-particle operations that have to be applied to realize this change. Let us assume we want to convert state  $|\psi_A\rangle$  into the state  $|\psi_B\rangle$ ; the following transformation exactly does the job

$$|\psi_B\rangle \propto \prod_{j=1}^D \hat{c}_{k'_j}^\dagger \hat{c}_{k_j} |\psi_A\rangle, \quad (2.2)$$

where  $k_j, k'_j$  label the single-particle momentum states of the left and right branch, respectively. The number of single-particle operations  $D$  would be a measure for the size of the quantum superposition of many-body states or from a geometric point of view the “distance” between the vectors  $|\psi_A\rangle$  and  $|\psi_B\rangle$  in the Hilbert-space  $\mathcal{H}$ .

When turning this into a general definition, we have to realize that the “target” state  $|\psi_B\rangle$  might be a superposition of components that can be created from  $|\psi_A\rangle$  by applying a different number  $d$  of single-particle operations. In that case one ends up with the probability distribution  $P(D = d)$ , defined as the weights of these components, for the distance  $D$  between  $|\psi_A\rangle$  and  $|\psi_B\rangle$  to equal  $d$ . Furthermore, repeated application of single-particle operations may lead to a state that could have been already created by a smaller number of these operations (e.g.  $|\psi_A\rangle \propto \hat{c}_k^\dagger \hat{c}_{k'} \hat{c}_{k'}^\dagger \hat{c}_k |\psi_A\rangle$ , if  $n_k = 1$  and  $n_{k'} = 0$ ). This has to be taken care of by projecting out the states which have been reached already.

The general definition of the distance between two many-body states works like this:

Start with a state  $|\psi_A\rangle$ , which spans a Hilbert-space  $\mathcal{H}_0$  of dimension 1,  $\mathcal{H}_0 = \text{span}(\{|\psi_A\rangle\})$ . Then apply all possible single-particle transformations on state  $|\psi_A\rangle$ , which create another Hilbert-space  $\mathcal{H}'_1$ . A vector  $|\tilde{v}'_1\rangle \in \mathcal{H}'_1$  differs from the initial state  $|\psi_A\rangle$  in exactly one particle. Given a Hilbert-space  $\mathcal{H}_{d-1}$ , apply all single-particle operators on its vectors. The resulting Hilbert-space is denoted by  $\mathcal{H}'_d$  but it still may contain vectors that have already been produced with fewer than  $d$  single-particle operations. To remedy this situation, we construct the subspace  $\mathcal{H}_d \subseteq \mathcal{H}'_d$  which is orthogonal to all previous  $\mathcal{H}_j$ , with  $j < d$ . Following this procedure, we ultimately construct the whole Hilbert-space  $\mathcal{H}$  as a direct sum of subspaces,

$$\mathcal{H} = \mathcal{H}_0 \oplus \mathcal{H}_1 \oplus \mathcal{H}_2 \oplus \cdots \oplus \mathcal{H}_N. \quad (2.3)$$

The Hilbert-space  $\mathcal{H}$  is spanned by the set of vectors  $\{|v_d\rangle | d = 0, \dots, M\}$ , where  $M$  is the dimension of the whole Hilbert-space,  $M = \dim \mathcal{H}$  and  $M = n_0 + n_1 + \dots + n_N$  where  $n_i = \dim \mathcal{H}_i$ . Finally, the target state  $|\psi_B\rangle$  can be expanded in this basis,

$$|\psi_B\rangle = \sum_{d=0}^M \lambda_d |v_d\rangle. \quad (2.4)$$

where  $\lambda_d$  is the expansion coefficient of the normalized vector  $|v_d\rangle \in \mathcal{H}_d$ . The expansion coefficients define a probability distribution  $P(D = d)$  for the distance  $D$ ,

$$P(D = d) \equiv |\lambda_d|^2. \quad (2.5)$$

One can express the distance between two many-body states  $\bar{D}_{\psi_A, \psi_B}$  as an expectation value,

$$\begin{aligned} \bar{D}_{\psi_A, \psi_B} &= \sum_{d=0}^M d P(D = d) \\ &= \sum_{d=0}^M d |\lambda_d|^2. \end{aligned} \quad (2.6)$$

### 2.2.1 Application to generalized GHZ-states

Here we present an important example for the derivation of the *distance*  $D$  between two many-body states. We consider a quantum superposition of two non-interacting pure Bose condensates,  $|\psi_A\rangle$  and  $|\psi_B\rangle$ , with a fixed number of particles  $N$  being simultaneously in the single-particle states  $|\alpha\rangle$  or  $|\beta\rangle$ , respectively. The Schrödinger cat state is of the form Eq. (2.1) and the single-particle states have a finite overlap, which can be parametrized by the angle  $\theta$ ,  $\langle \alpha | \beta \rangle = \cos \theta$ ,  $\theta \in [0, \pi]$ . We can express the two many-body states as

$$\begin{aligned} |\psi_A\rangle &= \frac{1}{\sqrt{N!}} (\hat{c}_1^\dagger)^{\otimes N} |\text{vac}\rangle, \\ |\psi_B\rangle &= \frac{1}{\sqrt{N!}} \left( \cos \theta \hat{c}_1^\dagger + \sin \theta \hat{c}_2^\dagger \right)^{\otimes N} |\text{vac}\rangle, \end{aligned} \quad (2.7)$$

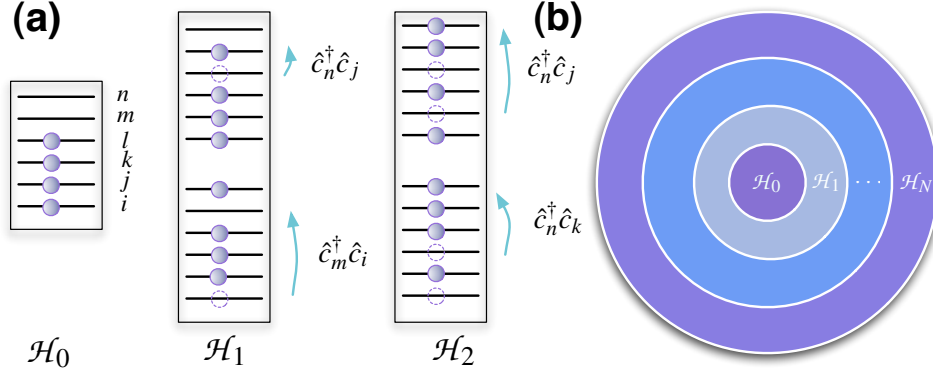


**Figure 2.2:** (a) Generation of states belonging to the Hilbert-spaces  $\mathcal{H}_0, \mathcal{H}_1, \dots, \mathcal{H}_N$  as a result of the action of repeated application of single-particle operators. (b) Schematic picture of the “shell” structure of the sequence of Hilbert-spaces  $\mathcal{H}_d$  generated by iterative application of single-particle operations on the initial state. The Hilbert-space  $\mathcal{H}_0$  is spanned by the initial state  $|\psi_A\rangle$ .

with  $\hat{c}_1^\dagger$  creating a particle in state  $|\alpha\rangle$  and  $\hat{c}_2^\dagger$  creating a particle in the state which defines the orthogonal direction in  $\text{span}\{|\alpha\rangle, |\beta\rangle\}$ , (we have dropped an eventually present but irrelevant global phase). Here  $|\text{vac}\rangle$  is the quantum mechanical vacuum state.

The state  $|\psi_B\rangle$  can be expanded into a series:

$$|\psi_B\rangle = \frac{1}{\sqrt{N!}} \sum_{d=0}^N \binom{N}{d} (\sin \theta \hat{c}_2^\dagger)^{\otimes d} (\cos \theta \hat{c}_1^\dagger)^{\otimes (N-d)} |\text{vac}\rangle. \quad (2.8)$$

Then we can easily find the states  $|v_d\rangle$  which span the Hilbert-space  $\mathcal{H}$  to be equal to

$$|v_d\rangle = \frac{1}{\sqrt{d!(N-d)!}} (\hat{c}_2^\dagger)^{\otimes d} (\hat{c}_1^\dagger)^{\otimes (N-d)} |\text{vac}\rangle, \quad (2.9)$$

which is a normalized state that can be reached from  $|\psi_A\rangle$  in exactly  $d$  applications of the single-particle operator  $\hat{c}_2^\dagger \hat{c}_1$ , i.e.  $|v_d\rangle \in \mathcal{H}_d$ . Thus, we have found a representation of the target state  $|\psi_B\rangle$  in the following form

$$|\psi_B\rangle = \sum_{d=0}^{\infty} \lambda_d |v_d\rangle, \quad (2.10)$$

with expansion coefficients  $\lambda_d$ ,

$$\lambda_d = \sqrt{\binom{N}{d}} \sin^d \theta \cos^{N-d} \theta. \quad (2.11)$$

As a result we obtain a binomial distribution  $P_\theta(D = d)$  with probability  $p = \sin^2 \theta = 1 - |\langle \psi_A | \psi_B \rangle|^2$ . Therefore the average distance between the states  $|\psi_A\rangle$  and  $|\psi_B\rangle$  is

$$\bar{D} = Np, \quad (2.12)$$

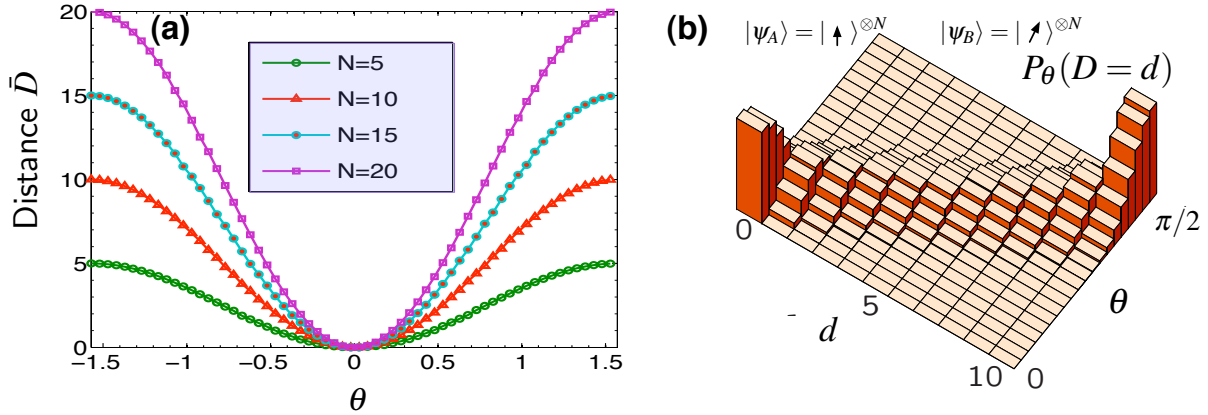


**Figure 2.3:** (a) Distance for generalized GHZ-states as a function of the angle  $\theta$  for different particle numbers  $N$ . The figure shows the results of the numerical evaluation for the distance. (b) Probability distribution  $P_\theta(D = d)$  for the distance  $d$  between two generalized GHZ-states as a function of the angle  $\theta$  between the corresponding single-particle states for  $N = 10$ .

with  $0 \leq p \leq 1$ . The maximal value of the average distance  $\bar{D} = N$  is reached when the two single-particle states  $|\alpha\rangle$  and  $|\beta\rangle$  become orthogonal to each other, i.e. at  $\theta = \pi/2$ . Figure 2.3(a) shows the numerical results for the average distance between two generalized GHZ-states as a function of  $\theta$  for different numbers of particle  $N$ .

One can draw a connection to generalized GHZ-states by considering the states

$$\begin{aligned} |\psi_A\rangle &= |\uparrow\rangle^{\otimes N} \\ |\psi_B\rangle &= (\cos \theta |\uparrow\rangle + \sin \theta |\downarrow\rangle)^{\otimes N}, \end{aligned} \quad (2.13)$$

where  $|\uparrow\rangle, |\downarrow\rangle$  are the eigenstates of the spin-1/2 operator  $\hat{S}_z = (\hbar/2)\hat{\sigma}_z$ , where  $\hat{\sigma}_z$  is the Pauli-matrix<sup>1</sup>. In this language the notion of the single-particle transformation  $\hat{c}_2^\dagger \hat{c}_1$  has to be replaced by  $\sum_{j=1}^N \hat{\sigma}_x^{(j)}$ , which flips a spin at site  $j$ . Identifying the probability  $p$  with  $\varepsilon$  we obtain exactly the same result as DCS.

## 2.3 General properties of the measure

### 2.3.1 Unitary changes of the basis

A straightforward requirement of our measure is that the Hilbert-space  $\mathcal{H}_d$  constructed by the procedure described above is independent from the choice of the single-particle basis used to

<sup>1</sup>The Pauli matrices are

$$\hat{\sigma}_x = \begin{pmatrix} 0 & 1 \\ 1 & 0 \end{pmatrix}, \quad \hat{\sigma}_y = \begin{pmatrix} 0 & -i \\ i & 0 \end{pmatrix}, \quad \hat{\sigma}_z = \begin{pmatrix} 1 & 0 \\ 0 & -1 \end{pmatrix}$$

define the operators  $\hat{c}_k^\dagger \hat{c}_{k'}$ . Thus no matter which single-particle basis we use to define the operators  $\{\hat{c}_k^\dagger \hat{c}_{k'}\}$  we arrive at the same Hilbert-space  $\mathcal{H}_d$ . Let  $\{\hat{c}_k |\text{vac}\rangle\}$  and  $\{\hat{c}'_k |\text{vac}\rangle\}$  be two basis-systems of the same Hilbert-space, with

$$\hat{c}'_i = \sum_j U_{ij} \hat{c}_j, \quad (2.14)$$

where  $U_{ij}$  is unitary. For an arbitrary vector  $|v\rangle \in \mathcal{H}$  the span of  $\hat{c}_i^\dagger \hat{c}_j |v\rangle$  should be the same irrespective of the basis we have chosen, i.e.  $\text{span}(\hat{c}_i^\dagger \hat{c}_j |v\rangle) = \text{span}(\hat{c}'_i \hat{c}'_j |v\rangle)$  (where  $i, j$  range over the basis). In fact any vector  $|w\rangle \in \text{span}(\hat{c}'_i \hat{c}'_j |v\rangle)$  can be written as

$$|w\rangle = \sum_{i', j', i, j} \mu_{i' j'} U_{i' i}^* U_{j' j} \hat{c}_i^\dagger \hat{c}_j |v\rangle, \quad (2.15)$$

where the right-hand side of Eq. (2.15) is an element of  $\text{span}(\hat{c}_i^\dagger \hat{c}_j |v\rangle)$ , and the left-hand side is an element of  $\text{span}(\hat{c}'_i \hat{c}'_j |v\rangle)$ . Indeed, the vector  $|w\rangle$  is contained in both spans and the same applies to the vector  $|v\rangle$ . As a consequence no particular basis (e.g. position) is singled out.

### 2.3.2 Symmetry

for an important class of states, namely those which are connected by time-reversal, such as clockwise and counterclockwise current states considered in Chap. 3, one can prove that the distance is symmetric under interchange of  $|\psi_A\rangle$  and  $|\psi_B\rangle$ , i.e.

$$D_{\psi_A, \psi_B} = D_{\psi_B, \psi_A}. \quad (2.16)$$

With respect to a position basis with real valued wave-functions this means  $|\psi_A\rangle = |\psi_B\rangle^*$ . In that case, since the single particle operators can be chosen real-valued, we have  $\mathcal{H}_d^{A \rightarrow B} = (\mathcal{H}_d^{B \rightarrow A})^*$ , making the weights  $P^{A \rightarrow B}(D = d) = P^{B \rightarrow A}(D = d)$  equal.

The example above can also be expressed in this way, by an appropriate change of basis, with  $|\psi_{A/B}\rangle \propto [\cos(\theta/2) \hat{c}_1^\dagger \pm i \sin(\theta/2) \hat{c}_2^\dagger]^{\otimes N} |\text{vac}\rangle$ . For other, non-symmetric pairs of states  $|\psi_A\rangle, |\psi_B\rangle$ , this is not true any longer, i.e.  $P^{A \rightarrow B}$  can become different from  $P^{B \rightarrow A}$ . An extreme example is provided by the states  $|\psi_A\rangle = (1/\sqrt{2})(|N, 0\rangle + |0, N\rangle)$  and  $|\psi_B\rangle = (1/\sqrt{2})(|N-1, 1\rangle)$ , for  $N$  bosons on two islands, where  $|n_1, n_2\rangle$  denoting the number of particles on each island. Here,  $P^{A \rightarrow B}(D = 1) = 1$ , but  $P^{B \rightarrow A}(D = 1) < 1$ , with  $P^{A \rightarrow B}(D = N-1) \neq 0$ . In the following chapter, we will restrict our discussion to time-reversed pairs of states.

## 2.4 Summary

We proposed a measure for the size of quantum superpositions of many-body states which is based on counting how many single-particle operations are needed to map one state into the other. This measure is independent of the basis, and moreover symmetric for time-reversed pairs of states. An analytical result for generalized GHZ-states coincides with previous results using a different approach (DCS).

# Chapter 3

## How fat is Schrödinger's cat?

### 3.1 Introduction

QUANTUM superpositions of macroscopically distinct states are commonly referred to as *Schrödinger cats* according to the famous gedankenexperiment by SCHRÖDINGER illustrating the counterintuitive nature of quantum mechanics. The term Schrödinger cat has nowadays become a synonym for a whole generation of experiments designed to investigate the potential limits of quantum mechanics as well as the crossover from the quantum-mechanical to the classical world.

In the present chapter we consider the experiment on the three-junction flux qubit performed in the Delft group [3] and address the question about the size of the Schrödinger cat in the three-junction flux qubit by a numerical implementation of the measure already introduced in Chap. 2 and we find the size calculated according to our measure to be unexpectedly small.

### 3.2 How fat is the cat in the ring?

When a small superconducting loop is subject to a magnetic field a small persistent supercurrent is generated inside the loop even when the loop is intersected by one or several Josephson-junctions. Depending on the externally applied magnetic flux  $\Phi$  the current has clockwise or counterclockwise direction thus reducing or enhancing the applied magnetic flux  $\Phi$  to approach integer multiples of the flux-quantum  $\Phi_0 = h/2e$ . The Josephson-junction comprises two superconducting islands which are separated by a thin oxide layer which allows for tunneling of Cooper-pairs. The junction is characterized by its charging energy  $E_C$ , which accounts for the electrostatic interaction of the Cooper-pairs, and the Josephson energy  $E_J$ , which accounts for tunneling across the junction. A schematic picture of the three-junction flux qubit which has been fabricated in Delft is shown in Fig. 3.1(a).

The current generated inside the loop corresponds to the collective motion of all Cooper-pairs condensed in the superconducting phase described by a collective wave-function  $\psi = |\Delta|e^{i\varphi}$ , describing the center of mass motion of the condensate, where  $\Delta$  is the superconducting order

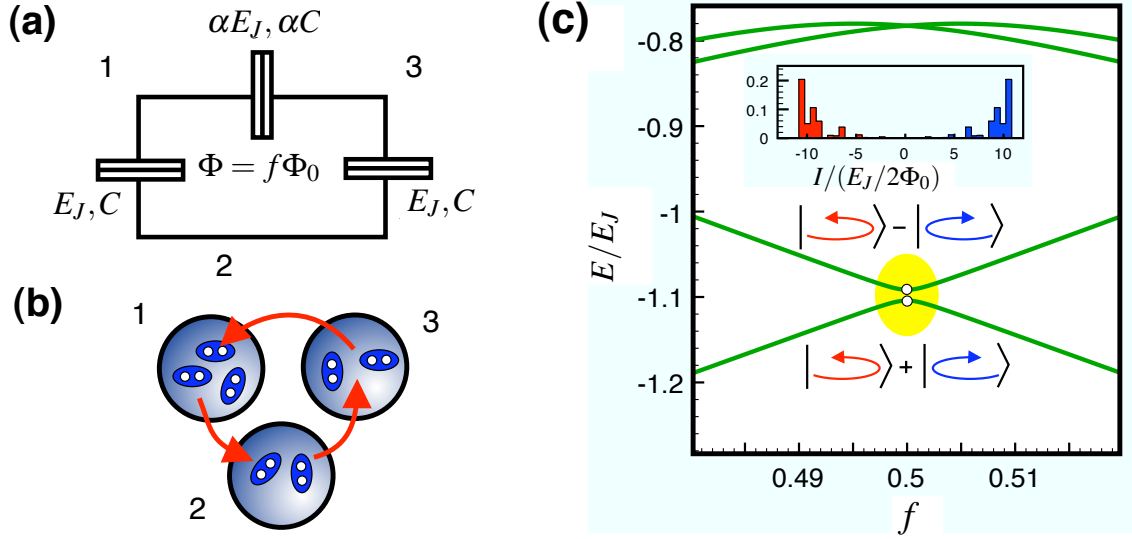


**Figure 3.1:** Three-junction flux qubit: (a) Circuit-diagram of the three-junction flux qubit. The left and right junctions have a capacitance  $C$  and Josephson coupling  $E_J$ . The top junction is by a factor  $\alpha$  smaller and has capacitance  $\alpha C$  and Josephson coupling  $\alpha E_J$ . (b) Equivalent picture of the three-junction flux qubit. Three superconducting islands are connected by tunnel junctions to each other. (c) Energies of the ground state and first excited state as a function of the applied magnetic flux  $f = \Phi/\Phi_0$ . Close to  $f = 0.5$  the ground state and first excited state are symmetric and anti-symmetric superpositions of clockwise or counterclockwise circulating current states. The inset shows the current contribution of clockwise (blue) and counterclockwise (red) circulating current states to the ground state.

parameter, and  $\varphi$  is the superconducting phase. At temperatures far below the superconducting transition temperature  $T \ll T_c$  excitations of quasi-particles are exponentially suppressed due to the large superconducting gap such that intrinsic dissipation associated with quasi-particle tunneling can safely be disregarded.

We now apply our measure for the size of the Schrödinger cat to a particular experimentally relevant case, the three-junction flux qubit that has been developed in Delft [3]. Three superconducting islands are connected by tunnel-junctions [Fig. 3.1(b)] where the tunneling amplitude is given by Josephson coupling  $E_J$ , and the charging energy is given by  $E_C = e^2/2C$  determined by the capacitance of the junctions. Such a superconducting circuit can be regarded as a collection of superconducting grains separated by an insulating layer which allows Cooper-pairs to tunnel coherently through the junctions. Adopting an effective bosonic description, tunneling is described by a term  $\hat{b}_i^\dagger \hat{b}_j$ , where  $\hat{b}_i^\dagger$  creates a Cooper-pairs on the island  $i$ . However, as the total “background” number of Cooper-pairs  $\bar{n}$  is very large and ultimately drops out of our calculation, the more convenient (and standard) approach is to consider instead operators  $e^{-i\hat{\varphi}_j} = \sum_n |n-1\rangle_j \langle n|_j$  that reduce the number of Cooper-pairs on island  $j$  by exactly one. Then, the tunneling becomes  $\bar{n}^{-1} \hat{b}_i^\dagger \hat{b}_j \rightarrow e^{i(\hat{\varphi}_i - \hat{\varphi}_j)}$ , while the total electrostatic energy may be expressed by the number operators  $\hat{n}_j$  that count the number of excess Cooper-pairs on each island. These two types of operators

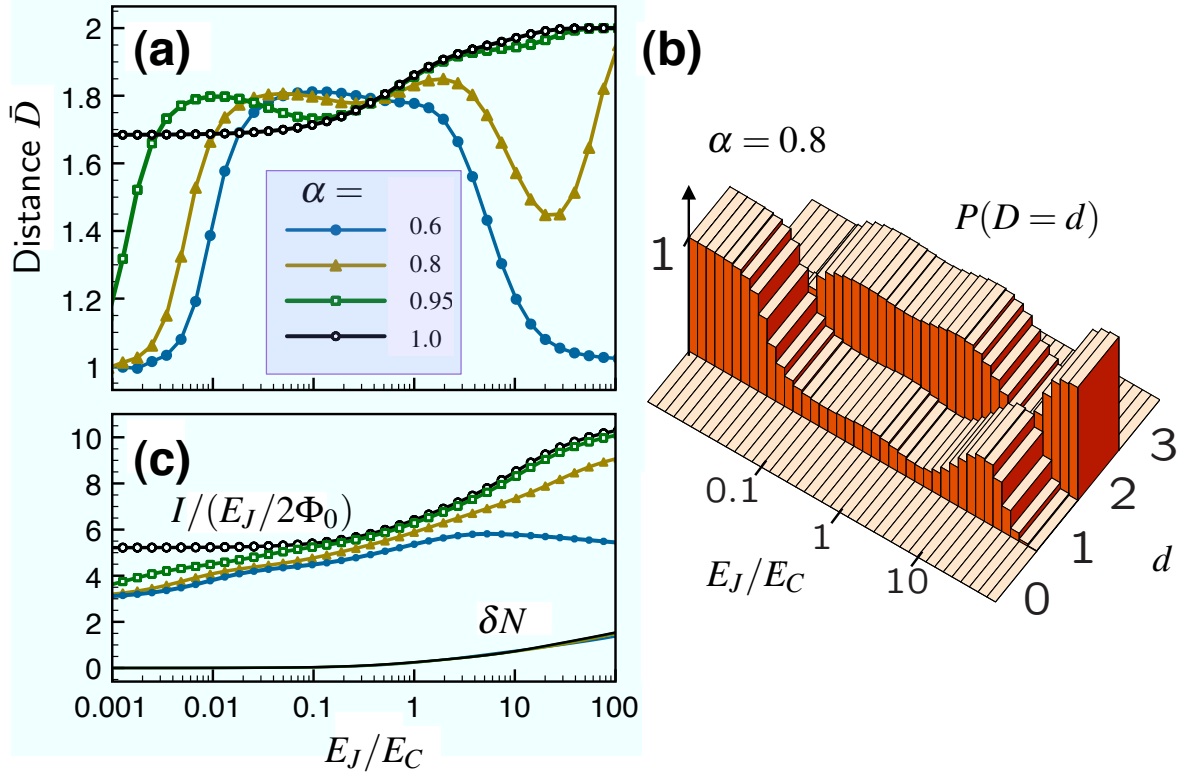


**Figure 3.2:** Size of Schrödinger's cat in the ring: (a) Numerical results for the average many-body distance  $\bar{D}$  between the clockwise and counterclockwise current states forming the ground state of the three-junction flux qubit at  $f = 0.5$  plotted as a function of  $E_J/E_C$  for various asymmetry parameters  $\alpha$ . (b) Corresponding probability distribution  $P(D = d)$  for  $\alpha = 0.8$  (c) Magnitude  $I$  of the average current in the two current states, and average charge fluctuations  $\delta N$  in the ground state.

define the single-particle operators needed in our approach. One of the junctions is smaller by a factor of  $\alpha$ , introducing an asymmetry that is important for the device to work as a qubit. The tunneling Hamiltonian [see App. A] is given by

$$\hat{\mathcal{H}}_T = -\frac{E_J}{2} \left( e^{i(\hat{\phi}_2 - \hat{\phi}_1)} + e^{i(\hat{\phi}_3 - \hat{\phi}_2)} + \alpha e^{i(\hat{\phi}_1 - \hat{\phi}_3 + 2\pi f)} + \text{h.c.} \right), \quad (3.1)$$

where the externally applied magnetic flux  $\Phi = f\Phi_0$  is measured in units of the flux quantum to define the frustration  $f$ . The charging Hamiltonian is equal to

$$\hat{\mathcal{H}}_C = \frac{1}{2C} \left( \hat{Q}_1^2 + \hat{Q}_2^2 + \frac{\hat{Q}_1^2 - \hat{Q}_3^2}{2 + 1/\alpha} \right), \quad (3.2)$$

with  $\hat{Q}_j = 2|e|\hat{n}_j$  and the restriction  $\sum_{j=1}^3 \hat{Q}_j = 0$  which imposes charge neutrality. For simplicity, we have neglected the small effects of the self-inductance and gate electrodes.

At  $f = 0.5$  the classical left and right-going current states are degenerate in energy, and quantum tunneling leads to an avoided crossing, with the ground- and first-excited state becoming a symmetric and anti-symmetric, respectively, superposition of the two classical current states, i.e.

$$|\psi_{\pm}\rangle = \frac{1}{\sqrt{2}} (|+I\rangle \pm |-I\rangle). \quad (3.3)$$

Figure 3.1(c) shows the eigenenergies of the ground state and first excited state as a function of  $f$ . The dots indicate the position where the energy levels of the classical states cross. However, the crossing is lifted by the charging energy which results in an avoided crossing of the two lowest lying energy levels.

We diagonalize the current operator  $\hat{I} = -\partial\hat{\mathcal{H}}/\partial\Phi$  in the two-dimensional subspace of ground- and first-excited states, which results in eigenvalues belonging to the two counter-propagating current states  $|\pm I\rangle$ . Whenever the excited and ground state are well separated from higher lying levels (as it should be the case in a flux qubit), an equivalent way of finding  $|\pm I\rangle$  is to write the ground state as a superposition of current operator eigenstates in the full Hilbert space, and keeping only the contributions with positive or negative current eigenvalues, respectively. A histogram displaying the current distribution in the ground state is shown in the inset of Fig. 3.1(c). The distance  $D$  between  $|\pm I\rangle$  then provides a measure of how ‘‘macroscopic’’ the ground (or excited) state superposition is.

Our calculations have been performed in the charge basis, by truncating the Hilbert-space to  $(2\Delta n + 1)^2$  states  $|n_1, n_2, n_3\rangle$  where  $n_{1,2} = -\Delta n, \dots, \Delta n$  (and  $n_3 = -n_1 - n_2$ ). Exact numerical diagonalization of  $\hat{\mathcal{H}}_C + \hat{\mathcal{H}}_J$  yields the ground state and the first excited state, and, from them, the current states  $|\pm I\rangle$ , as explained above. Our approach is then implemented by applying iteratively all possible single-particle operators (represented as  $(2\Delta n + 1) \times (2\Delta n + 1)$ -matrices in the charge basis), starting from  $|\psi_A\rangle = |+I\rangle$ . The target  $|\psi_B\rangle = |-I\rangle$  state is represented as a superposition in the Hilbert-space  $\mathcal{H}_d$ , which yields the weights  $P(D = d)$  [see Fig. 3.2(b)].

### 3.3 Numerical results and discussion

The results of our numerical evaluation are shown in Fig. 3.2(a) for different values of the asymmetry factor  $\alpha$ . It shows the average distance  $\bar{D}$  between the states  $|\psi_A\rangle = |+I\rangle$  and  $|\psi_B\rangle = |-I\rangle$  for  $\Delta n = 6$ . The fact that  $D \geq 1$  is a consequence of defining the states  $|\psi_A\rangle$  and  $|\psi_B\rangle$  as the eigenstates of the hermitean current operator, which makes them orthogonal by default, thus  $P(D = 0) = 0$ . At  $\alpha = 1$ , the monotonic rise of  $\bar{D}$  with  $E_J/E_C$  is expected, as a larger  $E_J/E_C$  allows the charges on the islands to fluctuate more strongly, implying that more Cooper-pairs effectively contribute to the current states. The non-monotonic dependence on  $E_J/E_C$  for  $\alpha < 1$  was unexpected, but is likely due to the fact that smaller values of  $\alpha$  tend to make the counter-propagating current states no longer a ‘‘good’’ basis (the ring is broken for  $\alpha = 0$ ).

In Fig. 3.2(c) we have plotted both the expectation value of the current operator in one of the superimposed states, as well as the average particle number fluctuation  $\delta N$  in the ground state, where  $\delta N^2 = \frac{1}{3} \sum_{j=1}^3 \langle (\hat{n}_j - \langle \hat{n}_j \rangle)^2 \rangle$ . Evidently, neither of these quantities can be correlated

to the average distance  $\bar{D}$ , apart from the general trend for all of them to usually increase with increasing  $E_J/E_C$ .

What is initially surprising is that the distance remains small, although the examples discussed earlier clearly show that much larger distances may be reached in principle when applying our measure. In contrast, the “disconnectivity” for the Delft setup was estimated [15] to be of the order of  $10^6$ , although a rigorous calculation is hard to do. Two reasons underly our findings for the flux qubit: First, it appears that the flux qubit considered here is really not far from the Cooper-pair box. In the Cooper-pair box [20], only a single Cooper-pair tunnels between two superconducting islands, yielding a distance  $D = 1$ . In fact, allowing only small charge fluctuations (e.g.  $\Delta n = 4$ ) on each island of the flux qubit is sufficient to reproduce the exact low-lying energy levels of this Hamiltonian to high accuracy for the parameter range considered here, since the charge fluctuations only grow slowly with  $E_J/E_C$ , as observed in Fig. 3.2(c) ( $\delta N \sim (E_J/E_C)^{1/4}$  at large  $E_J/E_C$ ). This means from the onset that very large values for  $D$  may not be expected. Second, when analyzing the structure of the generated Hilbert-spaces  $\mathcal{H}_d$ , it becomes clear that the dimensions of those spaces grow very fast with  $d$ , due to the large number of combinations of single-particle operators that are applied. For that reason, it turns out that the target state  $|\psi_B\rangle = |-I\rangle$  can accurately be represented as a superposition of vectors lying within the first few of those spaces, yielding a rather small distance  $\bar{D}$ .

### 3.4 Open questions

Future challenges include the extension to states without a fixed particle number and the comparison to other measures of catiness besides the DSC result [17]. In those cases in which different particles couple to independent environments (as was assumed in DCS), our measure is expected to be an indication of the decoherence rate with which the corresponding superposition is destroyed, and it would be interesting to verify this in specific cases.



## **Part II**

# **Decoherence by quantum telegraph noise**



# Chapter 4

## Basics of dephasing

### 4.1 Introduction

THE destruction of quantum mechanical interference induced by an environment is called *decoherence* or *dephasing*. Decoherence is important not only for fundamental questions like the quantum-classical crossover or the measurement problem but it is also of major relevance for applications of coherent quantum devices. Moreover, it is the main obstacle for achieving the long dephasing times necessary for building a quantum computer. The understanding of the underlying decoherence mechanisms as well as the search for methods to keep decoherence under control are of great importance in current research.

Let us see how the interfering particles are influenced by the environment in a double-slit experiment [see Fig. 4.1]. Two wave-packets (representing one and the same particle) have been separated and travel along different paths and combine later on a screen where the distribution of particles over many repeated runs of the experiment becomes visible. We observe an interference pattern in the probability density  $|\psi(x)|^2$  indicating the probability of the particle hitting the screen. When the particle is influenced by some fluctuating force on its way to the screen the interference pattern will be blurred.

The loss of interference “*visibility*” is due to the fluctuating force which results in an additional relative phase-factor  $e^{i\varphi}$  between the two wave-packets  $\psi_1$  and  $\psi_2$ . The interference pattern  $|\psi(x)|^2$  is then

$$\begin{aligned} |\psi(x)|^2 &= |\psi_1(x) + e^{i\varphi} \psi_2(x)|^2 \\ &= |\psi_1(x)|^2 + \underbrace{2\text{Re} [\psi_1^*(x) \psi_2(x) e^{i\varphi}]}_{\text{interference term}} + |\psi_2(x)|^2. \end{aligned} \tag{4.1}$$

What will be seen on the screen is the average interference pattern over many repeated runs of the same interferometer setup with a randomly fluctuating phase  $\varphi$  from run to run. As a consequence the interference contrast will be reduced by the average  $|\langle e^{i\varphi} \rangle|$ , which is a number equal or less than one. The angular brackets denote an average over the probability distribution

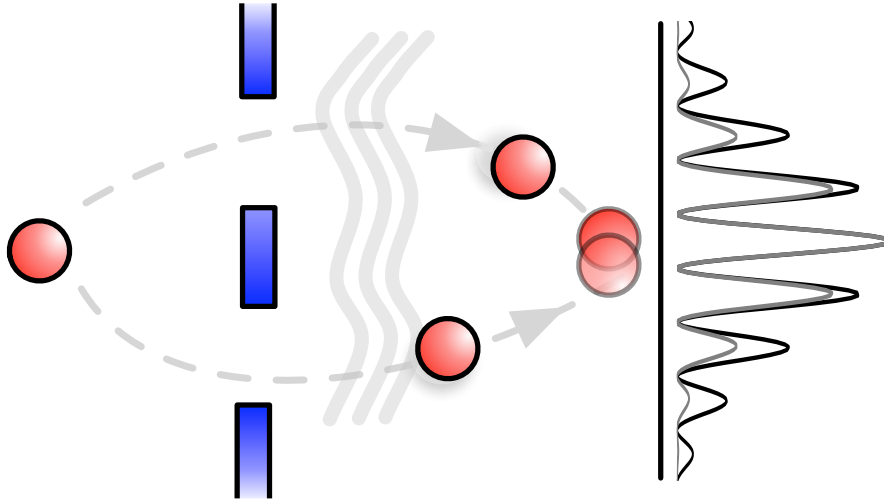


**Figure 4.1:** *Double-slit experiment: Two wave-packets of one and the same particle travel along different paths to recombine on the screen. The interference pattern will be blurred as a result of the unavoidable influence of the environment.*

of the phase  $\varphi$  and the decay of the interference pattern crucially depends on the distribution of the fluctuating force.

## 4.2 Dephasing in mesoscopic physics

Many of the interesting phenomena in mesoscopic physics are due to the quantum mechanical interference of electrons. In small electronic nanostructures these interference effects are most prominent when the wave-length of the electrons  $\sim \lambda_F$  (Fermi wave-length) becomes comparable to the typical size of the device.

The phenomena observed in mesoscopic devices include weak-localization corrections to the conductivity in disordered metals, Aharonov-Bohm interference and universal conductance fluctuations, to mention just a few of them.

An important realization of quantum interference manifests itself in disordered mesoscopic conductors as a result of the constructive interference of time-reversed electron paths that have been scattered off by randomly distributed impurities inside the metal. Let us consider two trajectories with amplitudes  $A_1$  and  $A_2$  of an electron and ask for its return probability when the particle is diffusing inside the disordered metal

$$\begin{aligned}
 P &= |A_1 + A_2|^2 \\
 &= |A_1|^2 + \underbrace{2|A_1||A_2|\cos(\varphi_1 - \varphi_2)}_{\text{interference term}} + |A_2|^2
 \end{aligned}
 \tag{4.2}$$

where  $\varphi_{1,2}$  is the phase accumulated along the paths 1, 2. After disorder averaging the interference-

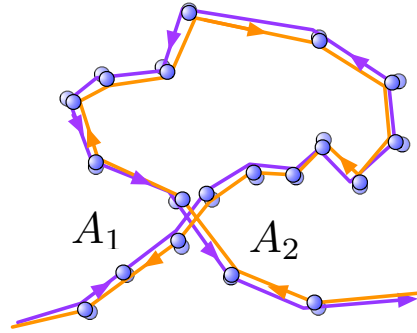


**Figure 4.2:** *Quantum interference in mesoscopic physics. Constructive interference of pairs of time-reversed electron trajectories in a disordered metal. The trajectories are diffusive (random walk) rather than ballistic.*

term in general vanishes. However, time-reversed pairs of trajectories, i.e.  $A_1 = A_2^*$ , will survive and as a consequence the return probability is equal to

$$P = 4|A_1|^2. \quad (4.3)$$

Thus the interference term doubles the classical contribution  $2|A_1|^2$ . This phenomenon is called *weak localization* and leads to a reduction of the conductivity (beyond its classical value). Figure 4.2 shows the constructive interference of a pair of time-reversed electron paths and only those pairs of paths survive after taking the ensemble average over many disorder configurations.

## 4.3 Dephasing of qubits

We discuss the dephasing of qubits induced by an external environment. A qubit is a two-level system which can have two states commonly denoted as  $|\uparrow\rangle$  and  $|\downarrow\rangle$  in order to emphasize the correspondence to spin-1/2. The most prominent physical implementation of a qubit in the solid state is the superconducting charge qubit which comprises two superconducting islands separated by an insulating oxide layer. By adjusting an external gate voltage one can achieve that only the two lowest lying energy states are relevant [20].

Studying dephasing of qubits has attained much interest because they serve as the quantum analogue of a classical bit and may serve as a building block for a quantum computer.

### 4.3.1 Classical noise

The Hamiltonian of the two-level system is equal to (we put  $\hbar, k_B = 1$  throughout this work)

$$\hat{\mathcal{H}} = \frac{\Delta}{2} \hat{\sigma}_z, \quad (4.4)$$

where  $\Delta$  is the energy-splitting between the energy levels of the qubit. We denote the eigenstates  $|\uparrow\rangle$  as the excited and  $|\downarrow\rangle$  as the ground state,  $\hat{\sigma}_z$  is the Pauli-matrix acting on the eigenstates of the qubit.

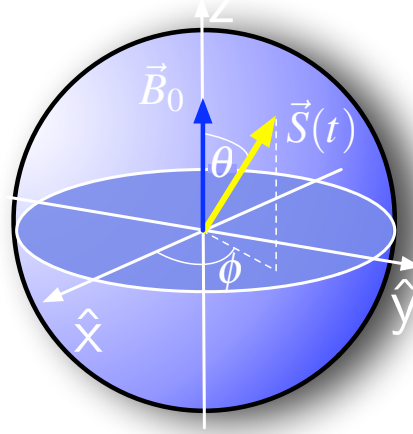


**Figure 4.3:** Representation of the density matrix by the vector  $\vec{S}(t)$  (yellow) on the Bloch sphere,  $\vec{B}_0$  (blue) represents an external magnetic field. The vector  $\vec{S}$  is parametrized by the angles  $\phi$  and  $\theta$ , i.e.  $\vec{S} = (\sin \theta \cos \phi, \cos \theta \cos \phi, \cos \theta)^T$ .

One can map the above Hamiltonian to a fictitious spin-1/2 in an effective magnetic field  $\vec{B}$  (measured in units of energy), i.e.

$$\hat{\mathcal{H}} = \frac{B_z}{2} \hat{\sigma}_z. \quad (4.5)$$

The density matrix of the qubit is equal to

$$\hat{\rho}(t) = \sum_{i,j=\uparrow,\downarrow} |i\rangle \rho_{ij}(t) \langle j|, \quad (4.6)$$

where  $\rho_{ij}(t)$  are the elements of the density matrix in the eigenbasis of the qubit. The unitary time evolution of the qubit's density matrix is determined by the *von Neumann equation*

$$\frac{\partial \hat{\rho}(t)}{\partial t} = -i[\hat{\mathcal{H}}, \hat{\rho}(t)], \quad (4.7)$$

and the solution can formally be expressed as  $\hat{\rho}(t) = e^{-i\hat{\mathcal{H}}t} \hat{\rho}(0) e^{i\hat{\mathcal{H}}t}$ . The unitary time evolution of the density matrix can be visualized as a vector  $\vec{S}(t)$  on the Bloch-sphere, parametrized by the two angles  $\theta$  and  $\phi$ . In this picture the qubit will precess around the  $\hat{z}$ -axis with a precession frequency  $B_z$  provided that the magnetic field is directed along the  $\hat{z}$ -axis  $\vec{B} = (0, 0, B_z)^T$ . The angles of the Bloch-sphere are related to the density matrix by

$$\hat{\rho}(t) = \frac{1}{2} (1 + \vec{S}(t) \cdot \vec{\sigma}), \quad (4.8)$$

where  $\vec{\sigma} = (\sigma_x, \sigma_y, \sigma_z)^T$ . The dynamics of the spin  $\vec{S}$  under the action of a time-dependent magnetic field can also be cast in form of the *Landau-Lifschitz equation*

$$\frac{d}{dt} \vec{S} = -\vec{S} \times \vec{B}. \quad (4.9)$$

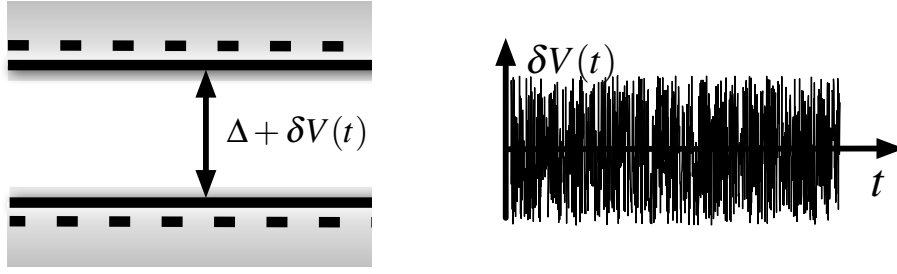


**Figure 4.4:** The position of the fluctuating energy levels around their average value (dashed line) is determined by the classical stochastic process  $\delta V(t)$ .

In a realistic physical situation the two-level system will be coupled to many degrees of freedom of an external environment (heat-bath). Let's suppose that the coupling to the qubit has the specific form

$$\frac{V(t)}{2} \hat{\sigma}_z, \quad (4.10)$$

where  $V(t) = \delta V(t) + \langle V \rangle$  describes the interaction of the qubit with the environment. Classically,  $V(t)$  may be described by some stochastic process (with mean  $\langle V \rangle$ ) which is indeed the high temperature limit of the quantum mechanical model where the coupling is of the form  $\hat{V} \hat{\sigma}_z / 2$  and  $\hat{V}$  is an operator whose dynamics is determined by the Hamiltonian of the heat-bath. For example,  $\hat{V}$  corresponds to the displacement of an atom in a crystal lattice or to the fluctuations of the electromagnetic field. The environments mentioned above may be modeled by a collection of harmonic oscillators and the quantum mechanical Hamiltonian (system + bath) represents an example of the so-called *spin-boson model* [22].

The form of the coupling to the heat-bath is crucial for all of our subsequent discussion. The coupling of the form  $V(t) \hat{\sigma}_z$  induces the energy levels  $\varepsilon_{\pm}(t) = \pm(\Delta + \delta V(t))/2$  fluctuating around their average position (we assume  $\langle V \rangle = 0$ ). However, the coupling  $V(t) \hat{\sigma}_x$  would induce transitions between first-excited  $|\uparrow\rangle$  and ground state  $|\downarrow\rangle$ . The effect of the environment on the qubit will be a loss of quantum mechanical phase coherence while no energy relaxation takes place. In the language of spin-1/2 the longitudinal coupling to an external bath corresponds to an additional fluctuating magnetic field  $\delta \mathcal{B}(t)$ . As consequence the spin  $\vec{S}$  will precess with a randomly fluctuating frequency around the  $\hat{z}$ -axis and this destroys phase coherence. Due to the diagonal coupling  $V \hat{\sigma}_z$  the diagonal elements of the density matrix are preserved whereas the off-diagonal elements acquire a random phase factor, i.e.

$$\rho_{\uparrow\downarrow}(t) = \rho_{\uparrow\downarrow}(0) e^{-i\Delta t} e^{i\varphi(t)}, \quad \varphi(t) = - \int_0^t dt' V(t'). \quad (4.11)$$

The diagonal model is commonly referred to as *pure dephasing* since the off-diagonal elements of the density-matrix will acquire a random phase-factor  $e^{i\varphi(t)}$ . In an experiment, measurements are performed not only for a single realization of the fluctuating force  $V(t)$  but over many repeated runs on the same qubit which requires averaging over many realizations of the fluctuating force.

Assuming the fluctuations  $\delta V(t)$  to be Gaussian-distributed because they originate from a very large number of environmental degrees of freedom and the central-limit theorem<sup>1</sup> is applicable, then we can use the following formula valid for Gaussian-distributed noise

$$\langle e^{i\varphi} \rangle = e^{i\langle \varphi(t) \rangle - \frac{1}{2}\langle \delta\varphi^2 \rangle}, \quad \delta\varphi(t) = \varphi(t) - \langle \varphi(t) \rangle, \quad (4.13)$$

where the angular brackets denote an average over the Gaussian-distributed fluctuations  $\delta\varphi$ ,  $\langle \dots \rangle = \int d\varphi(\dots)p(\varphi, t)$ , with the probability distribution  $p(\varphi, t) = (2\pi\langle \delta\varphi^2 \rangle)^{-1/2} e^{-\delta\varphi^2/(2\langle \delta\varphi^2 \rangle)}$  (we assume that  $\langle V \rangle = 0$ ). This is the simplest assumption for the probability distribution of  $\delta V$  and a quantum analogue of Eq. (4.13) exists when the environment is made of a collection of harmonic oscillators. In the case of Gaussian-distributed noise  $|\langle e^{i\varphi} \rangle|$  is determined by the variance  $\langle \delta\varphi^2 \rangle$  of the phase  $\varphi$ .

The quantity  $D(t) = \langle e^{i\varphi(t)} \rangle$  is called *coherence* and determines the interference contrast of any observable sensitive to the phase. For example, the expectation value of  $\hat{\sigma}_x$  averaged over fluctuations of  $\delta V$  is equal to

$$\langle \hat{\sigma}_x(t) \rangle = \cos(\Delta t) e^{-\frac{1}{2}\langle \delta\varphi^2(t) \rangle}. \quad (4.14)$$

One will observe decaying oscillations in the time evolution of  $\langle \hat{\sigma}_x(t) \rangle$  and the decay of these oscillations is determined by the coherence  $\langle e^{i\varphi(t)} \rangle$ . In the case of Gaussian-distributed noise the coherence is solely determined by the two-point correlation function  $\langle \delta V(t_1)\delta V(t_2) \rangle$  of  $\delta V(t)$ . To see this, we apply Eq. (4.13) on Eq. (4.11) and we get

$$\rho_{\uparrow\downarrow}(t) = \rho_{\uparrow\downarrow}(0) e^{-i\Delta t} \exp\left(-\frac{1}{2} \int_0^t dt' \int_0^t dt'' \langle \delta V(t')\delta V(t'') \rangle\right). \quad (4.15)$$

If the correlations decay sufficiently rapidly one may approximate the above integral as

$$\begin{aligned} \rho_{\uparrow\downarrow}(t) &\approx \rho_{\uparrow\downarrow}(0) e^{i\Delta t} \exp\left(-t \int_{-\infty}^{\infty} dt' \langle \delta V(t')\delta V(0) \rangle\right) \\ &= \rho_{\uparrow\downarrow}(0) e^{-i\Delta t} e^{-\Gamma_\varphi t}, \end{aligned} \quad (4.16)$$

in the long time limit. At long times the off-diagonal matrix elements of the density matrix decay exponentially with time at a *decoherence rate*  $\Gamma_\varphi$  defined as

$$\Gamma_\varphi = \int_{-\infty}^{\infty} dt' \langle \delta V(t')\delta V(0) \rangle \quad (4.17)$$

$$= \langle \delta V \delta V \rangle_{\omega=0}, \quad (4.18)$$

<sup>1</sup>Let  $X_1, X_2, \dots, X_N$  be a set of  $N$  independent random variables and each have an arbitrary probability distribution with mean  $\mu_i$  and a finite variance  $\sigma_i^2$ . Then the sum of random variables

$$X = \frac{\sum_{i=1}^N X_i - \sum_{i=1}^N \mu_i}{\sqrt{\sum_{i=1}^N \sigma_i^2}} \quad (4.12)$$

has a limiting cumulative distribution function which approaches a normal distribution.

where we have defined the noise-power  $\langle \delta V \delta V \rangle_\omega$  as the Fourier transform of the correlation function

$$\langle \delta V \delta V \rangle_\omega = \int_{-\infty}^{\infty} dt e^{i\omega t} \langle \delta V(t) \delta V(0) \rangle. \quad (4.19)$$

This concludes our discussion on dephasing of qubits due to classical Gaussian-distributed noise.

## 4.4 Quantum noise

At high temperatures the picture of classical noise as a stochastic process is a valid description of the environment and dephasing is due to the fluctuating energy levels of the qubit. However at low temperatures, the heat-bath cannot be described by a random external field but requires a quantum mechanical description taking into account the backaction of the qubit on the quantum bath. We now consider a qubit coupled to a quantum environment with an interaction of the form  $\hat{V} \hat{\sigma}_z / 2$ . The dynamics of  $\hat{V}$  is now determined by the Hamiltonian of the environment  $\hat{H}_B$  and the full Hamiltonian is equal to

$$\hat{H} = \frac{\Delta}{2} \hat{\sigma}_z + \frac{\hat{V}}{2} \hat{\sigma}_z + \hat{H}_B. \quad (4.20)$$

Let us imagine that the coupling between qubit and environment is switched on at  $t = 0$  and has been switched off before (i.e.  $\hat{V} = 0$  for  $t < 0$ ). The initial state of the system is a product state

$$|\psi(0)\rangle = \frac{1}{\sqrt{2}} (|\uparrow\rangle + |\downarrow\rangle) \otimes |\chi_0\rangle, \quad (4.21)$$

where  $|\chi_0\rangle$  is the ground state of the heat-bath. When we are dealing with finite temperatures one can proceed in a similar way including an average of all subsequent results over initial states of the heat-bath  $|\chi_0\rangle$  weighted by an appropriate Gibbs measure  $e^{-\beta(\hat{H}_B - \mu \hat{\mathcal{N}})} / Z$ , where  $\beta = 1/T$  is the inverse temperature,  $\hat{\mathcal{N}}$  is the particle number operator and  $Z$  is a normalization constant.

The dynamics of the bath states for subsequent times will be determined by  $\hat{H}_B + \hat{V}/2$  when the qubit is in the excited state  $|\uparrow\rangle$  and by  $\hat{H}_B - \hat{V}/2$  when the qubit is in its ground state  $|\downarrow\rangle$ , such that at time  $t$  the state of the system is equal to

$$|\psi(t)\rangle = \frac{1}{\sqrt{2}} \left( e^{-i\Delta t/2} |\uparrow\rangle \otimes |\chi_\uparrow(t)\rangle + e^{i\Delta t/2} |\downarrow\rangle \otimes |\chi_\downarrow(t)\rangle \right), \quad (4.22)$$

where  $|\chi_{\uparrow\downarrow}(t)\rangle$  is the state of the bath which evolves under the action of  $\hat{H}_B \pm \hat{V}/2$ ,

$$|\chi_{\uparrow\downarrow}(t)\rangle = \hat{U}_{\pm,t} |\chi_0\rangle, \quad \hat{U}_{\pm,t} = e^{-i(\hat{H}_B \pm \hat{V}/2)t}, \quad (4.23)$$

where  $\hat{U}_{\pm,t}$  is the unitary time evolution operator corresponding to the conditional Hamiltonian  $\hat{H}^\pm = \hat{H}_B \pm \hat{V}/2$ . The reduced density matrix of the qubit has the form

$$\hat{\rho}^{\text{red}}(t) = \begin{pmatrix} \rho_{\uparrow\uparrow}(0) & \rho_{\uparrow\downarrow}(0) e^{-i\Delta t} D(t) \\ \rho_{\downarrow\uparrow}(0) e^{i\Delta t} D^*(t) & \rho_{\downarrow\downarrow}(0) \end{pmatrix}, \quad (4.24)$$

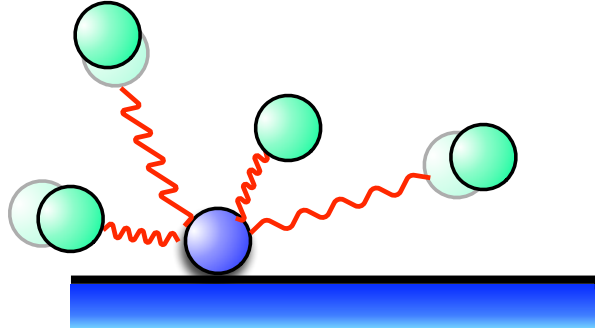


**Figure 4.5:** Schematic picture of a bath consisting of harmonic oscillators. The blue particle is coupled by springs (red) to the elongation of harmonic oscillator modes (green particles).

where the coherence can then be expressed as the overlap of the bath-states, i.e.

$$\begin{aligned} D(t) &= \langle \chi_{\downarrow}(t) | \chi_{\uparrow}(t) \rangle \\ &= \langle \chi_0 | e^{i(\hat{\mathcal{H}}_B - \hat{\nu}/2)t} e^{-i(\hat{\mathcal{H}}_B + \hat{\nu}/2)t} | \chi_0 \rangle. \end{aligned} \quad (4.25)$$

In the non-zero temperature case the above average has to be replaced by a trace over thermal bath states weighted by the Gibbs measure

$$D(t) = \frac{1}{Z} \text{tr} \left( e^{-\beta(\hat{\mathcal{H}}_B - \mu \hat{\mathcal{L}})} \hat{U}_{-,t}^{\dagger} \hat{U}_{+,t} \right) \quad (4.26)$$

The average phase factor  $\langle e^{i\varphi} \rangle$ , which we have already considered in the case of classical noise, is now replaced by the overlap between states of the heat-bath and averaging over fluctuations of the classical noisy field corresponds to taking the trace over states of the heat-bath.

## 4.5 Harmonic oscillator bath

We will now discuss an environment consisting of a collection of harmonic oscillators. A schematic picture of a particle coupled to the coordinates of a collection of harmonic oscillators is shown in Fig. 4.5. Many interesting physical phenomena arise from quantum systems coupled to a bath of harmonic oscillators like the *Caldeira-Leggett model of dissipative quantum tunneling* [21], the spin-boson model [22] and quantum Brownian motion [23]. In all of these cases, the bath variable coupling to the quantum system displays Gaussian-distributed fluctuations. This feature affords considerable technical simplifications, while at the same time these models are faithful descriptions of real environments: The vacuum electromagnetic field or the harmonic crystal lattice are indeed baths of harmonic oscillators. More importantly, in many other cases (like electronic Nyquist noise in a bulk metal), these models represent very good approximations. This is essentially a consequence of the central limit theorem, applied to the sum of contributions from many independent non-Gaussian noise sources. Moreover, a bath of harmonic oscillators can be regarded as the quantum analogue of classical noise in the sense that in

thermal equilibrium fluctuations are Gaussian-distributed (i.e. it would correspond to a random process with a Gaussian-distribution in the classical limit) and a quantum analogue of Eq. (4.13) is still valid.

For simplicity, we consider just a single oscillator with mass  $m$  and frequency  $\omega$ , the extension to many oscillators will be straightforward and one has to include a summation over oscillator modes when needed. We derive the coherence  $D(t)$  when the harmonic oscillator couples longitudinally to the qubit  $v\hat{\mathcal{V}}\hat{\sigma}_z/2$  with

$$\hat{\mathcal{V}} = v\hat{Q}, \quad (4.27)$$

where  $v$  is a coupling constant. The Hamiltonian of the environment consisting of a single harmonic oscillator is then equal to

$$\hat{\mathcal{H}}_B = \frac{\hat{P}^2}{2m} + \frac{m\omega^2}{2}\hat{Q}^2 \quad (4.28)$$

It is convenient to write  $\hat{\mathcal{V}}/2$  in the form

$$\frac{\hat{\mathcal{V}}}{2} = \frac{v\hat{Q}}{2} = -m\omega^2 Q_0 \hat{Q}, \quad (4.29)$$

where  $Q_0$  is the shift of the oscillator coordinate from its equilibrium position when the interaction with the qubit is switched on.

We first consider the zero temperature case  $T = 0$  when the harmonic oscillator is in its ground state denoted by  $|\chi_0\rangle$ . The extension to finite temperature is straightforward resulting in an average over all initial states weighted by the appropriate Gibbs factor.

The potential of the harmonic oscillator is shifted by  $Q_0$  after switching on the interaction with the qubit, i.e.

$$\frac{m\omega^2}{2}\hat{Q}^2 \rightarrow \frac{m\omega^2}{2}\hat{Q}^2 - m\omega^2 Q_0 \hat{Q} = \frac{m\omega^2}{2}(\hat{Q} - Q_0)^2 - \frac{m\omega^2}{2}Q_0^2. \quad (4.30)$$

The ground state of the harmonic oscillator bath (represented by a Gaussian wave-packet) will start to oscillate back and forth with a maximum displacement of  $2Q_0$ . The state of the harmonic oscillator can be written as a coherent state<sup>2</sup> with a complex amplitude, i.e.

$$|\chi_{\uparrow}(t)\rangle = e^{i\theta(t)}|\alpha(t)\rangle, \quad (4.33)$$

<sup>2</sup>Here we list just a few properties about bosonic coherent states: The coherent state  $|\alpha\rangle$  is an eigenstate of the annihilation operator with eigenvalue  $\alpha$ , i.e.  $\hat{a}|\alpha\rangle = \alpha|\alpha\rangle$  and can be represented as

$$|\alpha\rangle = e^{-|\alpha|^2/2} \sum_{n=0}^{\infty} \frac{\alpha^n}{\sqrt{n!}} |n\rangle. \quad (4.31)$$

The overlap between two coherent states is equal to

$$\langle\alpha|\alpha'\rangle = e^{-(|\alpha|^2 - 2\alpha^*\alpha' + |\alpha'|^2)/2}. \quad (4.32)$$

The solution for  $\alpha$  is equal to

$$\alpha = \sqrt{\frac{m\omega}{2}} \left( \bar{Q} + i \frac{\bar{P}}{m\omega} \right). \quad (4.34)$$

inserting Eq. (4.33) into the Schrödinger equation and applying  $\langle \chi_{\uparrow}(t) |$  from the left provides us with an equation for the dynamics of the complex phase  $\theta(t)$

$$\frac{d}{dt} \theta(t) = - \left[ E(t) + \frac{1}{2} \left( \bar{Q}(t) \frac{d}{dt} \bar{P}(t) - \bar{P}(t) \frac{d}{dt} \bar{Q}(t) \right) \right]. \quad (4.35)$$

The first term in Eq. (4.35) corresponds to the dynamical phase, whereas the second term in square brackets depends on the path in parameter-space (*geometrical phase* or *Berry-phase*). The expectation values  $\bar{Q}, \bar{P}$  obey the classical equation of motion for a harmonic oscillator and with the initial conditions  $\bar{Q} = 0, \bar{P} = 0$  at  $t = 0$  and we can immediately write down their solutions

$$\bar{Q}(t) = Q_0(1 - \cos \omega t), \quad \bar{P}(t) = m\omega Q_0 \sin \omega t. \quad (4.36)$$

The solution for  $\alpha(t)$  moves clockwise in the complex  $\alpha$ -plane along a circle centered at  $\alpha = (m\omega/2)^{-1/2} Q_0$ . The solution for  $\theta(t)$  is equal to

$$\theta(t) = \frac{m\omega Q_0^2}{2} (\omega t - \sin \omega t) - \frac{\omega t}{2}. \quad (4.37)$$

The coherence  $D(t) = \langle \chi_{\downarrow}(t) | \chi_{\uparrow}(t) \rangle$  is determined by the overlap of the bath states. The amplitudes are  $\alpha_{\uparrow}(t) = \alpha(t)$  for the excited- and  $\alpha_{\downarrow}(t) = -\alpha(t)$  for the ground-state of the bath and moreover, since the geometric phase  $\theta(t)$  is the same, the coherence yields

$$\begin{aligned} D(t) &= \langle \alpha_{\downarrow}(t) | \alpha_{\uparrow}(t) \rangle, \\ &= e^{-2|\alpha(t)|^2}, \end{aligned} \quad (4.38)$$

where the exponent is determined by the distance to the origin in the complex  $\alpha$  plane,

$$\begin{aligned} |\alpha(t)|^2 &= \frac{m\omega}{2} \left( \bar{Q}^2(t) + \frac{\bar{P}^2(t)}{m^2\omega^2} \right) \\ &= m\omega Q_0^2 (1 - \cos(\omega t)). \end{aligned} \quad (4.39)$$

The coherence  $D(t)$  is completely restored for times  $t = (2\pi/\omega)n, n = 0, 2, \dots$  and approaches its minimum value  $e^{-4\bar{n}}$  at half period when the distance between the two coherent states becomes largest. The average number of excitations of the coherent state is  $\bar{n} = m\omega Q_0^2$ , measured with respect to the new potential. The periodic revival of the coherence is a special feature of coupling to a single oscillator.

## 4.6 Spin-boson model with longitudinal coupling

The most paradigmatic model used to study dephasing of qubits is the *spin-boson model* where the qubit is coupled to a bath of harmonic oscillators. Here we consider the simplest limiting case of the spin-boson model, namely longitudinal coupling, i.e. the interaction is of the form  $\hat{\mathcal{V}}\hat{\sigma}_z/2$ . The Hamiltonian of the heat-bath is equal to

$$\hat{\mathcal{H}}_B = \sum_j \omega_j \hat{b}_j^\dagger \hat{b}_j, \quad (4.40)$$

where  $\omega_j$  is the frequency of the  $j$ -th oscillator mode and  $\hat{b}_j/\hat{b}_j^\dagger$  are bosonic annihilation / creation operators which obey the commutation relation  $[\hat{b}_i, \hat{b}_j^\dagger] = \delta_{ij}$ . The bath variable  $\hat{\mathcal{V}}$  which couples to the qubit is equal to

$$\hat{\mathcal{V}} = \sum_j v_j (\hat{b}_j + \hat{b}_j^\dagger), \quad (4.41)$$

where  $v_j$  is the coupling strength to the  $j$ -th oscillator. The coherence  $D(t)$  can be expressed in terms of the correlation function of  $\delta\hat{\mathcal{V}}$ ,

$$D(t) = \exp \left[ -i\langle \hat{\mathcal{V}} \rangle t - \frac{1}{2} \int_{-\infty}^{\infty} \frac{d\omega}{2\pi} \langle \delta\hat{\mathcal{V}} \delta\hat{\mathcal{V}} \rangle_{\omega} \frac{\sin^2(\omega t/2)}{(\omega/2)^2} \right], \quad (4.42)$$

where  $\delta\hat{\mathcal{V}} = \hat{\mathcal{V}} - \langle \hat{\mathcal{V}} \rangle$  and the symmetric correlation function is related to the spectral density of the heat-bath as  $\langle [\delta\hat{\mathcal{V}}, \delta\hat{\mathcal{V}}]_+ \rangle_{\omega} = 2J(\omega) \coth(\omega/2T)$ , where  $J(\omega)$  is the spectral density of the bath  $J(\omega) = \pi \sum_i v_i^2 \delta(\omega - \omega_i)$ .

### 4.6.1 Quantum noise correlator

We derive some general properties of the correlator  $\langle \delta\hat{\mathcal{V}}(t) \delta\hat{\mathcal{V}}(0) \rangle$  valid for arbitrary quantum operators  $\hat{\mathcal{V}}(t)$ , where  $\delta\hat{\mathcal{V}}(t) = \hat{\mathcal{V}}(t) - \langle \hat{\mathcal{V}} \rangle$ . The correlation function can be written as

$$\langle \delta\hat{\mathcal{V}}(t) \delta\hat{\mathcal{V}}(0) \rangle = \sum_{\alpha} P_{\alpha} \langle \alpha | \delta\hat{\mathcal{V}}(t) \delta\hat{\mathcal{V}}(0) | \alpha \rangle, \quad (4.43)$$

where  $|\alpha\rangle$  is an eigenstate of the system with energy  $\varepsilon_{\alpha}$  and probability  $P_{\alpha}$ . Using  $\langle \alpha | \delta\hat{\mathcal{V}}(t) | \beta \rangle = e^{i(\varepsilon_{\alpha} - \varepsilon_{\beta})t} \langle \alpha | \delta\hat{\mathcal{V}} | \beta \rangle$  and taking the Fourier transform, we obtain for the noise-power

$$\langle \delta\hat{\mathcal{V}} \delta\hat{\mathcal{V}} \rangle_{\omega} = 2\pi \sum_{\alpha, \beta} P_{\alpha} |\delta V_{\beta\alpha}|^2 \delta[\omega - (\varepsilon_{\beta} - \varepsilon_{\alpha})]. \quad (4.44)$$

For a system in equilibrium at finite temperature  $T$  and  $P_{\alpha}/P_{\beta} = e^{-\beta(\varepsilon_{\alpha} - \varepsilon_{\beta})}$  and when the system is symmetric under time-inversion we obtain the well known relation

$$\langle \delta\hat{\mathcal{V}} \delta\hat{\mathcal{V}} \rangle_{\omega} = \langle \delta\hat{\mathcal{V}} \delta\hat{\mathcal{V}} \rangle_{-\omega} e^{-\beta\omega}. \quad (4.45)$$

In the classical limit  $T \gg \omega$  the noise-power is approximately symmetric, which implies that emission or absorption of a bath mode (e.g. in the case of the crystal lattice the emission or absorption of a phonon) are equally likely. On the other hand, in the quantum limit  $T = 0$  the noise-power vanishes for  $\omega < 0$  which means that emission is not possible when the bath is in the ground state.

## 4.7 Summary

We have reviewed the basics of dephasing of qubits for classical as well as for quantum noise. Classical noise can be regarded as the high temperature limit of quantum noise and corresponds to a stochastic process. The spin-boson model is the most paradigmatic model to study dephasing of qubits. Specifically, in this model the environment is modelled by a collection of harmonic oscillators and the coherence of the qubit is determined by the two-point correlation function of the bath-variable. We have discussed the simple, yet relevant limiting case of coupling longitudinally to the qubit (pure dephasing).

# Chapter 5

## Charge qubit subject to non-Gaussian noise

### 5.1 Introduction

THE unavoidable coupling of any quantum system to a noisy environment leads to decoherence. Understanding the mechanisms of decoherence is not only interesting for fundamental reasons (the quantum-classical crossover, the measurement problem etc.), but it is also essential for achieving the long dephasing times necessary for building a quantum computer and other applications of coherent quantum dynamics.

Various sources of noise have been described by baths of harmonic oscillators [see. Sec. 4.5 for examples], which afford great technical simplification while at the same time these environments are faithful descriptions of real environments. The approximation finally breaks down when one couples strongly to a few noise sources. This situation is becoming more prevalent nowadays, as one studies the coherent dynamics of smaller and smaller nanostructures. In fact, the decoherence times of solid state qubits are often mainly determined by a few fluctuators [24, 25, 26].

This challenge has given rise to a number of theoretical studies of qubits subject to fluctuators producing telegraph noise [27, 28, 29, 30, 31, 32, 33, 34, 35, 36, 37, 38, 39], some of them with surprising discoveries. The most straightforward but realistic fully quantum-mechanical model for an electronic fluctuator consists of a single resonant level that is tunnel-coupled to an electron reservoir, thereby producing non-Gaussian charge fluctuations. Models of this type may be reasonably termed “*quantum telegraph noise*” since they correspond to stochastic processes of the telegraph noise type of Poissonian-distributed random jumps between two possible charge states with  $Q \in \{0, 1\}$  in the classical limit [see Chap. 6].

GRISHIN, YURKEVICH and LERNER recently studied this model in the long-time limit and derived the dephasing rate for a qubit coupled longitudinally to a single fluctuator [31, 32]. They found a striking non-analytic dependence of the dephasing rate  $\Gamma_\varphi$  on the coupling strength and temperature (we briefly discuss the dephasing rate in Sec. 7.5). However, in the present work the focus is on analyzing the non-Gaussian features of quantum telegraph noise and we evaluate the full time evolution of the reduced density matrix. Our analysis covers arbitrary coupling strengths and temperatures, and predicts a non-trivial temporal evolution of the coherence.

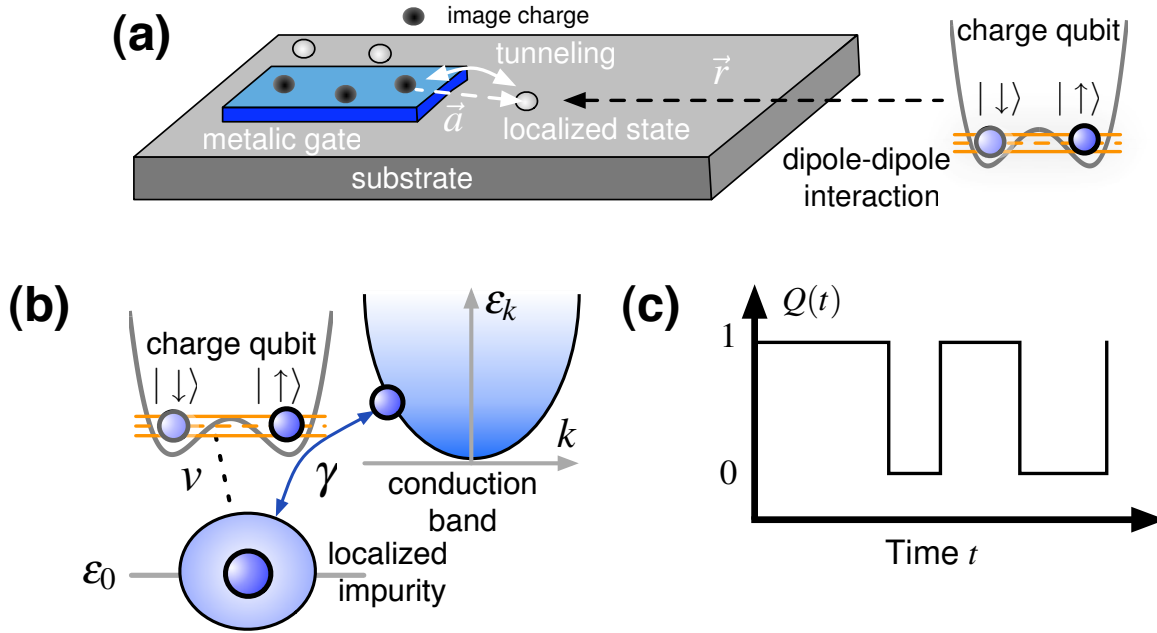


**Figure 5.1:** (a) Schematic picture of the model discussed in the text: The qubit interacts via a random dipole field produced by the fluctuating charge on the defect levels distributed on the substrate. When an electron tunnels from the gate electrode to a localized level it leaves a positive image charge on the gate which produces an electric dipole field with a nearby negative charge on the impurity level. Defect levels are denoted by light dots and the image charge produced inside the gate electrode when an electron tunnels onto the defect level by black dots. The connection between image charge and localized level is denoted by  $\vec{a}$ . (b) A qubit is longitudinally coupled to the fluctuating population on a single localized impurity. Electrons can hop from the impurity level onto the reservoir at a rate  $\gamma$  and the coupling strength between qubit and fluctuator is  $v$ . (c) time evolution of the charge  $Q(t)$  in the classical limit (high temperature). In this regime the charge on the impurity level may be described by a classical stochastic process which jumps randomly between 0 and 1 at the classical switching rate  $\gamma^{cl}$ .

Please note: This and the following chapters are partly based on our publication on “Decoherence by quantum telegraph noise: A numerical evaluation” in [40].

## 5.2 The model: Fluctuating background charges

We study decoherence in a Josephson charge qubit which interacts with an environment consisting of an ensemble of electronic fluctuators. A 2D metallic gate grown on a substrate is surrounded by nearby localized impurities such that electrons can tunnel from the gate-electrode on an impurity level thereby leaving a positive image charge on the gate-electrode [see Fig. 5.1(a)]. This gives rise to a randomly fluctuating electric dipole field which interacts with the qubit. The qubit itself can be considered as an electric dipole since one superconducting island has an excess number of Cooper pairs whereas the other superconducting island exactly lacks the same

number of Cooper pairs and therefore the qubit and the fluctuating background charges interact via dipole-dipole interaction. The interaction strength depends on the distance  $r$  between qubit and fluctuator, i.e.  $v = e^2(\vec{a} \cdot \vec{r})/r^3 \propto 1/r^2$ , where  $a$  is the tunneling distance. In a realistic sample the impurities are widely dispersed on the substrate and the distribution of coupling strengths depends on the distance between the charge qubit and the fluctuator, i.e.  $P(v) \propto 1/v^2$ . This is exactly the same distribution of coupling constants as observed in glasses where an ensemble of two-level systems interact via dipole-dipole interaction, [41].

Loss of coherence is due to the fluctuating charge on the defect level which gives rise to a randomly fluctuating electric dipole field affecting the qubit. A static dipole-field caused by static image charges would only result in a renormalization of the qubit's interlevel distance but not to a loss of quantum mechanical phase coherence.

The effect from many randomly distributed impurities gives rise to  $1/\omega$ -noise, [34, 39], which is a result of averaging over randomly distributed couplings  $v$  with the probability distribution  $P(v) \propto 1/v^2$ . However, in nanostructures only a few individual fluctuators play an important role and decoherence will be produced by fluctuators with non-Gaussian noise statistics. In our analysis we are primarily interested in decoherence produced by a single fluctuator.

The two lowest lying states of the qubit are discriminated by their excess number of Cooper pairs and therefore feel a different interaction depending on the charge state, thus enforcing the longitudinal coupling  $\hat{\mathcal{V}}\hat{\sigma}_z/2$  between qubit and fluctuator. This type of interaction leads to pure dephasing only and not to energy relaxation (the populations of the qubit levels are conserved). The Hamiltonian of the model is equal to

$$\hat{\mathcal{H}} = \frac{\Delta}{2}\hat{\sigma}_z + \frac{\hat{\mathcal{V}}}{2}\hat{\sigma}_z + \hat{\mathcal{H}}_B, \quad (5.1)$$

where  $\Delta$  is the energy splitting of the eigenenergies of the qubit and  $\hat{\mathcal{H}}_B$  is the Hamiltonian of the heat-bath. The heat-bath consists of  $N$  defect levels inside the metal which are tunnel-coupled to the metallic gate. The hopping of electrons between the defect levels and the lead results in a randomly fluctuating ‘‘charge’’

$$\hat{\mathcal{V}} = \sum_{i=1}^N v_i \hat{d}_i^\dagger \hat{d}_i, \quad (5.2)$$

where  $v_i$  is the coupling strength to the  $i$ -th impurity level. Due to the Pauli-principle, a single defect level is either empty or singly occupied which results in a discretely fluctuating charge on the impurity level. The ensemble of  $N$  fluctuators is described by

$$\hat{\mathcal{H}}_B = \sum_{i=1}^N \varepsilon_i^0 \hat{d}_i^\dagger \hat{d}_i + \sum_{i=1}^N \sum_{\mathbf{k}} \left( T_{ki} \hat{c}_{\mathbf{k}}^\dagger \hat{d}_i + \text{h.c.} \right) + \sum_{\mathbf{k}} \varepsilon_{\mathbf{k}} \hat{c}_{\mathbf{k}}^\dagger \hat{c}_{\mathbf{k}}, \quad (5.3)$$

here  $\varepsilon_i^0$  is the bare energy of the  $i$ -th impurity level,  $T_{ki}$  is the tunneling amplitude for hopping of an electron from impurity  $i$  to a state with momentum  $\mathbf{k}$  inside the lead electrode. The operators  $\hat{d}_i^\dagger/\hat{d}_i$  create / annihilate an electron with energy  $\varepsilon_i^0$  on the defect level and  $\hat{c}_{\mathbf{k}}^\dagger/\hat{c}_{\mathbf{k}}$  create / annihilate an electron with momentum  $\mathbf{k}$  inside the electronic reservoir. We assume the reservoir to be a normal metal since this is the usual case in semiconductor quantum dots.

The width of each impurity level  $\varepsilon_i^0$  is broadened due to hybridization with the Fermi sea, such that the density of states near  $\varepsilon_i^0$  has a Lorentzian shape. The width of the Lorentzian is set by the *tunneling rate*  $\gamma$  for flips between the two possible states of the impurity level which can be either occupied or unoccupied.

There are four parameters with dimension of energy: coupling strength  $v_i$ , energy of the impurity level  $\varepsilon_i^0$ , the impurity level broadening  $\gamma_i = 2\pi \sum_{\mathbf{k}} |T_{\mathbf{k}}|^2 \delta(\omega - \varepsilon_{\mathbf{k}})$  and temperature  $T$ . For many fluctuators with a broad distribution of parameters some of them may be considered as “high-energy” ( $\varepsilon_i^0 > T$ ) and some of them as “low-energy” ( $\varepsilon_i^0 < T$ ) when compared against temperature. As shown in [32] the low energy impurities are effectively absent and the contribution of high energy impurities is suppressed due to the Lorentzian tail of the density of states but still not negligible. Thus, the main contribution to decoherence comes mainly from high energy impurities  $\varepsilon_i^0 \gg T$  which imposes the low temperature regime and therefore requires a quantum mechanical treatment. The full quantum mechanical analysis of the model is subject of Chap. 7.

In the high temperature limit, one can neglect the backaction of the qubit onto the heat-bath and treat the charge on the impurity as a classical stochastic process. Such a stochastic process is described by a random variable which flips randomly between 0 and 1 at the classical *switching rate*  $\gamma^{cl}$ . The classical limit is studied in Chap. 6.

### 5.3 Summary

We have discussed the major source of decoherence in Josephson charge qubits caused by the fluctuating charge on intrinsic impurity levels. The resulting noise produced by these defect levels is non-Gaussian and its high-temperature limit corresponds to classical telegraph noise, therefore we term models of the type *quantum telegraph noise*. In small nanostructures the effect of decoherence will be strongest when the qubit couples only to a few fluctuators. Besides temperature  $T$ , the relevant parameters are  $v$  the coupling strength of the qubit to the fluctuator, and  $\gamma$ , the is the tunneling rate.

# Chapter 6

## Decoherence by classical telegraph noise

### 6.1 Introduction

IT is useful to begin by reviewing the classical limit for the heat-bath, where the charge  $Q(t)$  is a stochastic process of the “telegraph noise” type, which flips randomly between 0 and 1 at a rate  $\gamma^{cl}$ . We will see further below that this corresponds precisely to the high-temperature limit of the quantum model which we will discuss thoroughly in Chap. 7.

Telegraph noise is an example of non-Gaussian noise and cannot be described by any Gaussian theory, e.g. a harmonic oscillator bath. This makes telegraph noise interesting because the simple Gaussian approximation is no longer reliable and more sophisticated methods are required for the calculation of the time evolution of the coherence  $D(t)$ .

In the present chapter we will derive the full time evolution of the coherence for a charge qubit subject to classical telegraph noise. Furthermore, we investigate the non-Gaussian probability distribution  $p(\varphi, t)$  for the relative phase  $\varphi$  accumulated by the qubit’s eigenstates and finally we calculate the decoherence rate  $\Gamma_\varphi$  as a function of the coupling  $\nu$  of the qubit to the fluctuator.

### 6.2 Classical telegraph noise

Classical telegraph noise describes a discrete stochastic process denoted by  $Q(t)$ ,  $t \in [0, \infty]$ , where the random variable  $Q$  can only have two possible values,  $Q(t') = 0/1$ , at some certain time  $t'$ . Jumps between the two possible states of  $Q$  occur at a *switching rate*  $\gamma^{cl}$  such that in a time-interval  $[0, t]$  the average number of flips is equal to  $\gamma^{cl}t$ . Figure. 6.2 (left panel) shows a realization of the time evolution of  $Q(t)$  for increasing switching rate  $\gamma^{cl}$  (from top to bottom). Surprisingly, the regime where the fluctuator rarely flips in a given time-interval is most interesting and shows many unexpected features as compared to Gaussian noise.

Telegraph noise has the Markoff-property, i.e. in a given time-interval the probability for a flip to occur is independent of the history of preceding jumps. Furthermore, telegraph noise is an example of non-Gaussian noise. In contrast to the case of Gaussian-distributed noise where the two-point correlation function  $\langle Q(t)Q(0) \rangle$  of the random variable  $Q(t)$  determines all higher

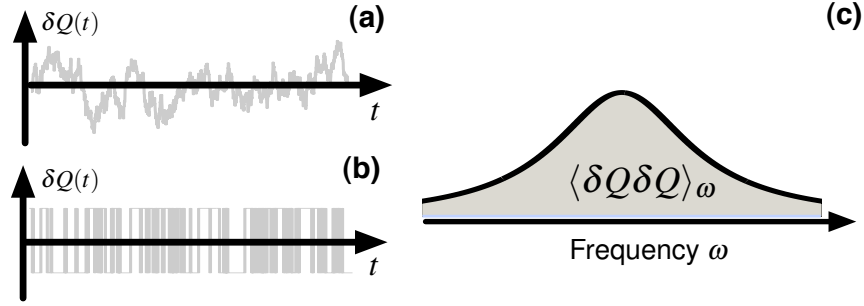


**Figure 6.1:** Two types of stochastic processes with the same noise-power: Shown are the time evolution for two types of stochastic processes  $\delta Q(t)$  which have the same noise-spectrum  $\langle \delta Q \delta Q \rangle_\omega$ . (a) The upper panel displays Gaussian Lorentzian noise and in comparison with (b) non-Gaussian telegraph noise (lower panel). (c) Lorentzian noise-power  $\langle \delta Q \delta Q \rangle_\omega$  for the stochastic processes displayed in (a), (b).

correlation functions, for non-Gaussian noise the knowledge of all higher correlation functions is necessary <sup>1</sup>.

It is instructive to calculate the probability for the fluctuator  $Q(t)$  to switch  $n$  times between the two possible states during the time-interval  $[0, t]$ . Let us divide the interval  $[0, t]$  into  $N$  pieces of equal length  $\delta t$  such that  $t = N\delta t$ . The probability for the fluctuator to flip  $n$  times in  $N$  trials is given by a binomial distribution

$$P_n(N) = \frac{N!}{n!(N-n)!} p^n (1-p)^{N-n}, \quad (6.2)$$

where  $p$  is the probability for the fluctuator to flip during the time-interval  $\delta t$ . The expected number of flips is  $\nu = Np$ , taking the limit  $N \rightarrow \infty$  while keeping  $\nu$  constant we obtain the expected Poisson distribution for the fluctuator to switch  $n$  times after the elapsed time  $t$

$$P_n(t) = \frac{(\gamma^{cl} t)^n}{n!} e^{-\gamma^{cl} t}, \quad (6.3)$$

where  $\gamma^{cl} = p/\delta t$  is the *switching rate* of the fluctuator. The average number of flip-flops is then  $\mu_n(t) = \gamma^{cl} t$  and the variance  $\sigma_n^2(t) = \gamma^{cl} t$ . Correlations between jumps fall off exponentially in time and the two-point correlation function is equal to

$$\langle \delta Q(t_1) \delta Q(t_2) \rangle = \frac{1}{4} e^{-2\gamma^{cl} |t_1 - t_2|}, \quad (6.4)$$

<sup>1</sup>This means for a Gaussian process  $X(t)$  with zero mean  $\langle X(t) \rangle_{\text{Gauss}} = 0$  and the two-point correlation function  $C(t_1, t_2) = \langle X(t_1) X(t_2) \rangle_{\text{Gauss}}$ :

$$\langle X(t_1) X(t_2) X(t_3) X(t_4) \rangle_{\text{Gauss}} = C(t_1, t_2) C(t_2, t_3) + C(t_1, t_4) C(t_2, t_3) + C(t_1, t_3) C(t_2, t_4). \quad (6.1)$$

where  $\delta Q(t) = Q(t) - \langle Q \rangle$  and  $\langle Q \rangle = 1/2$ . The time-scale on which these correlations decay is set by the inverse of the switching rate  $\tau_c = 1/\gamma^{cl}$ . The power-spectrum defined as the Fourier transform of the correlation function,  $\langle \delta Q \delta Q \rangle_\omega = \int dt e^{i\omega t} \langle \delta Q(t) \delta Q(0) \rangle$  of the charge fluctuations has a Lorentzian shape

$$\langle \delta Q \delta Q \rangle_\omega = \frac{\gamma^{cl}}{\omega^2 + (2\gamma^{cl})^2}. \quad (6.5)$$

Figure 6.1 displays possible realizations of the stochastic process  $\delta Q(t)$  for Gaussian (a) and non-Gaussian noise (b) which both have the same noise-spectrum  $\langle \delta Q \delta Q \rangle_\omega^2$ .

Let us start with a semi-classical analysis of the quantum model of a two-level system coupled to the charge fluctuations of a localized impurity level tunnel-coupled to a fermionic reservoir [see Eq. (5.1)]. In contrast to the full quantum mechanical model we now assume the charge on the impurity  $\hat{Q}$  to be a classical stochastic process of the ‘‘telegraph noise’’ type, which flips randomly between 0/1 at a rate  $\gamma^{cl}$ . Models of this type have been studied in [42, 43] discussing spectral diffusion in glasses and in [34, 35] considering dephasing of qubits.

The switching rate  $\gamma^{cl}$  can be derived from the full quantum mechanical model by second order perturbation theory in the tunneling amplitude  $T_{\mathbf{k}}$ . In the full quantum mechanical model the switching rate is connected to the classical rate by the relation  $\gamma^{cl} = \gamma(1 - f_T(\epsilon_0))$ . In order to compare the classical results with the full quantum mechanical model [see Chap 7], we perform all calculations in this chapter at the rate  $\gamma^{cl} = \gamma/2$  for  $\epsilon_0 = 0$ .

The two-level system coupled longitudinally to the random variable  $Q(t)$  experiences randomly fluctuating energy-levels  $\epsilon_\pm(t) = \pm(\Delta + vQ(t))/2$ . Averaging over these temporal fluctuations results in the decay of an initially prepared coherent superposition of quantum states. For simplicity we assume the heat-bath to act like a classical potential, thereby neglecting the back-action of the qubit on the environment. The Hamiltonian in the semi-classical approximation then reads

$$\hat{\mathcal{H}} = \frac{\Delta}{2} \hat{\sigma}_z + \frac{v}{2} Q(t) \hat{\sigma}_z, \quad (6.7)$$

where  $Q(t) = 0/1$ ,  $\Delta$  is the splitting between the qubit’s eigenenergies,  $v$  is the coupling of the qubit to the fluctuator and  $\hat{\sigma}_z$  is the Pauli matrix acting on the qubit’s eigenstates. For a given realization of the random potential  $Q(t)$  the solution of the time-dependent Schrödinger-equation is a superposition of the qubit’s eigenstates  $\{|\uparrow\rangle, |\downarrow\rangle\}$ ,

$$|\psi(t)\rangle = \frac{1}{\sqrt{2}} \left( e^{-i\Delta t/2} e^{i\varphi(t)/2} |\uparrow\rangle + e^{i\Delta t/2} e^{-i\varphi(t)/2} |\downarrow\rangle \right), \quad (6.8)$$

<sup>2</sup>The Gaussian stochastic process corresponds to an *Ornstein-Uhlenbeck* process  $\{X_t : t \geq 0\}$  which is the solution of the stochastic differential equation

$$dX_t = -\rho(X_t - \mu)dt + \sigma dW_t, \quad (6.6)$$

where  $\{W_t : t \geq 0\}$  is a Wiener-process of unit variance and  $\rho, \mu, \sigma$  are constants. The mean  $\langle X_t \rangle = \mu$  and variance  $\langle \delta X_t \delta X_s \rangle = (\sigma^2/(2\rho))e^{-\rho|s-t|}$ , where  $\delta X_t = X_t - \langle X_t \rangle$ . Figure 6.1(a) has been calculated using the Euler-Murayama method for the parameters  $\mu = 0$ ,  $\rho = 2\gamma^{cl}$  and  $\sigma = \sqrt{\gamma^{cl}}$ .

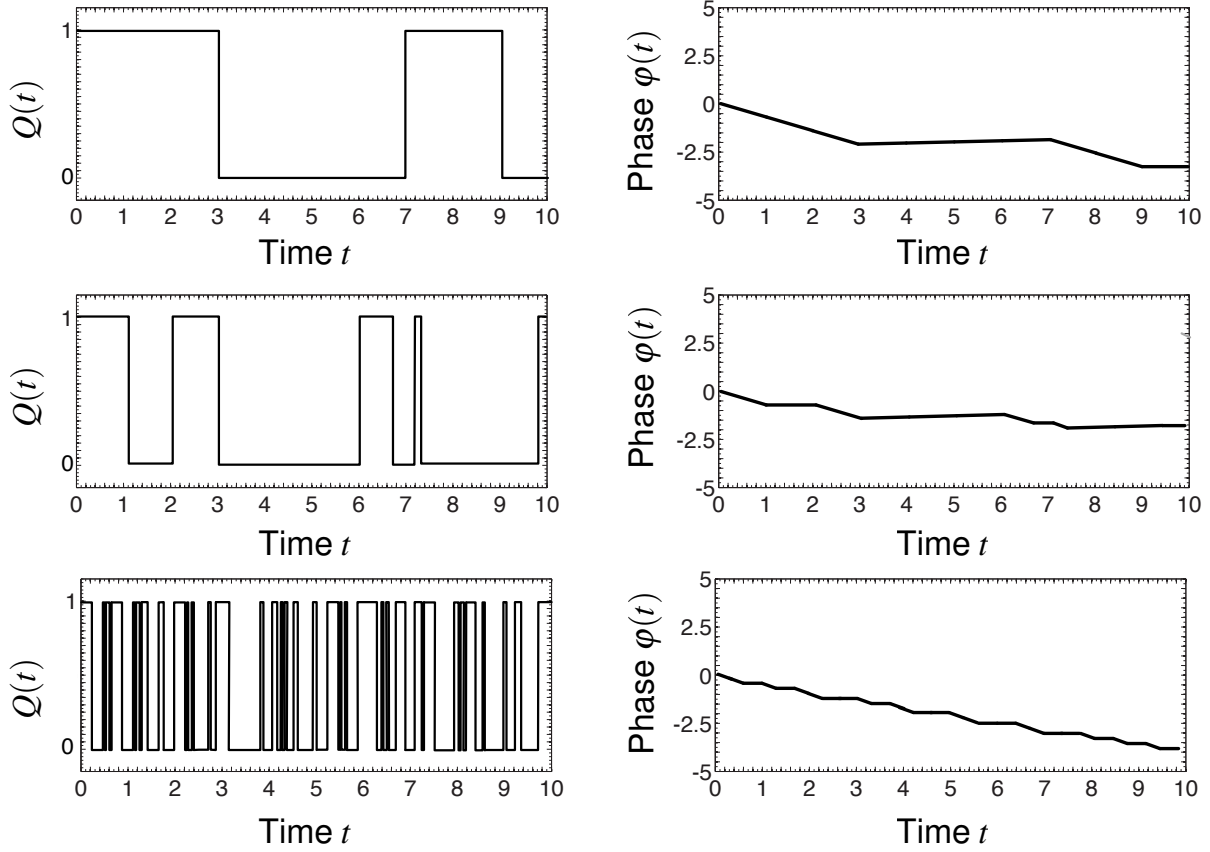


**Figure 6.2:** Time evolution of possible realizations of random trajectories of the fluctuating charge  $Q(t)$  on the impurity level and the random phase  $\varphi(t) = -v \int_0^t dt' Q(t')$  picked up during the time-interval  $[0, t]$  (right panel). The switching rate  $\gamma$  increases from top to bottom. For large switching rate  $\gamma$  the phase  $\varphi$  is a sum of many random contributions and performs almost a random walk with a drift. The phase  $\varphi(t)$  is always negative and is drifting with a velocity  $-v/2$ .

which acquire an additional phase-factor  $e^{\mp i\varphi(t)/2}$  to their oscillatory time evolution with the random phase

$$\varphi(t) = -v \int_0^t dt' Q(t'). \quad (6.9)$$

Equation (6.8) is the solution of the Schrödinger-equation for a given specific realization of the random potential  $Q(t)$ . However, in an experiment one is not interested in a single measurement for a specific realization of the random phase  $\varphi(t)$  but in an average over many repeated runs on the same qubit. Suppose that we wish to measure an observable  $\hat{\mathcal{A}}$ . Then the expectation value averaged over many realizations of the random phase is equal to

$$\langle\langle \hat{\mathcal{A}} \rangle\rangle_{\varphi} = \text{tr} \int d\varphi p(\varphi, t) \hat{\rho}(\varphi, t) \hat{\mathcal{A}}, \quad (6.10)$$

where the double angle brackets  $\langle\langle \dots \rangle\rangle_\varphi$  on the left hand side of Eq. (6.10) denote a quantum mechanical average and an average over realizations of the random phase  $\varphi$ ,  $p(\varphi, t)$  is the distribution function of the phase  $\varphi$  and  $\hat{\rho}(\varphi, t)$  is the density matrix of the qubit. Since the operator  $\hat{\mathcal{A}}$  is independent of the phase one can perform the statistical average independently of the quantum mechanical and as a consequence the expectation value of an observable  $\hat{\mathcal{A}}$  can be written as the trace of the reduced density-matrix multiplied with the observable  $\hat{\mathcal{A}}$

$$\langle\langle \hat{\mathcal{A}} \rangle\rangle_\varphi(t) = \text{tr} \left[ \hat{\rho}^{\text{red}}(t) \hat{\mathcal{A}} \right], \quad (6.11)$$

where  $\hat{\rho}^{\text{red}}(t)$  is called the *reduced* density matrix of the qubit and it is equal to

$$\hat{\rho}^{\text{red}}(t) = \begin{pmatrix} \rho_{\uparrow\uparrow}(0) & \rho_{\uparrow\downarrow}(0)e^{-i\Delta t}D(t) \\ \rho_{\downarrow\uparrow}(0)e^{i\Delta t}D^*(t) & \rho_{\downarrow\downarrow}(0) \end{pmatrix}. \quad (6.12)$$

The diagonal elements of the reduced density-matrix  $\hat{\rho}_{ii}^{\text{red}}(0)$  remain constant during the time evolution of the qubit, thus there is no change of the population of the qubit's levels. This is due to the specific form of the coupling to the heat-bath:  $vQ\hat{\sigma}_z/2$  (pure dephasing). However, the off-diagonal elements of the reduced density matrix pick-up an additional *coherence-factor* in their oscillatory time evolution. The coherence is defined as the average of the phase-factor  $e^{i\varphi(t)}$

$$D(t) = \left\langle \exp \left[ -iv \int_0^t dt' Q(t') \right] \right\rangle, \quad (6.13)$$

where  $\langle \dots \rangle_\varphi$  is an average over many random realizations of the fluctuating phase:

$$\langle \dots \rangle_\varphi = \int d\varphi (\dots) p(\varphi, t), \quad (6.14)$$

where  $p(\varphi, t)$  is the non-Gaussian probability distribution of the phase  $\varphi$  for classical telegraph noise. The magnitude of the time-dependent coherence determines the decay of the off-diagonal matrix elements of the density matrix which we will term *visibility*

$$v(t) = |D(t)|. \quad (6.15)$$

The interference contrast of any observable sensitive to the relative phase between the qubit's levels is reduced by a factor  $v(t)$ , e.g.  $\langle \hat{\sigma}_x(t) \rangle = \text{Re} \rho_{\uparrow\downarrow}(t)$  [see Fig. 6.4]. The possible values for the visibility are ranging from 0 to 1 corresponding to total loss of coherence and totally constructive interference, respectively.

### 6.3 Gaussian approximation

As we will see in Sec. 6.4 the probability distribution has a pronounced non-Gaussian shape. Nevertheless, it is insightful to calculate the coherence as if the probability distribution would be Gaussian-distributed, according to

$$p(\varphi, t) = \frac{1}{\sqrt{2\pi \langle \delta\varphi^2 \rangle}} \exp \left( -\frac{\delta\varphi^2}{2 \langle \delta\varphi^2 \rangle} \right), \quad (6.16)$$

with mean  $\langle \varphi \rangle$  and variance  $\langle \delta\varphi^2(t) \rangle$  of the phase,  $\delta\varphi(t) = \varphi(t) - \langle \varphi \rangle$ . Then the Gaussian approximation for the coherence is equal to

$$D_{\text{Gauss}}(t) = \exp\left(i\langle \varphi \rangle - \frac{1}{2}\langle \delta\varphi^2(t) \rangle\right). \quad (6.17)$$

The mean of the phase is  $\langle \varphi(t) \rangle = -vt/2$  and the variance are equal to

$$\langle \delta\varphi^2(t) \rangle = v^2 \int_0^t dt_1 \int_0^t dt_2 \langle \delta Q(t_1) \delta Q(t_2) \rangle. \quad (6.18)$$

Inserting Eq. (6.4) for the correlation function we obtain for the variance of the phase

$$\langle \delta\varphi^2(t) \rangle = \frac{v^2}{2\gamma} \left[ t - \frac{1}{\gamma} (1 - e^{-\gamma|t|}) \right]. \quad (6.19)$$

Finally, the coherence for classical telegraph noise is equal to

$$D_{\text{Gauss}}(t) = \exp\left\{-\frac{ivt}{2} - \frac{v^2}{4\gamma} \left[ t - \frac{1}{\gamma} (1 - e^{-\gamma|t|}) \right]\right\}. \quad (6.20)$$

This is the *Gaussian approximation* for the coherence of a two-level system coupled to the charge fluctuations on a localized impurity in the semi-classical model. The time evolution of the visibility  $v_{\text{Gauss}}(t) = |D_{\text{Gauss}}(t)|$  is shown in Fig. 6.4(b) (dashed line). The decay of the coherence is monotonous and  $v_{\text{Gauss}}(t)$  doesn't have any zeros on the real axis. In the weak-coupling limit  $v/\gamma \ll 1$ , the Gaussian result is a good approximation for the exact result (solid line) whereas for strong coupling  $v/\gamma > 1$  the Gaussian approximation fails even qualitatively. At long times  $\gamma t \gg 1$  the visibility decays exponentially with time  $D_{\text{Gauss}}(t) \propto e^{-\Gamma_\varphi t}$  at a *decoherence rate*  $\Gamma_\varphi = v^2/4\gamma$  (for the Gaussian case).

## 6.4 Probability distribution

In this section we derive the probability distribution  $p(\varphi, t)$  of the phase  $\varphi$  for classical telegraph noise which may be used to calculate the coherence  $D(t)$  (beyond the Gaussian approximation) appearing in the reduced density matrix of the qubit, Eq. (6.12). It turns out that the probability distribution cannot be described by a simple Gaussian distribution function. Nevertheless, at times typically much larger than the correlation time  $t \gg \gamma^{-1}$ , the probability distribution approaches asymptotically a Gaussian distribution.

The probability distribution  $p(\varphi, t)$  is described by a set of two coupled Markoff master-equations. Let us denote the probability of finding the random variable at  $Q(t) = +1$  at a certain phase and time by  $p^+(\varphi, t)$  and the probability of finding the random variable at  $Q(t) = 0$  by  $p^-(\varphi, t)$ , respectively. Next we introduce a rate  $\gamma^+$  for an “up-jump”  $Q: 0 \rightarrow +1$  and a rate  $\gamma^-$ ,

$Q : +1 \rightarrow 0$  for a “down-jump”<sup>3</sup>. The phase is always negative and the minimal value which can be acquired during the time-interval  $[0, t]$  is equal to  $\varphi = -vt$  which corresponds to  $Q(t) = 1$  during the whole time-interval. On the other hand the maximal phase which can be acquired is  $\varphi = 0$  corresponding to  $Q(t) = 0$ . Since the mean of the phase  $\langle \varphi \rangle$  is not vanishing the probability distribution will be drifting with a velocity  $-v/2$ . This can be accounted for by shifting the probability distribution  $p(\varphi, t)$  in  $\varphi$  by  $vt/2$ , i.e.  $\varphi(t) \rightarrow \varphi(t) + vt/2$  and  $p(\varphi, t) \rightarrow p(\varphi + vt/2, t)$ , which will be assumed in the following for simplicity. Then we can write down a set of master-equations for  $p^+(\varphi, t)$  and  $p^-(\varphi, t)$ :

$$\frac{d}{dt}p^+(\varphi, t) = \frac{v}{2}\frac{\partial}{\partial\varphi}p^+(\varphi, t) + \gamma^+p^-(\varphi, t) - \gamma^-p^+(\varphi, t), \quad (6.22)$$

$$\frac{d}{dt}p^-(\varphi, t) = -\frac{v}{2}\frac{\partial}{\partial\varphi}p^-(\varphi, t) + \gamma^-p^+(\varphi, t) - \gamma^+p^-(\varphi, t).$$

The deterministic evolution of the probability-distribution is described by the drift-term on the right-hand side of Eq. (6.22). If there is no switching it takes into account the phase evolution according to  $\dot{\varphi}(t) = -vQ$ . The second term is responsible for random jumps between the two states (0/1) at a rate  $\gamma^\pm$ . For simplicity we assume that both rates  $\gamma^+$  and  $\gamma^-$  are equal to each other,  $\gamma^\pm = \gamma/2$ . Moreover, at the initial time  $t = 0$  both probabilities are equal,  $p^+(\varphi, 0) = p^-(\varphi, 0) = \delta(\varphi)/2$ , where  $\delta(\varphi)$  is the Dirac  $\delta$ -function. Without any switching of the fluctuator ( $\gamma = 0$ ) the probability distribution is just a superposition of two  $\delta$ -functions:  $p(\varphi, t) = (1/2)(\delta(\varphi - vt/2) + \delta(\varphi + vt/2))$ .

We define the sum and the difference of the probabilities,  $p(\varphi, t) = p^+(\varphi, t) + p^-(\varphi, t)$  and  $\delta(\varphi, t) = p^+(\varphi, t) - p^-(\varphi, t)$ . Then Eq. (6.22) is equal to

$$\frac{d}{dt}p(\varphi, t) = \frac{v}{2}\partial_\varphi\delta(\varphi, t) \quad (6.23)$$

$$(6.24)$$

$$\frac{d}{dt}\delta(\varphi, t) = \frac{v}{2}\partial_\varphi p(\varphi, t) - \gamma\delta(\varphi, t).$$

Differentiating the upper one of Eq. (6.23), and inserting the lower one results in<sup>4</sup>

$$\frac{\partial^2}{\partial t^2}p(\varphi, t) - \left(\frac{v}{2}\right)^2 \frac{\partial^2}{\partial \varphi^2}p(\varphi, t) = -\gamma \frac{\partial}{\partial t}p(\varphi, t). \quad (6.26)$$

<sup>3</sup>In order to make contact with the quantum mechanical model (see Chap. 5): The ratio of the rates is  $\gamma^+/\gamma^- = \exp(\varepsilon/T)$ , where  $\varepsilon$  is the energy of the impurity counted from the Fermi-level  $\mu$  and  $T$  is the temperature of the bath of fluctuators. It follows that

$$\frac{\Delta\gamma}{\gamma} = 1 - 2f_T(\varepsilon), \quad (6.21)$$

where  $f_T(\varepsilon)$  is the Fermi-Dirac distribution.

<sup>4</sup>This is a special case of the telegraph equation:

$$\frac{\partial^2}{\partial t^2}w(x, t) - a^2 \frac{\partial^2}{\partial x^2}w(x, t) = -b \frac{\partial}{\partial t}w(x, t) + cw(x, t), \quad (6.25)$$

with  $b > 0$  and  $c \leq 0$ . For  $a = v/2$ ,  $b = \gamma$  and  $c = 0$  we recover Eq. (6.23).

The substitution  $p(\varphi, t) = e^{-\gamma/2} u(\varphi, t)$  leads to the well-known *Klein-Gordon* equation with an imaginary mass

$$\frac{\partial^2}{\partial t^2} u(\varphi, t) - \left(\frac{v}{2}\right)^2 \frac{\partial^2}{\partial \varphi^2} u(\varphi, t) = \left(\frac{\gamma}{2}\right)^2 u(\varphi, t), \quad (6.27)$$

with the initial conditions  $u(\varphi, 0) = \delta(\varphi)$  and  $\frac{d}{dt}u(\varphi, 0) = (\gamma/2)\delta(\varphi)$ . We make the following ansatz  $u(\varphi, t) = e^{i(\kappa\varphi - \omega t)}$  from which the dispersion relation follows:

$$\omega_{\pm}(\kappa) = \pm \frac{1}{2} \sqrt{v^2 \kappa^2 - \gamma^2}, \quad (6.28)$$

thus a general solution of  $u(\varphi, t)$  can be written as

$$u(\varphi, t) = \int \frac{d\kappa}{2\pi} [a_{\kappa} e^{-i\omega_+ t} + b_{\kappa} e^{-i\omega_- t}] e^{i\kappa\varphi}. \quad (6.29)$$

The coefficients  $\{a_{\kappa}, b_{\kappa}\}$  then follow from the initial conditions:

$$\begin{aligned} u(\varphi, 0) = \delta(\varphi) : \int \frac{d\kappa}{2\pi} [a_{\kappa} + b_{\kappa}] e^{i\kappa\varphi} &= 1 \\ \Rightarrow a_{\kappa} + b_{\kappa} &= 1, \end{aligned} \quad (6.30)$$

and

$$\begin{aligned} \frac{d}{dt}u(\varphi, 0) = \frac{\gamma}{2}\delta(\varphi) : -i \int \frac{d\kappa}{2\pi} [\omega_+ a_{\kappa} + \omega_- b_{\kappa}] e^{i\kappa\varphi} &= \frac{\gamma}{2}\delta(\varphi) \\ \Rightarrow \omega_+ a_{\kappa} + \omega_- b_{\kappa} &= \frac{i\gamma}{2}. \end{aligned} \quad (6.31)$$

From which  $a_{\kappa} = (1/2)(1 + i\gamma/2\omega_+(\kappa))$  and  $b_{\kappa} = (1/2)(1 + i\gamma/2\omega_-(\kappa))$  follow. Inserting the coefficients  $\{a_{\kappa}, b_{\kappa}\}$  into Eq. (6.29) and reshiftig the phase  $\varphi$ , we finally obtain for the distribution function [35],

$$\begin{aligned} p(\varphi, t) = & \\ e^{-\gamma/2} \left[ \frac{\delta(\varphi) + \delta(\varphi + vt)}{2} + \frac{\gamma}{v} \cdot \frac{I_1 \left( \frac{\gamma}{2} \sqrt{1 - (2/vt)^2 (\varphi + vt/2)^2} \right)}{\sqrt{1 - (2/vt)^2 (\varphi + vt/2)^2}} \right] & (\theta(\varphi + vt) - \theta(\varphi)), \end{aligned} \quad (6.32)$$

where  $I_1(z)$  is the modified Bessel-function of the first kind and  $\theta(\varphi)$  is the Heaviside-function. Figure 6.3 shows the probability distribution  $p(\varphi, t)$  as a function of the phase  $\varphi$  for different times  $\gamma t$ . For short times the probability distribution consists of a large central part which is cut by  $\delta$ -functions at  $vt/2$ . At times larger than the typical correlation time of the fluctuator  $\gamma t \gg 1$

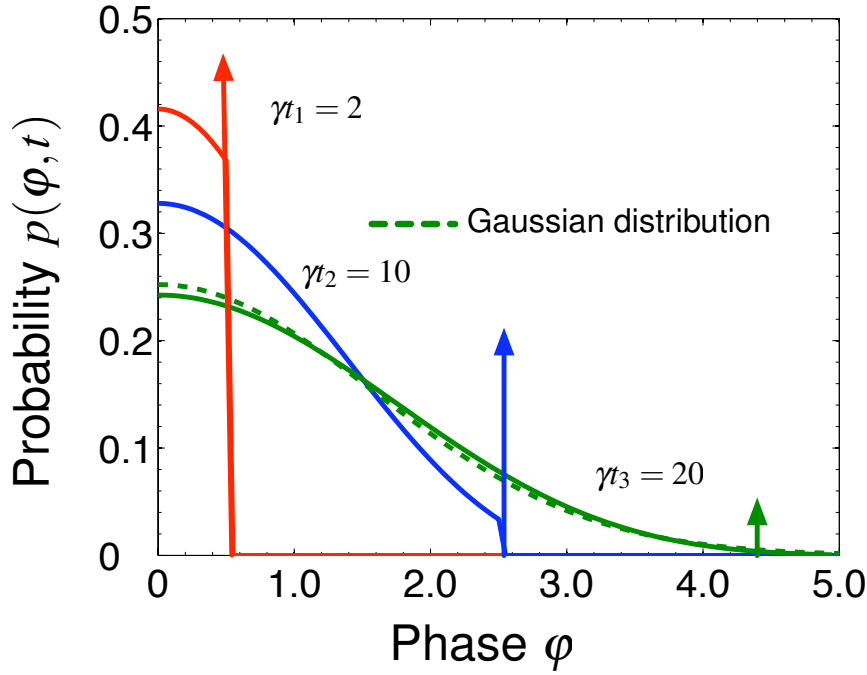


**Figure 6.3:** Probability distribution function  $p(\varphi, t)$  as a function of the phase  $\varphi$  plotted in a coordinate-system moving with a velocity  $-v/2$  for weak-coupling  $v/\gamma = 0.5$ . The dashed line shows the asymptotic Gaussian distribution and the arrows indicate the  $\delta$ -function which cuts the probability distribution at  $\varphi = vt/2$ .

the central part of the distribution-function approaches a Gaussian-distribution. Indeed, this can be seen from the asymptotic behaviour of the modified Bessel-function<sup>5</sup>

$$e^{-\gamma t/2} \frac{\gamma}{v} \cdot \frac{I_1 \left( \gamma t/2 \sqrt{1 - (2/vt)^2 (\varphi + vt/2)^2} \right)}{\sqrt{1 - (2/vt)^2 (\varphi + vt/2)^2}} \sim \sqrt{\frac{\gamma}{\pi v^2 t}} \exp \left( -\frac{\gamma (\varphi + vt/2)^2}{v^2 t} \right). \quad (6.34)$$

Thus in the long-time limit  $\gamma t \gg 1$  we obtain exactly the distribution of the phase that we have expected from a Gaussian distribution with  $\langle \varphi^2(t) \rangle = v^2 t / (2\gamma)$  which coincide with Eq. (6.19) at long times. Note that the drift-term in the probability-distribution is absolutely necessary for the coherence to have the correct phase-factor. This can already be seen in the Gaussian approximation of the coherence Eq. (6.20) and in Eq. (6.35) [see below].

The coherence  $D(t) = \int d\varphi p(\varphi, t) e^{i\varphi}$  can be easily obtained from the probability distribution

<sup>5</sup>For  $|z|$  large the asymptotic form of the modified Bessel function is

$$I_1(z) \sim \frac{e^z}{\sqrt{2\pi z}}. \quad (6.33)$$

in Fourier-space (Eq. 6.29). It is just the  $\kappa = -1$  component of  $p(\kappa, t)$

$$D(t) = \int \frac{d\kappa}{2\pi} [a_\kappa e^{-i\omega_+ t} + b_\kappa e^{i\omega_+ t}] e^{i\kappa vt/2} \delta(\kappa + 1). \quad (6.35)$$

Then the coherence is equal to

$$D(t) = \frac{1}{2} e^{-i(v-i\gamma)t/2} \left[ \left(1 + \frac{\gamma}{2\delta}\right) e^{\delta t} + \left(1 - \frac{\gamma}{2\delta}\right) e^{-\delta t} \right], \quad (6.36)$$

where  $\delta = \frac{1}{2} \sqrt{\gamma^2 - v^2}$ . We will present another way based on an equation of motion approach to derive the coherence in Sec. 6.5.

## 6.5 Time evolution of the visibility for classical telegraph noise

In the present section we derive the coherence  $D(t)$  from an equation of motion approach. The advantage of this approach in comparison to the derivation of the probability distribution first and then compute all averages by means of the probability distribution as we have done in Sec. 6.4 is that in the current derivation of the visibility it is not necessary to know the probability distribution explicitly. We will deduce a system of coupled differential equations for the coherence of a stochastic process with  $\xi(t) = \pm 1$ , thus we will derive  $D(t) = \langle e^{i\varphi_\xi(t)} \rangle$ , with the phase  $\varphi_\xi(t) = -v \int_0^t dt' \xi(t')$ . The bonus of this auxiliary quantity is that all of the calculations below considerably simplify due to  $\xi^2(t') = 1, \forall t' \in [0, t]$ . At the end of the derivation one can get the coherence  $D(t)$  corresponding to the stochastic process  $Q(t') = 0/1, t' \in [0, t]$  simply by the replacement<sup>6</sup>

$$D(t; v) = e^{-ivt/2} \langle e^{i\varphi_\xi(t)} \rangle|_{v/2}, \quad (6.37)$$

where the left-hand side corresponds to the coherence  $D(t)$  of the stochastic process  $Q = 0/1$ . We start with the time-derivative of  $\langle e^{i\varphi_\xi(t)} \rangle$

$$\begin{aligned} \frac{d}{dt} \langle e^{i\varphi_\xi(t)} \rangle &= i \langle \dot{\varphi}_\xi(t) e^{i\varphi_\xi(t)} \rangle \\ &= -iv \langle \xi(t) e^{i\varphi_\xi(t)} \rangle, \end{aligned} \quad (6.38)$$

where we have used that  $\dot{\varphi}_\xi(t) = -v\xi(t)$ . A similar derivation for the right-hand side of Eq. (6.38) shows that

$$\frac{d}{dt} \langle \xi(t) e^{i\varphi_\xi(t)} \rangle = -iv \langle \xi(t) \xi(t) e^{i\varphi_\xi(t)} \rangle + \langle \dot{\xi}(t) e^{i\varphi_\xi(t)} \rangle, \quad (6.39)$$

One can “considerably” simplify Eq. (6.39) by taking into account that  $\xi^2(t') = 1$ . The time-derivative of  $\xi(t)$  can be rendered using a stochastic process  $\eta_\pm(t)$  such that

$$\dot{\xi}(t) = \underbrace{\frac{1 + \xi(t)}{2}}_{=1 \text{ for } \xi=1} (2 \cdot \eta_-(t)) + \underbrace{\frac{1 - \xi(t)}{2}}_{=1 \text{ for } \xi=-1} (2 \cdot \eta_+(t)), \quad (6.40)$$

<sup>6</sup>The stochastic process  $Q(t'), t' \in [0, t]$  can be rendered by the auxiliary stochastic process  $\xi(t') = \pm 1, t' \in [0, t]$  with the same switching rate. The coherence phase  $\varphi(t)$  is then related to the auxiliary phase  $\varphi_\xi(t)$  by a shift of  $-vt/2$ , i.e.  $\varphi(t) = \varphi_\xi(t) - vt/2$ .

where  $\eta_{\pm}(t) = \pm \sum_j \delta(t - t_j)$  is a sum of Poisson-distributed  $\delta$  peaks. A factor of 2 is explicitly written in order to indicate the size of the jumps. Inserting Eq. (6.40) into  $\langle \dot{\xi}(t) e^{i\varphi_{\xi}(t)} \rangle$ , we obtain

$$\langle \dot{\xi}(t) e^{i\varphi_{\xi}(t)} \rangle = \Delta\gamma \langle e^{i\varphi_{\xi}} \rangle - \gamma \langle \xi(t) e^{i\varphi_{\xi}} \rangle, \quad (6.41)$$

where we have used that  $\langle \eta_{\pm}(t) \rangle = \gamma^{\pm}$ . Finally, we obtain a system of coupled equations determining  $\langle e^{i\varphi_{\xi}(t)} \rangle$ ,

$$\begin{aligned} \frac{d}{dt} \langle e^{i\varphi_{\xi}(t)} \rangle &= -i\nu \langle \xi(t) e^{i\varphi_{\xi}(t)} \rangle \\ \frac{d}{dt} \langle \xi(t) e^{i\varphi_{\xi}(t)} \rangle &= -\gamma \langle \xi(t) e^{i\varphi_{\xi}(t)} \rangle + (\Delta\gamma - i\nu) \langle e^{i\varphi_{\xi}(t)} \rangle. \end{aligned} \quad (6.42)$$

If we assume that the probabilities for an ‘‘up-jump’’ and a ‘‘down-jump’’ are equal ( $\Delta\gamma = 0$ )<sup>7</sup> it is easy to verify that these equations describe a damped harmonic oscillator with frequency  $\omega = \nu$  and friction coefficient  $\gamma$ . We just present the solution for the coherence  $D(t)$  and leave details of the derivation to App. B. The result for the coherence  $D(t)$  is equal to,

$$D(t) = \frac{1}{2} e^{-i(\nu t/2 - i\gamma t/2)} \left[ \left(1 + \frac{\gamma}{2\delta}\right) e^{\delta t} + \left(1 - \frac{\gamma}{2\delta}\right) e^{-\delta t} \right], \quad (6.43)$$

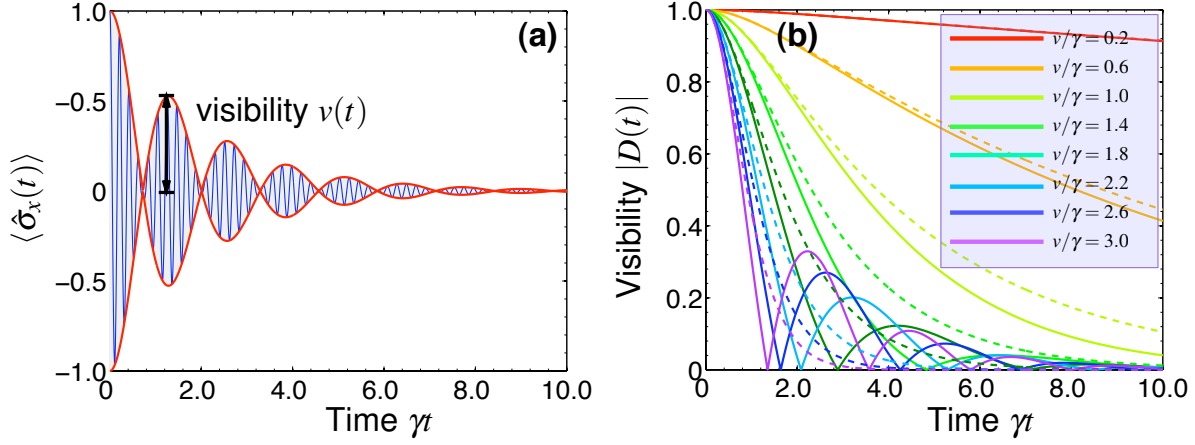
where  $\delta = \frac{1}{2} \sqrt{\gamma^2 - \nu^2}$ . Figure 6.4(b) shows the time evolution of the visibility  $|D(t)|$  for various coupling strengths  $\nu$  of a two-level system subject to pure dephasing by telegraph noise. When  $\delta$  becomes imaginary ( $\nu > \gamma$ ), damped oscillations in the time evolution of the coherence appear with a magnitude not greater than one, i.e.  $|\langle e^{i\varphi(t)} \rangle| \leq 1$ , and the coherence gets always negative  $D < 0$  when oscillations are present. Such a behaviour is qualitatively different from the behaviour predicted by the Gaussian approximation for telegraph noise [see Eq. (6.20)] where the coherence is a monotonous function with always positive values. Indeed, telegraph noise cannot be mimicked by any Gaussian process e.g. a random walk.

Figure 6.5 shows the time evolution of the visibility and the corresponding time evolution of the phase  $\alpha(t)$  [i.e, the complex argument of  $D(t)$ ] for different detunings  $\Delta\gamma/\gamma$ . In the weak-coupling limit  $\nu/\gamma = 0.5$  at  $\Delta\gamma = 0$  (equal probabilities of the up / down switching rates  $\gamma^{\pm}$ ), Fig. 6.5(a) shows an exponential decay of the visibility and a linear time evolution of the phase with slope  $-\nu/2$ , as expected from Eq. (6.43). In the strong-coupling limit [Fig. 6.5 right panel] the visibility shows sharp zero crossings for  $\Delta\gamma = 0$  and phase jumps of size  $\pi$  whenever the visibility vanishes. If the detuning  $\Delta\gamma$  grows the sharp zero crossings are vanishing and turn into local minima whereas the the sharp jumps of corresponding phase are smeared out.

Assuming  $\nu > \gamma$ , such that  $\delta$  is imaginary, the position of the  $k$ -th zero-crossing is given by

$$t_k^* = \frac{1}{\delta} \left[ k\pi - \operatorname{atanh} \left( \frac{2\delta}{\gamma} \right) \right]. \quad (6.44)$$

<sup>7</sup>This corresponds to  $\varepsilon = 0$  in the full quantum mechanical model.



**Figure 6.4:** (a) Time evolution of the observable  $\langle \hat{\sigma}_x(t) \rangle$  (blue) and the envelope (red) of the oscillations,  $v = |D(t)|$  for  $v/\gamma = 5.0$ . (b) Time evolution of the visibility  $|D(t)|$  of a qubit subject to classical telegraph noise for increasing couplings  $v/\gamma$  (solid line from top to bottom). The dashed line shows the Gaussian approximation  $|D_{\text{Gauss}}(t)|$ .

The zero-crossings appear regularly with a period of  $\pi/\delta$ . Zero-crossings of the visibility first appear at  $vt^* = \infty$  beyond the threshold  $v = \gamma$  and saturate at a finite value  $vt^* = \pi$ . Below this threshold no zeros show up in the time evolution of the visibility.

The Gaussian process Eq. (6.20) is expected to become a good approximation to the telegraph process when the switching rate is large,  $v/\gamma \rightarrow 0$ . Then one can imagine that the phase is a sum of small independent random contributions (from the time-interval of order  $\gamma^{-1}$ ). As a consequence of the central-limit theorem the phase should become a Gaussian random variable performing an almost continuous random walk. Expanding Eq. (6.43) to the leading order in  $v/\gamma$  while keeping  $v^2 t/\gamma = \text{const}$  results in

$$\langle e^{i\varphi(t)} \rangle \approx e^{-ivt/2} \left( 1 + \frac{v^2}{4\gamma^2} \right) \exp\left( -\frac{v^2 t}{4\gamma} \right), \quad (6.45)$$

an expansion of Eq. (6.20) in the same limit gives the same result. For very small switching rate  $\gamma \rightarrow \infty$  the fluctuator is almost at rest and the two possible values of the phase  $\varphi = -vt$  or  $\varphi = 0$  occur with equal probabilities  $1/2$  in the coherence. Then the coherence is just  $\langle e^{i\varphi(t)} \rangle = \frac{1}{2}(e^{-ivt} + 1) = e^{-ivt/2} \cos(vt/2)$ .

For the calculation of the two-point correlation function  $\langle \delta Q(t) \delta Q(0) \rangle$  it is easier to make use of the symmetric fluctuator with  $\xi = \pm 1$  and make the replacement to  $Q(t) = (\xi(t) + 1)/2$  at the end of the derivation. The two-point correlation function Eq. (6.4) then reads in terms of  $\xi(t)$  as

$$\begin{aligned} \langle \delta Q(t) \delta Q(0) \rangle &= \langle Q(t) Q(0) \rangle - \langle Q(t) \rangle \langle Q(0) \rangle \\ &= \frac{1}{4} [\langle \xi(t) \xi(0) \rangle - \langle \xi(t) \rangle \langle \xi(0) \rangle]. \end{aligned} \quad (6.46)$$

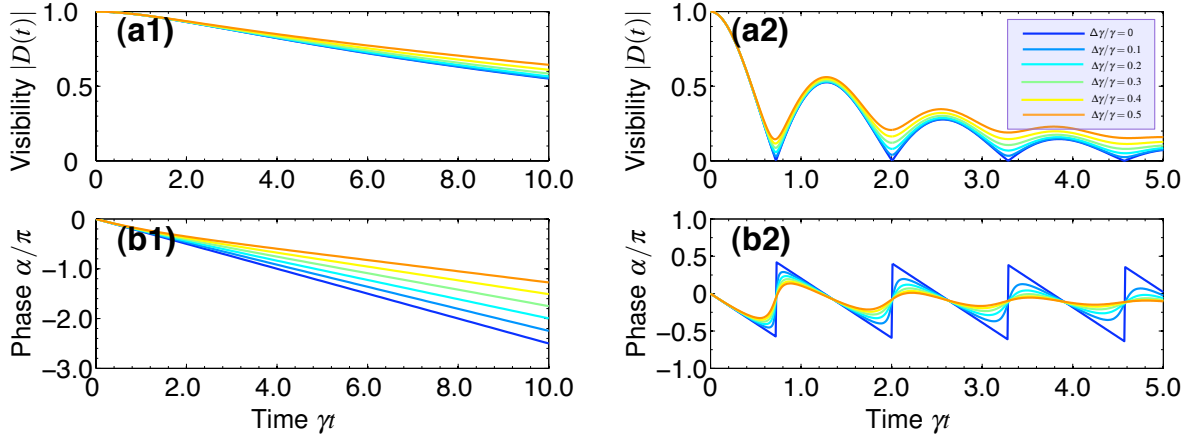


**Figure 6.5:** Effect of the detuning  $\Delta\gamma$  on the time evolution of the visibility (a)  $|D(t)|$  and the corresponding phase  $\alpha(t)$  (i.e. the complex argument of  $D(t)$ ) for different  $\Delta\gamma/\gamma$ . left panel (1)  $v/\gamma = 0.5$ , right panel (2)  $v/\gamma = 5.0$ .

The two-point correlation function is the sum of the conditional probabilities  $P_{\alpha|\beta}(t)$  weighted by the initial probability, thus

$$\langle \xi(t)\xi(0) \rangle = \frac{1}{2} (P_{++}(t) - P_{+-}(t) - P_{-+}(t) + P_{--}(t)), \quad (6.47)$$

where  $P_{\alpha|\beta}(t)$ ,  $\alpha, \beta \in \{\pm\}$ , is the conditional probability to find the fluctuator in state  $\alpha$  when it had previously been in the state  $\beta$  at  $t = 0$ . For example  $P_{-|+}(t)$  is the conditional probability to find the fluctuator in a “down”-state ( $-1$ ) when it had previously been in an “up”-state ( $+1$ ) at  $t = 0$ . The factor of  $1/2$  in Eq. (6.47) describes the initial probability to find the fluctuator either in an “up”-state or “down”-state. The probabilities can be found by solving the Markoff rate equation,

$$\begin{aligned} \frac{d}{dt}p_+(t) &= \frac{\gamma}{2}(p_-(t) - p_+(t)) \\ \frac{d}{dt}p_-(t) &= -\frac{\gamma}{2}(p_-(t) - p_+(t)), \end{aligned} \quad (6.48)$$

with initial conditions  $p_+(0) = 0$  and  $p_-(0) = 1$  for obtaining  $P_{+|-}(t)$ . The solution is equal to  $P_{+|-}(t) = \frac{1}{2}(1 - e^{-\gamma t})$ . The other probabilities can be obtained in a similar way, finally summing up to  $\langle \xi(t)\xi(0) \rangle = e^{-\gamma|t|}$ . Using the relation Eq. (6.46) we obtain the two-point correlation function for the fluctuator  $Q = 0/1$  to be equal to Eq. (6.4). The time evolution of  $\langle \xi(t) \rangle = (p_+(t) - p_-(t))$  is

$$\langle \xi(t) \rangle = \pm e^{-\gamma|t|}, \quad (6.49)$$

where the sign depends on the initial conditions of the fluctuator  $\xi$  at  $t = 0$ . After averaging over the initial state of the fluctuator we obtain  $\langle \xi(t) \rangle = 0$ . Finally, one gets the result for the two-

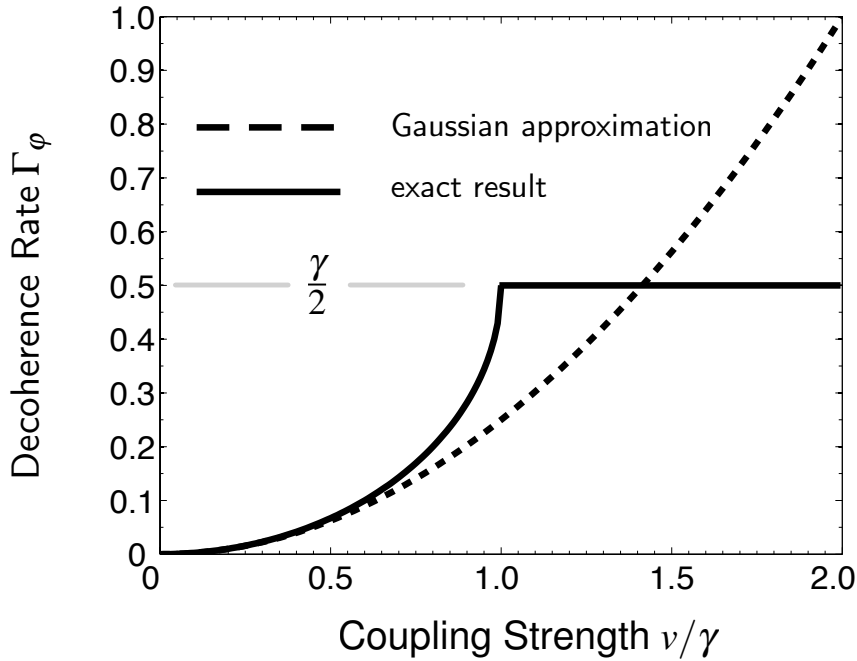


**Figure 6.6:** Decoherence rate of a qubit subject to classical telegraph noise as a function of the coupling strength  $v/\gamma$ . The solid line shows the exact result and the dashed line shows result of the Gaussian approximation. The exact result has a kink at  $v/\gamma = 1$  and saturates at  $\gamma/2$  for  $v > \gamma$ .

point correlation function Eq. 6.4. The result for  $t < 0$  follows from  $\langle \xi(-t)\xi(0) \rangle = \langle \xi(t)\xi(0) \rangle$  that holds for any classical stationary stochastic process.

## 6.6 Decoherence rate for classical telegraph noise

The rate  $\Gamma_\phi$  at which the coherence decays can be inferred from the long-time behaviour of  $D(t)$ . The decoherence rate  $\Gamma_\phi$  is defined by

$$\Gamma_\phi = -\lim_{t \rightarrow \infty} \frac{1}{t} \ln |D(t)|. \quad (6.50)$$

In the Gaussian approximation, the coherence Eq. (6.20) decays exponentially in time at the decoherence rate  $\Gamma_\phi^{\text{Gauss}}(v) = v^2/4\gamma$ . In contrast to the Gaussian approximation, the exact decoherence rate for classical telegraph noise shows a pronounced non-Gaussian behaviour,

$$\Gamma_\phi(v) = \begin{cases} \frac{1}{2} \left( \gamma - \sqrt{\gamma^2 - v^2} \right), & v \leq \gamma \\ \frac{\gamma}{2}, & v > \gamma. \end{cases} \quad (6.51)$$

For small coupling strengths  $v/\gamma \ll 1$  the Gaussian approximation coincides with the exact result which is again a manifestation of the central limit theorem. Indeed, this can be understood from

the point of view of the probability distribution. At large times  $\gamma t \gg 1$  the central part of the distribution approaches a Gaussian which results in a decoherence rate  $\Gamma_\varphi^{\text{Gauss}}$ . However, the distribution is cut by  $\delta$ -functions at the end which only decay at a rate  $\gamma/2$ . The coherence decay will be controlled by  $\Gamma_\varphi^{\text{Gauss}}$  as long as  $\Gamma_\varphi^{\text{Gauss}} < \gamma$  and the Gaussian approximation is valid. However, if  $\Gamma_\varphi^{\text{Gauss}}$  becomes larger than  $\gamma/2$  then the effect arising from the  $\delta$ -functions is dominant and the decoherence rate will be set by  $\gamma/2$ , i.e. the decay rate of the  $\delta$ -functions.

## 6.7 Summary

We have reviewed the semi-classical model of a two-level system coupled longitudinally to a non-Gaussian bath of the “telegraph noise” type, [34, 35, 39, 43]. This model corresponds to the high-temperature limit of the background fluctuator model already introduced in Chap. 5. We have calculated the visibility of the qubit which displays an oscillatory time evolution with regions of complete loss of visibility and visibility revivals in-between. The exponential decay of the visibility oscillations at the rate  $\Gamma_\varphi$  show an unusual dependence on the coupling strength to the fluctuator. We also calculated the probability distribution of the phase which has a non-Gaussian shape. However, at times much larger than the typical correlation time the probability distribution approaches asymptotically a Gaussian distribution. The Gaussian asymptotic is a consequence of the central-limit theorem.



Chapter
7

# Decoherence by quantum telegraph noise

## 7.1 Introduction

**I**N this chapter we analyze the full time evolution of the reduced density matrix for a qubit subject to the fluctuating charge on a single impurity level tunnel-coupled to an electronic reservoir. We are able to fully include quantum fluctuations as well as non-equilibrium effects. Our analysis is based on a numerical evaluation of the exact solution for the reduced density matrix for arbitrary temperatures and for the full range of parameters. Our findings show that in the strong-coupling regime (beyond a certain threshold) the rather simple sub-threshold decay of the qubit's coherence  $D(t)$  turns into temporal oscillations, with complete loss of coherence interspersed between coherence revivals. These qualitative features persist when going to lower temperatures, but the threshold increases and we characterize this effect in detail. The result is a “phase diagram” which displays the temperature-dependence of the strong-coupling threshold.

## 7.2 Calculation of the coherence

We present an exact formalism to study systems coupled to non-equilibrium environments exhibiting non-Gaussian fluctuations. In particular we analyze the dynamics of the coherence of a qubit coupled to the fluctuations of intrinsic background charges already introduced in Chap. 5. The effects of non-Gaussian fluctuations of the environment are pronounced when the system strongly couples to only a small number of environmental degrees of freedom which is of major importance in nanostructures at low temperatures.

We primarily focus on understanding the non-Gaussian properties of the model and therefore we neglect relaxation effects which would contribute as an additional source of decoherence. The interaction between qubit and environment is of the general form:  $(v/2)\hat{Q}\hat{\sigma}_z$ , where  $\hat{Q}$  is the charge on the localized impurity, the Pauli matrix  $\hat{\sigma}_z$  acts on the eigenstates of the qubit and  $v$  is a coupling constant. The reservoir consists of a single localized impurity level tunnel-coupled to an electronic reservoir. The electrons on the impurity level can hop onto the gate-electrode which gives rise to a fluctuating charge with  $\hat{Q} = 0/1$  as the possible charge states of the impurity level.

The Hamiltonian of the heat-bath for a single fluctuator is equal to

$$\hat{\mathcal{H}}_B = \varepsilon_0 \hat{d}^\dagger \hat{d} + \sum_{\mathbf{k}} \left( T_{\mathbf{k}} \hat{c}_{\mathbf{k}}^\dagger \hat{d} + \text{h.c.} \right) + \sum_{\mathbf{k}} \varepsilon_{\mathbf{k}} \hat{c}_{\mathbf{k}}^\dagger \hat{c}_{\mathbf{k}}, \quad (7.1)$$

where  $\varepsilon_0$  is the bare energy of the impurity level,  $T_{\mathbf{k}}$  is the tunneling amplitude for hopping of an electron from the impurity level to a state with momentum  $\mathbf{k}$  inside the reservoir. The operators  $\hat{d}^\dagger / \hat{d}$  create / annihilate an electron with energy  $\varepsilon_0$  on the impurity and  $\hat{c}_{\mathbf{k}}^\dagger / \hat{c}_{\mathbf{k}}$  create / annihilate an electron with momentum  $\mathbf{k}$  inside the lead. The full Hamiltonian of the system is equal to

$$\hat{\mathcal{H}} = \frac{\Delta}{2} \hat{\sigma}_z + \frac{v}{2} \hat{Q} \hat{\sigma}_z + \hat{\mathcal{H}}_B, \quad (7.2)$$

where  $\Delta$  is the energy splitting of the eigenenergies of the qubit, and  $\hat{Q} = \hat{d}^\dagger \hat{d}$  is the fluctuating charge on the localized level.

We start with an initial quantum superposition at  $t = 0$ :  $|\psi(0)\rangle = (1/\sqrt{2})(|\uparrow\rangle + |\downarrow\rangle) \otimes |\chi\rangle$ , where  $|\chi\rangle$  is a thermal state of the heat-bath and then switch on the interaction of the qubit with the environment. The state of the system is described at time  $t$  by

$$|\psi(t)\rangle = \frac{1}{\sqrt{2}} \left( e^{-i\Delta t/2} |\uparrow\rangle \otimes |\chi_\uparrow(t)\rangle + e^{i\Delta t/2} |\downarrow\rangle \otimes |\chi_\downarrow(t)\rangle \right). \quad (7.3)$$

Due to the specific qubit-bath interaction the diagonal components  $\rho_{ii}$  of the reduced density matrix are conserved during the time evolution but the off-diagonal components  $\rho_{ij}(t)$  with  $i, j \in \{\uparrow, \downarrow\}$  acquire an additional coherence factor  $D(t)$  in their oscillatory time evolution which can be expressed as an overlap  $D(t) = \langle \chi_\downarrow(t) | \chi_\uparrow(t) \rangle$  of the bath states  $|\chi_\uparrow(t)\rangle, |\chi_\downarrow(t)\rangle$  that evolve under the influence of the conditional Hamiltonian  $\hat{\mathcal{H}}^\pm = \hat{\mathcal{H}}_B \pm (v/2) \hat{Q}$ .

The reduced density matrix has the same form as in Eq. (4.24) and the coherence factor  $D(t)$  describing the decay of the off-diagonal elements of the reduced density-matrix is equal to [see Sec. 4.4]

$$D(t) = \left\langle e^{i(\hat{\mathcal{H}}_B - v\hat{Q}/2)t} e^{-i(\hat{\mathcal{H}}_B + v\hat{Q}/2)t} \right\rangle. \quad (7.4)$$

The average  $\langle \dots \rangle = \text{tr} (e^{-\beta(\hat{\mathcal{H}}_B - \mu\hat{\mathcal{N}})} \dots) / Z$  is a trace over thermal states of the heat-bath weighted by a Gibbs factor,  $\beta = 1/T$  is the inverse temperature,  $\hat{\mathcal{N}}$  is the particle number operator and  $Z$  is a normalization such that  $Z = 1$  for  $v = 0$ .

### 7.2.1 Time evolution of the visibility: General exact solution

Several methods have been developed to calculate averages of products of exponentials like Eq. (7.4), e.g. linked-cluster expansions [see App. D.1.2] or non-equilibrium Keldysh path-integral techniques [31, 44]. In App. D we give an introduction to the Keldysh path-integral technique and show a detailed calculation of the coherence.

Here we implement a variant of a formula well-known from the theory of full-counting statistics [45, 46, 47, 48], which can be evaluated numerically efficiently. Our derivation is based on a trace formula which relates certain traces in Fock-space to single particle determinants. We will

first derive the underlying trace formula for fermions and then apply it to the definition of the coherence  $D(t)$ , Eq. (7.4).

We first define the second quantized version of a single-particle operator  $\hat{A}$  (i.e. acting on the single-particle Hilbert space) to be the Fock space operator  $\hat{\mathcal{A}}$ ,

$$\hat{\mathcal{A}} = \sum_{\alpha\beta} \underbrace{\langle \alpha | \hat{A} | \beta \rangle}_{=\hat{A}_{\alpha\beta}} \hat{a}_{\alpha}^{\dagger} \hat{a}_{\beta}, \quad (7.5)$$

where  $\{|\alpha\rangle\}$  is an arbitrary single-particle basis of the Hilbert-space,  $\hat{A}_{\alpha\beta}$  are the matrix-elements of the operator  $\hat{A}$  in the single-particle basis, and  $\hat{a}_{\alpha}^{\dagger}/\hat{a}_{\beta}$  are fermionic creation / annihilation operators which obey the anti-commutation relation  $[\hat{a}_{\alpha}, \hat{a}_{\beta}^{\dagger}]_{+} = \delta_{\alpha\beta}$ .

The central formula for the calculation of the coherence  $D(t)$  is the following *trace formula*

$$\text{tr} \left( e^{\hat{\mathcal{A}}} \right) = \det \left( 1 + e^{\hat{A}} \right), \quad (7.6)$$

where the left-hand side of Eq. (7.6) is a trace over the many-body Hilbert-space and the right-hand side is a determinant in the single-particle basis.

Essentially, this formula is known from calculating the partition sum for non-interacting fermions. However, here we will briefly show how it arises. We start to prove Eq. (7.6) by noting that any matrix  $\hat{A}$  can be brought into the diagonal form  $\hat{A} = \text{diag}(\lambda_1, \lambda_2, \dots, \lambda_N)$ , where  $\lambda_i$  is an eigenvalue of the matrix  $\hat{A}$  and  $N$  is the dimension of the Hilbert-space<sup>1</sup>. Then the trace in Eq. (7.6) can be written as

$$\begin{aligned} \text{tr} \left( e^{\hat{\mathcal{A}}} \right) &= \text{tr} \left( e^{\sum_{\alpha} \lambda_{\alpha} \hat{a}_{\alpha}^{\dagger} \hat{a}_{\alpha}} \right) \\ &= \sum_{(n_1=0/1, n_2=0/1, \dots, n_N=0/1)} e^{\sum_{\alpha} \lambda_{\alpha} n_{\alpha}}. \end{aligned} \quad (7.7)$$

The sum in the equation above is over all occupations of the level  $\alpha$ , i.e.  $n_{\alpha} = 0/1$  for fermions,

$$\begin{aligned} \sum_{(n_1=0/1, n_2=0/1, \dots, n_N=0/1)} e^{\sum_{\alpha} \lambda_{\alpha} n_{\alpha}} &= \prod_{\alpha} (1 + e^{\lambda_{\alpha}}) \\ &= \det \left( 1 + e^{\hat{A}} \right). \end{aligned} \quad (7.8)$$

This completes the proof of the trace formula for fermionic systems. For completeness we note that in the bosonic case the analog of the trace formula can be written as

$$\text{tr} \left( e^{\hat{\mathcal{A}}} \right) = \det \left( 1 - e^{\hat{A}} \right)^{-1}, \quad (7.9)$$

<sup>1</sup>We assume a finite dimensional Hilbert-space.

where  $\hat{\mathcal{A}} = \sum_{\alpha\beta} \langle \alpha | \hat{A} | \beta \rangle \hat{b}_\alpha^\dagger \hat{b}_\beta$ . The operators  $\hat{b}_\alpha^\dagger / \hat{b}_\alpha$  create / annihilate a boson in state  $\alpha$  and they fulfill the commutation relation  $[\hat{b}_\alpha, \hat{b}_\beta^\dagger] = \delta_{\alpha\beta}$ . The proof of Eq. (7.9) basically follows the same lines as in the fermionic case but the occupations  $n_\alpha$  are now positive integers.

Equation (7.6) is valid for a single fermionic operator  $\hat{A}$  but can be easily extended to an arbitrary number of exponentials; just put  $e^{\hat{D}} = e^{\hat{A}} e^{\hat{B}} e^{\hat{C}}$  and apply the rule above

$$\text{tr} \left( e^{\hat{\mathcal{A}}} e^{\hat{\mathcal{B}}} e^{\hat{\mathcal{C}}} \right) = \det \left( 1 + e^{\hat{A}} e^{\hat{B}} e^{\hat{C}} \right). \quad (7.10)$$

Now, we are able to apply the formula above to the definition of the coherence  $D(t)$ . We recover the right-hand side of Eq. (7.4) if we replace  $\hat{\mathcal{A}}, \hat{\mathcal{B}}$  by  $\pm i(\hat{\mathcal{H}}_B \mp (v/2)\hat{\mathcal{Q}})t$  in Eq. (7.10) and identify  $e^{\hat{\mathcal{C}}}$  with the many-body density matrix of the heat-bath  $\hat{\rho}_B$  for an uncorrelated state with independently fluctuating occupations. The full many-body density matrix can be written in an exponential form which is applicable to Eq. (7.10)

$$\begin{aligned} \hat{\rho}_B &= \prod_{\alpha} \left[ n_{\alpha} \hat{c}_{\alpha}^{\dagger} \hat{c}_{\alpha} + (1 - n_{\alpha})(1 - \hat{c}_{\alpha}^{\dagger} \hat{c}_{\alpha}) \right] \\ &= \prod_{\alpha} (1 - n_{\alpha}) e^{\sum_{\alpha} \hat{c}_{\alpha}^{\dagger} \hat{c}_{\alpha} \ln[n_{\alpha}/(1-n_{\alpha})]}, \end{aligned} \quad (7.11)$$

where  $0 \leq n_{\alpha} \leq 1$  is the probability of the level  $\alpha$  to be occupied. Inserting Eq. (7.11) into Eq. (7.6) we obtain for the coherence,

$$\begin{aligned} D(t) &= \left[ \prod_{\alpha} (1 - \hat{n}_{\alpha}) \right] \det \left[ 1 + e^{i(\hat{H}_B - v\hat{Q}/2)t} e^{-i(\hat{H}_B + v\hat{Q}/2)t} \frac{\hat{n}}{1 - \hat{n}} \right] \\ &= \det \left[ 1 - \hat{n} + e^{i(\hat{H}_B - v\hat{Q}/2)t} e^{-i(\hat{H}_B + v\hat{Q}/2)t} \hat{n} \right], \end{aligned} \quad (7.12)$$

where the determinant is taken with respect to some single-particle basis, the operator  $\hat{H}_B = \sum_{\alpha} \varepsilon_{\alpha} \hat{c}_{\alpha}^{\dagger} \hat{c}_{\alpha}$  is the Hamiltonian of the bath which is diagonal in the single-particle basis  $\{|\alpha\rangle\}$  and  $\hat{n}$  is the single-particle density matrix  $\hat{n}_{\alpha\beta} = \langle \hat{c}_{\alpha}^{\dagger} \hat{c}_{\beta} \rangle$  which is just equal to the occupation probability of level  $\alpha$  when diagonalized. We are assuming everywhere that the many-body state, with respect to which all expectation values are calculated, is an uncorrelated state. Then there exists some single-particle basis where the occupations of the levels fluctuate independently, and the state is thus fully described by the average occupations, i.e. the eigenvalues of  $\hat{n}_{\alpha\beta}$ . This might be the thermal state with

$$\hat{n}_{\alpha\beta} = f_T(\varepsilon_{\alpha}) \delta_{\alpha\beta}, \quad (7.13)$$

in the eigenbasis of the single-particle Hamiltonian,  $f_T(\varepsilon)$  the Fermi-Dirac distribution function and  $\varepsilon_{\alpha}$  the eigenenergies of  $\hat{\mathcal{H}}_B$  when diagonalized.

What is left to do, is to calculate the matrix-elements of the charge operator  $\hat{Q}_{\alpha\beta}$  in the basis  $\{|\alpha\rangle\}$ . The charge operator  $\hat{Q}$  can be written as the projector onto the defect level  $|d\rangle \langle d|$ , where  $|d\rangle$  is the state of the defect level. Therefore the matrix elements of  $\hat{Q}$  in the single-particle basis

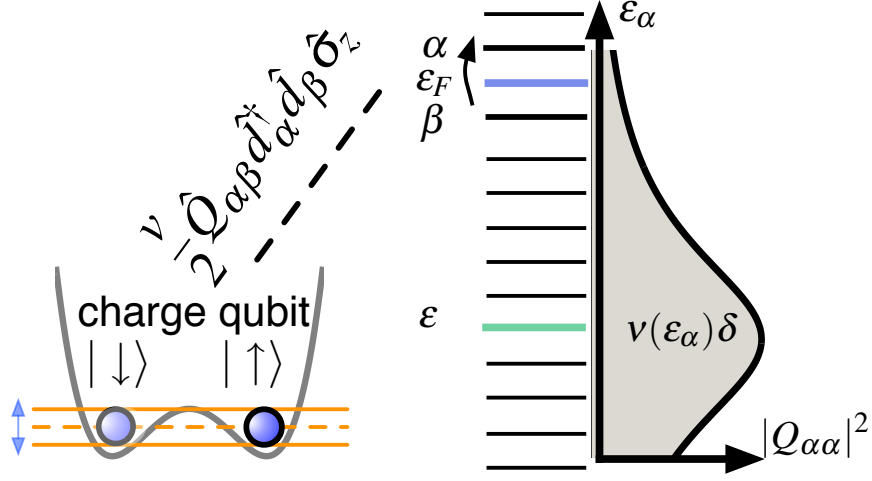


**Figure 7.1:** Schematic representation of the interaction between qubit and heat-bath. In the diagonal basis the qubit interacts with a fluctuating  $\hat{Q}_{\alpha\beta}$  which is due to transitions between all exact states of the heat-bath. The strength of the interaction is determined by the Lorentzian DoS  $v(\omega)$ . At low temperature the strength of the interaction of remote lying (measured from the Fermi energy  $\varepsilon_F$ ) impurity-levels will be controlled by the tail of the Lorentzian rather than the Fermi-Dirac distribution.

are equal to  $\hat{Q}_{\alpha\beta} = \langle \alpha | d \rangle \langle d | \beta \rangle$ . The matrix elements may be expressed by the retarded Green's function of the impurity level. Using the definition of  $G^R(t, t')$ ,

$$G^R(t, t') = -i\theta(t - t') \langle [\hat{\psi}(t), \hat{\psi}^\dagger(t')]_+ \rangle, \quad (7.14)$$

where  $\theta(t)$  is the Heavidiide function. One may expand the quantum field operators  $\hat{\psi}(t)$ ,  $\hat{\psi}^\dagger(t)$  in terms of the basis  $\alpha$  such that  $\hat{\psi}(t) = \sum_{\alpha} \hat{d}_{\alpha} \varphi_{\alpha} e^{-i\varepsilon_{\alpha}t}$  and  $\hat{\psi}^\dagger(t) = \sum_{\alpha} \hat{d}_{\alpha}^{\dagger} \varphi_{\alpha}^* e^{i\varepsilon_{\alpha}t}$ , where  $\varphi_{\alpha} = \langle \alpha | d \rangle$ . The retarded Green's function is then

$$G^R(t, t') = -i\theta(t - t') \sum_{\alpha, \alpha'} \langle \alpha | d \rangle \langle d | \alpha' \rangle \langle [\hat{d}_{\alpha}, \hat{d}_{\alpha'}^{\dagger}]_+ \rangle e^{-i(\varepsilon_{\alpha}t - \varepsilon_{\alpha'}t')}. \quad (7.15)$$

Using the anti-commutation relation  $[\hat{d}_{\alpha}, \hat{d}_{\beta}^{\dagger}]_+ = \delta_{\alpha\beta}$  and representing the equation above in Fourier-space we obtain

$$G^R(\omega) = \sum_{\alpha} \frac{|\langle \alpha | d \rangle|^2}{\omega - \varepsilon_{\alpha} + i\delta}, \quad (7.16)$$

and thus

$$\text{Im}G^R(\omega) = -\pi \sum_{\alpha} |\langle \alpha | d \rangle|^2 \delta(\omega - \varepsilon_{\alpha}). \quad (7.17)$$

Assuming (w.o. loss of gen.) the matrix-elements to be real valued, we obtain for the matrix-elements of the charge operator  $\hat{Q}_{\alpha\beta}$

$$\hat{Q}_{\alpha\beta} = \frac{1}{\pi v_0} \sqrt{\text{Im}G^R(\omega = \varepsilon_{\alpha}) \text{Im}G^R(\omega = \varepsilon_{\beta})}, \quad (7.18)$$

where  $v_0$  is the density of states (DoS) of the electron states in the conduction band and  $G^R(\omega)$  is the retarded Green's function of the broadened impurity level

$$G^R(\omega) = \frac{1}{\omega - \varepsilon + i\gamma/2}, \quad (7.19)$$

where  $\varepsilon$  is the energy of the impurity level potentially renormalized due to hybridization with the Fermi sea and  $\gamma$  is the broadening of the impurity level. The matrix elements of the charge operator  $\hat{Q}$  may be related to the Lorentzian density of states of the broadened impurity level by

$$\hat{Q} = \sum_{\alpha,\beta} \hat{Q}_{\alpha\beta} \hat{c}_\alpha^\dagger \hat{c}_\beta, \quad (7.20)$$

where  $|\hat{Q}_{\alpha\alpha}|^2 = v(\omega = \varepsilon_\alpha) \delta$ , where  $\delta = 1/v_0$ , where  $v(\omega) = (1/\pi) \text{Im}G^R(\omega)$  and

$$v(\omega) = \frac{1}{\pi} \frac{\gamma/2}{(\omega - \varepsilon)^2 + \gamma^2/4}. \quad (7.21)$$

Equation (7.12) together with Eq. (7.18) and Eq. (7.19) provide an exact formula for the coherence  $D(t)$  for a qubit subject to non-Gaussian quantum telegraph noise.

Figure 7.1 displays the interaction between qubit and heat-bath. A fluctuating charge is due to transitions between all exact states of the heat-bath. At low temperatures, transitions close to the Fermi energy  $\varepsilon_F$  are the dominant process. However the strength of the interaction is controlled by the tail of the Lorentzian DoS  $v(\omega)$  rather than the Fermi-Dirac distribution. As a consequence the influence of a remote impurity level with energy  $\varepsilon$  will be power-law suppressed.

### 7.3 Gaussian approximation

Before we present the results of our numerical simulations of the visibility  $v(t) = |D(t)|$ , it is advisable to derive the Gaussian approximation. The key assumption here is that  $\hat{Q}$  is a linear superposition of harmonic oscillator coordinates, which are in thermal equilibrium, and fluctuations are Gaussian distributed (i.e. it would correspond to a random process with a Gaussian distribution in the classical limit). The Gaussian approximation for the coherence is equal to

$$D_{\text{Gauss}}(t) = \exp \left[ -iv \langle \hat{Q} \rangle t - \frac{v^2}{2} \int_0^t dt_1 \int_0^t dt_2 \langle \delta \hat{Q}(t_1) \delta \hat{Q}(t_2) \rangle \right], \quad (7.22)$$

where  $\delta \hat{Q}(t) = \hat{Q}(t) - \langle \hat{Q} \rangle$ . If one is interested in the time evolution of the visibility  $v(t) = |D_{\text{Gauss}}(t)|$  then

$$v_{\text{Gauss}}(t) = \exp \left[ -\frac{v^2}{2} \int_0^t dt_1 \int_0^t dt_2 \frac{1}{2} \langle [\delta \hat{Q}(t_1), \delta \hat{Q}(t_2)]_+ \rangle \right], \quad (7.23)$$

where the visibility only depends on the symmetrized version of the quantum correlator. Defining the quantum noise-spectrum

$$\langle \delta \hat{Q} \delta \hat{Q} \rangle_\omega = \int_{-\infty}^{+\infty} dt e^{i\omega t} \langle \delta \hat{Q}(t) \delta \hat{Q}(0) \rangle, \quad (7.24)$$

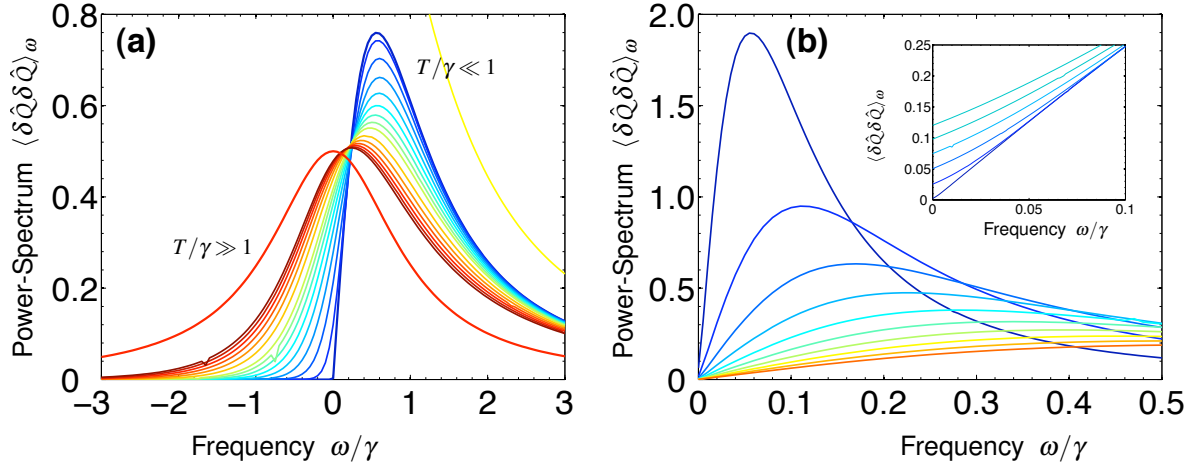


**Figure 7.2:** (a) Power-Spectrum  $\langle \delta \hat{Q} \delta \hat{Q} \rangle_{\omega}$  of the charge fluctuations for decreasing temperatures, (from top to bottom)  $T/\gamma = 1.0, 0.9, 0.8, \dots, 0.5, 0.45, 0.4, \dots, 0$ . At non-zero temperature the visibility decays exponentially in time with a decoherence rate  $\Gamma_{\phi}$  that is controlled by the value of  $\langle \delta \hat{Q} \delta \hat{Q} \rangle_{\omega}$  at  $\omega = 0$ . At low temperatures  $T \ll \gamma$  the nose-power is asymmetric and vanishes for zero temperature  $T = 0$  (blue line). The high-temperature limit represents the classical symmetric noise-power (red line). (b) Power-Spectrum for different switching-rates  $\gamma$ , (from top to bottom)  $\gamma = 1.0, 0.9, \dots, 0.1$  at zero-temperature  $T = 0$ . The slope of the noise-power at  $\omega = 0$  determines the exponent  $K$  of the power-law decay of the visibility. The inset shows the noise-power in the vicinity of  $\omega = 0$  for decreasing temperature (from top to bottom).

we find the general expression for the visibility which is valid for an arbitrary noise-spectrum

$$v_{\text{Gauss}}(t) = \exp \left[ -\frac{v^2}{2} \int \frac{d\omega}{2\pi} \langle \delta \hat{Q} \delta \hat{Q} \rangle_{\omega} \frac{\sin^2(\omega t/2)}{(\omega/2)^2} \right]. \quad (7.25)$$

Inserting the relation between the charge operator  $\hat{Q}$  and the density fluctuations, Eq. (7.20) we obtain

$$\langle \delta \hat{Q} \delta \hat{Q} \rangle_{\omega} = 2\pi \sum_{\alpha\beta} |\hat{Q}_{\beta\alpha}|^2 n_{\alpha} (1 - n_{\beta}) \delta[\omega - (\epsilon_{\beta} - \epsilon_{\alpha})]. \quad (7.26)$$

Equation (7.25) together with the noise-power Eq. (7.26) define the Gaussian approximation of the visibility  $v_{\text{Gauss}}(t)$ . The noise-power of the charge fluctuations on a single impurity level  $\langle \delta \hat{Q} \delta \hat{Q} \rangle_{\omega}$  is shown in Fig. 7.2 for various temperatures (a) and for various switching rates  $\gamma$  as displayed in (b).

### 7.3.1 Results for the visibility according to the Gaussian approximation

We now discuss the results of the Gaussian approximation for certain special cases. At zero-temperature  $T = 0$  the linear slope of the noise-power  $\langle \delta \hat{Q} \delta \hat{Q} \rangle_{\omega}$  at  $\omega = 0$  gives rise to a power-law decay of the visibility with an exponent depending on the coupling strength  $v/\gamma$ .

The integral in Eq. (7.25) considerably simplifies for times  $t$  which are much larger than the typical correlation-time  $\omega_c^{-1}$  of the bath, i.e.  $\omega_c t \gg 1$ . As a consequence the rapidly oscillating function  $\sin^2(\omega t/2)$  may be replaced by its mean (equal to 1/2) and  $\int d\omega \rightarrow \int_{1/t}^{\omega_c} d\omega$ . The long-time limit of the visibility in the Gaussian approximation at  $T = 0$  is equal to

$$v_{\text{Gauss}}^{T=0}(t) = \text{constant} \cdot t^{-K}, \quad K = \frac{4}{\pi^2} \left( \frac{v}{\gamma} \right)^2, \quad (7.27)$$

where the exponent  $K$  is determined by the slope of the noise-power  $\langle \delta \hat{Q} \delta \hat{Q} \rangle_{\omega}$  at  $\omega = 0$ . This result is well known from the physics of the orthogonality catastrophe, which underlies the physics of many important phenomena like the X-ray edge singularity or the Kondo-effect [49, 50, 51]. After turning on the interaction between the two-level system and the fermionic bath, the two bath states  $|\chi_{\uparrow}(t)\rangle$  and  $|\chi_{\downarrow}(t)\rangle$  evolve in time such that their overlap decays in time according to a power-law. The vanishing overlap  $\langle \chi_{\downarrow} | \chi_{\uparrow} \rangle$  at long times is due the fact that the states  $|\chi_{\uparrow\downarrow}\rangle$  of the fermionic bath which evolve under the action of the conditional Hamiltonian  $\hat{H}^{\pm} = \hat{H}_B \pm v\hat{Q}/2$  are orthogonal.

Figure 7.3(a) displays the time evolution of the visibility at  $T = 0$  which has been obtained by direct numerical evaluation of Eq. (7.25) and the inset shows a log – log plot of the visibility compared against the power-law decay indicating the exponent  $K$  (dashed lines).

At finite temperatures  $T > 0$  the noise-power  $\langle \hat{Q} \delta \hat{Q} \rangle_{\omega}$  is finite at  $\omega = 0$  and we may make the following replacement inside Eq. (7.25) to obtain the long-time asymptotics for the visibility:  $\sin^2(\omega t/2)/(\omega/2)^2 \rightarrow 2\pi t \delta(\omega)$ . Then we obtain

$$v_{\text{Gauss}}(t) \sim \exp\left(-\frac{v^2 t}{2} \langle \delta \hat{Q} \delta \hat{Q} \rangle_{\omega=0}\right). \quad (7.28)$$

At high temperatures  $T$

if  $\gamma$  the zero-frequency noise-power is equal to

$$\begin{aligned} \langle \delta \hat{Q} \delta \hat{Q} \rangle_{\omega=0} &= 2\pi \int_{-\infty}^{\infty} d\omega' v^2(\omega') f_T(\omega') (1 - f_T(\omega')) \\ &= \frac{1}{2\gamma}. \end{aligned} \quad (7.29)$$

In this “classical”, high-temperature limit ( $T \gg \gamma$ ), we find the visibility to decay exponentially in the long-time limit,

$$v_{\text{Gauss}}(t) \sim e^{-\Gamma_{\varphi} t}, \quad \Gamma_{\varphi} = \frac{v^2}{4\gamma}, \quad (7.30)$$

with a decoherence rate  $\Gamma_{\varphi}$ , which is compatible with the classical result in the Gaussian approximation.

## 7.4 Exact numerical results and discussion

We now present the exact time evolution of the visibility  $v(t) = |D(t)|$  for a qubit subject to quantum telegraph noise. These results have been obtained by direct numerical evaluation of

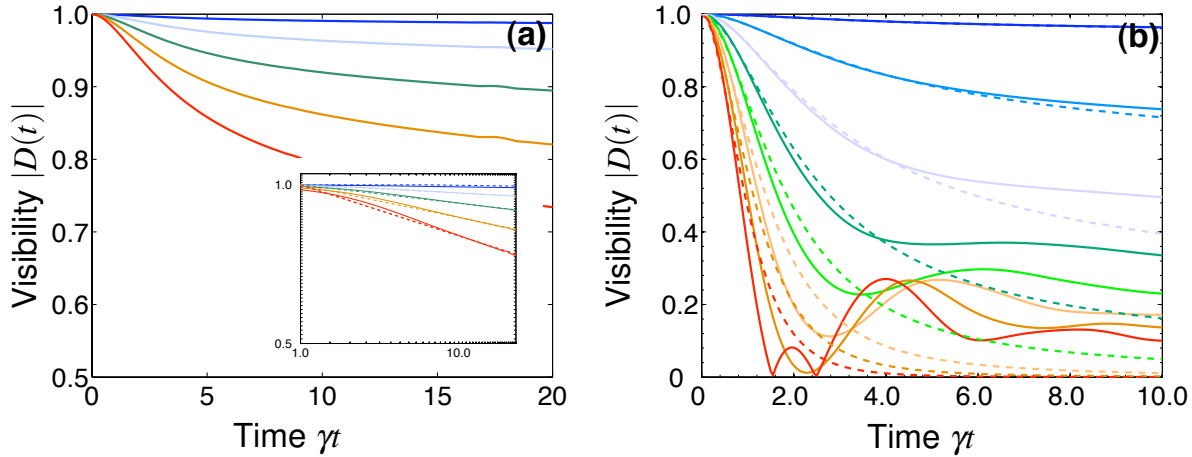


**Figure 7.3:** Time evolution of the visibility  $|D(t)|$  for a qubit coupled to the charge fluctuations on a single impurity level at zero temperature  $T = 0$  ( $\varepsilon = 0$ ). (a) Visibility according to the Gaussian approximation [see Eq. (7.25)] for increasing coupling strength  $v/\gamma = 0.1, 0.2, 0.3, 0.4, 0.5$  (from top to bottom), displaying the power-law decay at long times as expected from the physics of the orthogonality catastrophe. The inset shows a log-log-plot, where the dashed lines indicate the exponent  $K = (4/\pi^2)(v/\gamma)^2$ . (b) Exact time evolution of the visibility for increasing coupling strength (from top to bottom)  $v/\gamma = 0.2, 0.6, 1.0, 1.4, 1.8, 2.2, 2.6, 3.0$ . These curves have been obtained by direct numerical evaluation of Eq. (7.12). Beyond a certain temperature dependent threshold the visibility has zeros in the time evolution with complete loss of visibility and coherence revivals in-between. This phenomenon is a manifestation of the non-Gaussian nature of quantum telegraph noise. The dashed lines show the corresponding Gaussian-approximation.

the determinant in Eq. (7.12). We have discretized the determinant using a spectrum of equally spaced energy levels  $\varepsilon_n = n\delta$  in a band  $\varepsilon_n \in [-W, W]$ , where  $\delta = 1/v_0$ . The width of the band  $W \gg \gamma$  is chosen such that a good resolution of the Lorentzian density of states is achieved. The determinant of the resulting  $N \times N$ -matrix,  $N = 2W/\delta$ , already converges for  $W = 20$  and  $N = 400$ .

In Fig. 7.3(b) we show the time evolution of the visibility  $v(t)$  at zero temperature  $T = 0$  for different coupling strengths (solid lines) compared against the Gaussian approximation (dashed lines). For weak-coupling  $v/\gamma \ll 1$  the Gaussian result is a good approximation of the visibility. However for increasing coupling strength the Gaussian approximation fails even qualitatively indicating the non-Gaussian nature of quantum telegraph noise.

In the case of classical telegraph noise, [Fig. 6.4], the important feature had been the occurrence of visibility oscillations beyond a critical coupling strength,  $v_c^{cl}$ . This threshold is set by the inverse of the correlation time of the fluctuating charge,  $v_c^{cl} = \gamma$ . The visibility vanishes at certain times and shows coherence revivals in-between these zeros. These features continue to exist for quantum telegraph noise where we first observe a transition to a non-monotonous behaviour as a precursor to the visibility oscillations in contrast to the classical limit discussed above. Moreover,

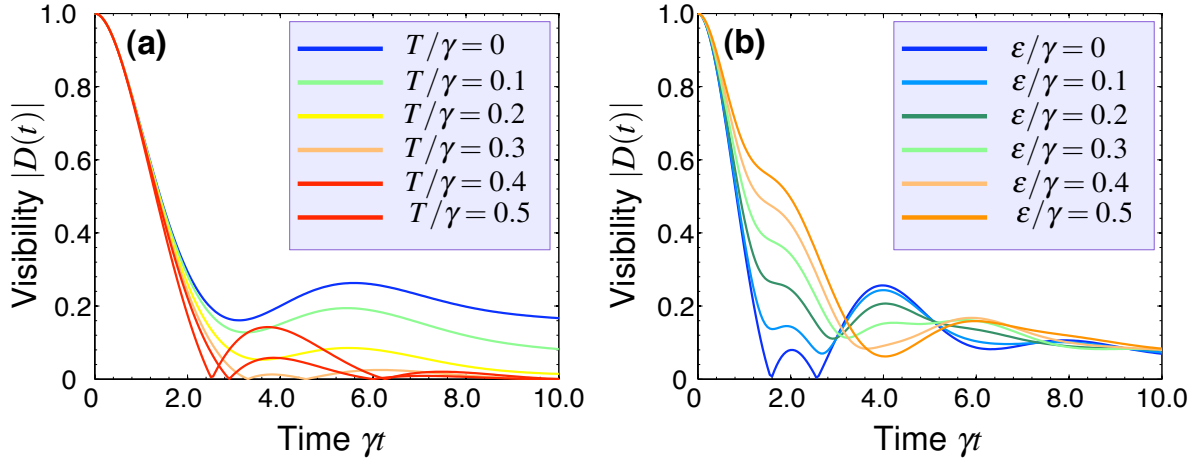


**Figure 7.4:** (a) Time evolution of the visibility  $v(t)$  for increasing temperature  $T$  (from top to bottom) and  $v/\gamma = 2.0$ . At zero-temperature the visibility has no zero in the time evolution but when the temperature is increased zeros appear beyond a certain temperature. (b) These curves display the effect of shifting the impurity level  $\epsilon$  away from the Fermi energy  $\epsilon_F$  for increasing energy  $\epsilon$  (from top to bottom),  $v/\gamma = 3.0$  and  $T = 0$ . The first zero-crossing is lifted but visibility oscillations are still present.

zeros in the visibility develop only at much larger (temperature dependent) coupling strengths  $v_c^q$ . We will study the appearance of zeros in the time evolution of the visibility in more detail, [see Sec. 7.6]. Zeros in the time evolution of the visibility may be used to characterize the fluctuator since their appearance is due to the non-Gaussian statistics of quantum telegraph noise. Another notable feature is the non-monotonous evolution of peak heights for strong coupling which is not seen in the classical analogue, where the height of the peaks decays exponentially with time.

Figure 7.4(a) displays the transition for a fluctuator in a state without any zero in the time evolution of  $v(t)$  to a state where at least one zero appears as temperature is increased. The first zero appears at approximately at  $T/\gamma \approx 0.3$ . This is a strong indication of a temperature dependent critical coupling strength  $v_c^q(T)$  beyond which zeros in the time evolution of the visibility occur. The precise form of the critical coupling  $v_c^q(T)$  as a function of temperature  $T$  will be analyzed in Sec. 7.6. Finally, the effect of shifting the energy of the impurity level  $\epsilon$  away from the Fermi level  $\epsilon_F$  is shown in Fig. 7.4(b). The zero crossings in the time evolution of the visibility are lifted even for small  $\epsilon$  but visibility oscillations still appear. This is due to the fact that far away from the Fermi energy  $\epsilon_F$  the strength of the qubit-fluctuator interaction is power-law suppressed due to the Lorentzian DoS [see Fig. 7.1].

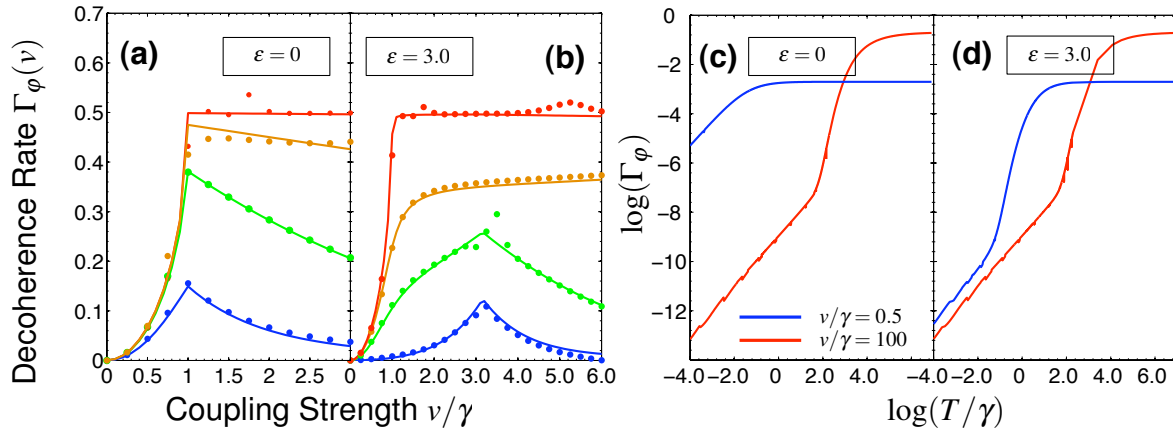


**Figure 7.5:** Decoherence rate  $\Gamma_\phi$  of a qubit coupled to the charge fluctuations on a single impurity level hybridized with a Fermi sea. (a) and (b) Decoherence rate  $\Gamma_\phi$  for different temperatures (from top to bottom)  $T/\gamma = 100, 5, 1, 0.2$  as a function of the coupling strength  $v/\gamma$ . The energy of the impurity level is (a)  $\varepsilon/\gamma = 0$  and (b)  $\varepsilon/\gamma = 3.0$  measured from the Fermi energy  $\varepsilon_F$ . The solid line corresponds to the analytical result of [31, 32] and the solid circles corresponds to the direct numerical evaluation of Eq. (7.12). (c) and (d) log – log-plot of the analytical results for the decoherence rate as a function of temperature. Some spurious deviations are entirely due to the numerical method used for obtaining the decoherence rate.

## 7.5 Decoherence rate

In the long-time limit  $t \rightarrow \infty$  the visibility decays exponentially in time,  $|D(t)| \propto e^{-\Gamma_\phi t}$  at a decoherence rate  $\Gamma_\phi$  which is defined as

$$\Gamma_\phi = -\lim_{t \rightarrow \infty} \frac{1}{t} \log |D(t)|. \quad (7.31)$$

Figure 7.5 shows the decoherence rate  $\Gamma_\phi$  as a function of the coupling strength  $v/\gamma$  for different temperatures. The solid line corresponds to the analytical results obtained in [31, 32] and the dots corresponds to the numerical evaluation of the slope of the visibility using Eq. (7.12). In Figs. 7.5(a) and (b) the decoherence rate  $\Gamma_\phi$  displays a non-analytic behavior as a function of the coupling strength and has a cusp whenever  $v/\gamma = \sqrt{(2\varepsilon/\gamma)^2 + 1}$  for the whole range of temperatures. However, there is an additional temperature-induced rounding as a precursor of the cusp for  $\varepsilon \neq 0$ . The high-temperature limit corresponds to the classical limit of telegraph noise discussed in Chap. 6.

The reason for the deviations of our numerical results from the analytical one is due to the fact that  $\log |D(t)|$  is a linearly decaying function with a slope equal to  $-\Gamma_\phi$  with rapid oscillations on top of it, which makes it difficult to extrapolate the linear slope numerically.

Figures 7.5(c) and (d) display the decoherence rate  $\Gamma_\phi$  as a function of temperature in a log – log-plot for small (blue) and very large coupling (red). The low-temperature regime  $T \ll \gamma$  is characterized by a linear dependence  $\Gamma_\phi \propto T$ . That behaviour could already be inferred from a

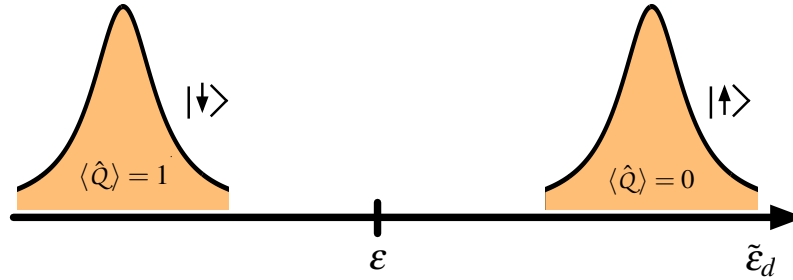


**Figure 7.6:** Schematic picture of the shifted energy level  $\tilde{\epsilon}_d$  of the impurity level depending on the state of the qubit. When the qubit is in its ground state the energy is shifted far below  $\epsilon$  and when the qubit is in its excited state  $\tilde{\epsilon}_d$  is shifted far above  $\epsilon$ . The average occupation on the impurity level is either  $\langle \hat{Q} \rangle = 0$  when  $\hat{\sigma}_z = |\uparrow\rangle$  or  $\langle \hat{Q} \rangle = 1$  when  $\hat{\sigma}_z = |\downarrow\rangle$ .

spin-boson model with an Ohmic noise-spectrum [see Sec. 4.6]. In contrast, the high temperature decoherence rate is always stronger for a strongly coupled fluctuator. In the weak-coupling limit  $\nu \ll \gamma$  at finite temperature  $T$  the quadratic increase of decoherence rate  $\Gamma_\varphi \sim \nu^2$  can be inferred from the long-time behaviour of the Gaussian approximation for the coherence Eq. (7.28). In the strong-coupling limit the energy of the impurity level  $\tilde{\epsilon}_d^{\uparrow\downarrow} = (\epsilon \pm \nu/2)$  is either pushed far above or far below the bare impurity energy  $\epsilon_0$  depending on the state of the qubit. Figure 7.6 shows a qualitative picture of the shifted DoS of the impurity level. In thermal equilibrium the average occupation of impurity  $\langle \hat{Q} \rangle = \langle \hat{d}^\dagger \hat{d} \rangle$  is  $\langle \hat{Q} \rangle = 0$  if the qubit is in its excited state  $|\uparrow\rangle$  and  $\langle \hat{Q} \rangle = 1$  if the qubit is in its ground state  $|\downarrow\rangle$ . In both cases the charge fluctuations on the impurity are frozen which results in a decreasing decoherence rate  $\Gamma_\varphi$  despite of a large coupling strength  $\nu$ .

## 7.6 Phase diagram

We propose a scheme to identify the regime of strong fluctuator-qubit coupling characterized by the specifically non-Gaussian dynamics of the density matrix, i.e. the occurrence of zeros in the time evolution of the visibility. Another approach for the characterization of the dynamics of the reduced density matrix for a non-Gaussian environments identified the time-scale separating Gaussian and non-Gaussian dynamical regimes [52] for a non-Gaussian spin-bath.

The appearance of zeros is a genuine effect of non-Gaussian noise and cannot be mimicked by any Gaussian theory, e.g. by a bath of harmonic oscillators. For Gaussian-distributed noise  $|\langle e^{i\varphi} \rangle| = |e^{-\langle \varphi^2 \rangle / 2}| > 0$ , irrespective of the power-spectrum which fully determines all properties of the harmonic oscillator heat-bath. A peculiar feature of telegraph noise is the occurrence of zeros in the time evolution of the visibility. We characterize the onset of the strong-coupling regime by the temperature dependent coupling strength  $\nu_c^q(T)$ , beyond which the zeros in the time evolution of  $\nu(t)$  appear. The result is a "phase diagram" which shows the critical coupling strength  $\nu_c^q$  as a function of temperature.

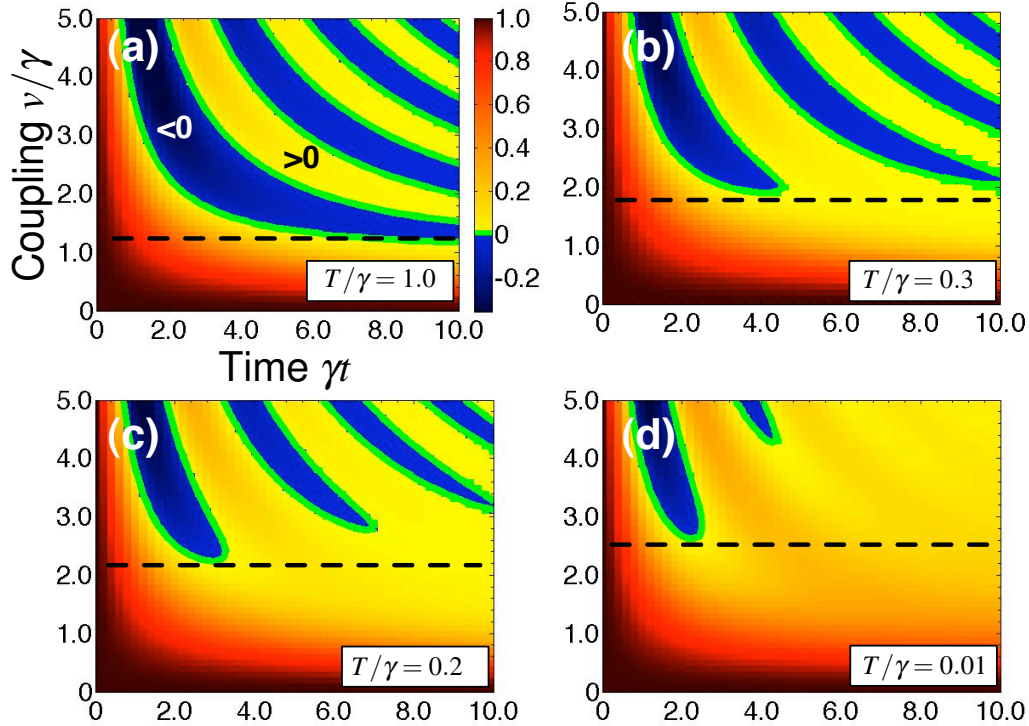


**Figure 7.7:** Time evolution of the coherence  $D(t)$  (densityplot) as a function of the coupling  $v/\gamma$  (vertical) and time  $\gamma t$  (horizontal axis) for decreasing temperatures, (a)-(d)  $T/\gamma = 1.0, 0.3, 0.2, 0.01$  (with  $\varepsilon = 0$ ). The bold green lines indicate the contours of vanishing coherence,  $D(t; v, T) = 0$ . The dashed black line indicates the critical coupling strength for the appearance of the first zero-crossing in  $D(t)$ . Zeros in the time evolution of the visibility start beyond the threshold (from (a)-(d))  $v/\gamma \approx 1.0, 1.9, 2.2, 2.7$ .

### 7.6.1 Temperature-dependence of the strong-coupling threshold

In order to illustrate both the dependence on coupling strength  $v$  and temperature  $T$  we have plotted the time evolution of the coherence  $D(t)$  as a function of the coupling-strength  $v$  for various temperatures, omitting the trivial phase-factor  $e^{-ivt/2}$ , [see Fig. 7.7]. Then the coherence is a real-valued function. It displays oscillations between positive ( $D > 0$ , light shading) and negative ( $D < 0$ , dark shading) values. Bold green contour-lines indicate the location of zeros in the  $v - T$ -plane, i.e. where  $D(t; v, T) = 0$ .

At high temperatures  $T \gg \gamma$  [Fig. 7.7(a)] visibility oscillations set in beyond a certain threshold  $v_c^q/\gamma \approx 1$ . The visibility vanishes at certain times and shows coherence revivals in-between. This was expected from the semi-classical model studied in Chap. 6 where zeros appear as soon as  $v = \gamma$ . However, for decreasing temperatures [Fig. 7.7(b-d)], the first zero-crossing appears beyond a larger coupling strength  $v > \gamma$ . In particular, in the low-temperature limit [Fig. 7.7(d)] the first zero-crossing appears approximately at the critical coupling  $v_c^q/\gamma \approx 2.7$ .

One can characterize the onset of the specifically non-Gaussian strong coupling regime by the temperature-dependent critical coupling strength  $v_c^q(T)$  beyond which the zeros in the time

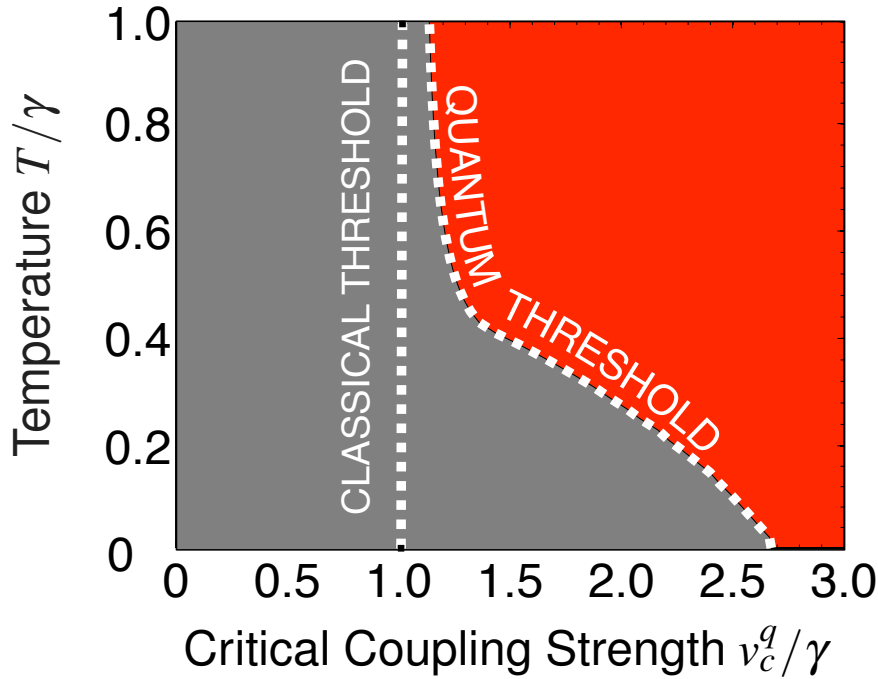


**Figure 7.8:** “Phase diagram”: Critical coupling strength  $v_c^q(T)$  as a function of temperature. The dashed line indicate the parameters  $(v, T)$  where zeros in the coherence first appear. Above the dashed line one observes always zeros in the coherence. At high temperatures  $v_c^q \rightarrow 1$  according to the classical limit.

evolution of the coherence appear. At a fixed temperature  $T$  the critical coupling-strength  $v_c^q$  and the corresponding zero in  $D(t)$  at time  $t^*$  are found by a bisection procedure [see Sec. 7.6.2]. The result is a phase diagram showing the critical coupling-strength  $v_c^q$  as a function of the temperature  $T$ , [Fig. 7.8]. The critical threshold  $v_c^q(T)$  separates the  $v - T$ -plane into two regions: At high temperatures  $T \gg \gamma$  the critical coupling  $v_c^q$  converges to its classical value  $v_c^q \rightarrow 1$  (the slight offset in Fig. 7.8 is due to limited numerical accuracy). For low temperatures the critical coupling strength increases and saturates at a finite value, as  $D(t; v, T)$  is continuous in the limit  $T \rightarrow 0$  and  $D(t; v, T = 0)$  still displays oscillations beyond some threshold. This means the equilibrium quantum Nyquist noise of the fluctuator is enough to observe visibility oscillations, in contrast to the strong coupling regime studied in [53, 54], where only the nonequilibrium shot noise of discrete electrons could yield these effects.

## 7.6.2 Algorithm

A schematic picture of the way to find the first zero  $t_1^*$  and the corresponding critical coupling  $v_c^q$  is shown in Fig. 7.9. We begin with zero temperature  $T = 0$  and determine the location of the first zero crossing and the corresponding critical coupling.

We are starting with an arbitrary initial coupling, i.e.  $v_1$  which is sufficiently large enough

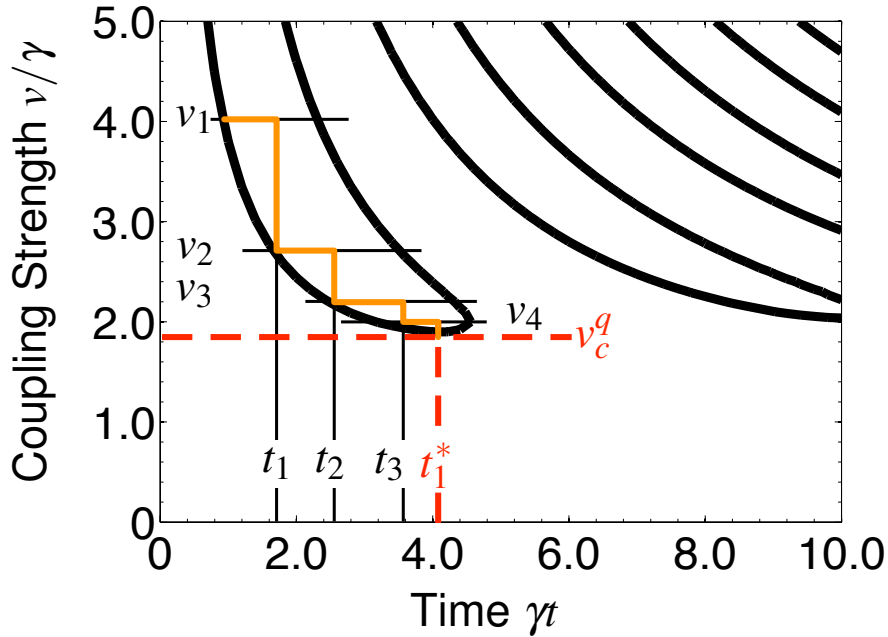


**Figure 7.9:** Schematic picture of the algorithm used to find the first zero-crossing of the coherence. The bold black lines show the contour lines of the coherence for  $D(t;v,T) = 0$  for a specific temperature  $T$ . Our goal is to find the first zero of the coherence  $(t_1^*, v_c^q)$  which is indicated by red dashed lines. The initial value is  $v_1$ . The combination of two bisection procedures in the  $t - v$ -plane produces a sequence  $(t_n, v_n)$  which converges to the critical coupling  $v_c^q$  and the corresponding zero  $t_1^*$ .

such that the time evolution of  $D(t;v,T)$  has at least one zero. Then we determine the positions of the first two zero-crossings of  $D(t;v_1)$ , e.g.  $t_1'$  and  $t_1''$  and take the middle of the interval  $t_1 = (t_1' + t_1'')/2$ . The value of  $v_2$  where  $D(t_1 : v, T)$  is equal to zero is denoted by  $v_2$  and can be found by a standard bisection-algorithm to find zeros of an arbitrary function. The procedure explained above is iterated until the sequence  $t_2, t_3, \dots, t_N$  converges to  $t^*$  and the corresponding coupling strengths  $v_2, v_3, \dots, v_N$  converge to  $v_c^q$ . The trajectory of  $(t_n, v_n)$  is indicated by the orange line in Fig. 7.9. The full phase diagram is obtained by increasing the temperature and using the last critical coupling strength as an initial value for the coupling  $v$  at the increased temperature  $T + \delta T$ .

## 7.7 Summary

We have studied the decoherence of a qubit subject to quantum telegraph noise. We derived an exact fully quantum mechanical formula for the time evolution of the coherence and found the strong-coupling regime with an oscillatory time-dependence that cannot be mimicked by any Gaussian noise source. We have characterized this regime by the appearance of the first zero in the time evolution of the coherence and summarized the result in a “phase diagram”.



*It should be possible to explain the laws of physics to a barmaid.*

ALBERT EINSTEIN

## Chapter 8

# Spin-Echo

## 8.1 Introduction

ONE of the typical problems where the current standard silicon-based computer technology seems to be insufficient is the decomposition of large numbers into prime factors at a reasonable speed, a technique which is frequently used in cryptography and security related applications. It is widely believed that the computational time for that problem grows exponentially with the length of the number which makes it intractable for large numbers. In his breakthrough article SHOR [55] proposed in the year 1994 an algorithm which would greatly improve the performance of the encoding of large numbers. The basic ingredient of that algorithm was the use of the quantum mechanical superposition principle which allows for parallel processing of many classical registers (bits). This quantum-parallelism allows a reduction for the computational time to polynomial order.

The quantum analogue of a classical bit (0/1) is a two-level system (qubit  $|\uparrow\rangle, |\downarrow\rangle$ ). In order to make use of quantum parallelism for computation the qubit needs to be protected from the irreversible dynamics of the environment in order to maintain its quantum state not only with respect to its two eigenstates  $|\uparrow\rangle$  and  $|\downarrow\rangle$  but also with respect to its relative phase. The inevitable coupling of the qubit to the environment destroys any initially prepared superposition of quantum states (decoherence).

Various methods have been proposed to fight decoherence and protect the qubit from dephasing. For example error-correcting codes [56, 57], decoherence free subspace coding [58, 59], noiseless subsystem coding [60], dynamical decoupling [61, 62, 63, 64], quantum feedback control [65, 66, 67] and quantum reservoir engineering [68]. Among these techniques we focus here on dynamical decoupling schemes applied to a qubit subject to quantum telegraph noise.

The idea of dynamical decoupling is borrowed from spin-echo pulses first invented by HAHN in *nuclear magnetic resonance* (NMR), where ensembles of spins are considered. Dynamical decoupling schemes are based on stroboscopic pulsing of the qubit effectively averaging out the environment by external control fields. Schemes of repeated pulse-sequences are applied on the qubit in the hope to maintain phase coherence. For static but non-uniform coupling to the environment a single  $\pi$ -pulse is sufficient to compensate perfectly the environment. The idea of

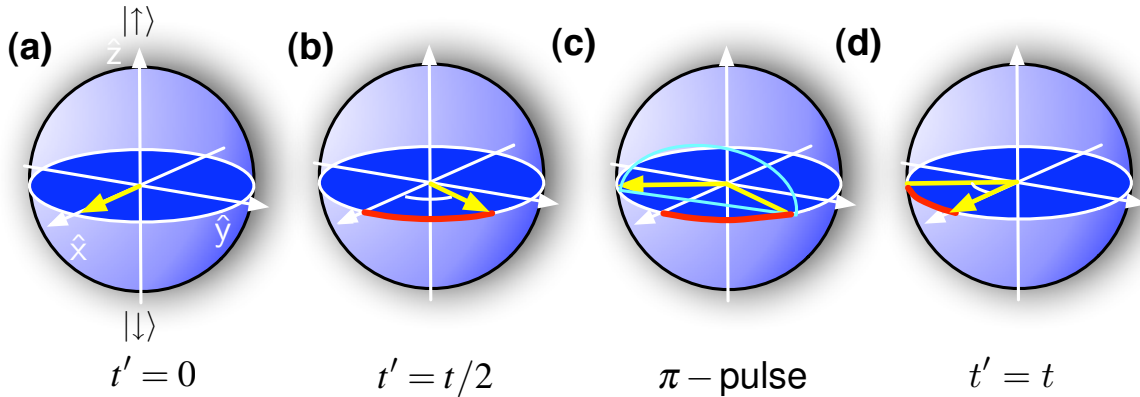


**Figure 8.1:** Time evolution of the qubit in a spin-echo experiment represented on the Bloch sphere. The qubit evolves under the influence of a static but random magnetic field with direction along the  $\hat{z}$ -axis. (a) The initial state of the qubit is a superposition  $|\psi(0)\rangle = 1/\sqrt{2}(|\uparrow\rangle + |\downarrow\rangle)$ . (b) During its time evolution the qubit accumulates the phase  $\varphi(t') = B_z t'$ ,  $t' \in [0, t/2]$  and the state of the qubit is  $|\psi(t)\rangle = 1/\sqrt{2}(e^{i\varphi/2}|\uparrow\rangle + e^{-i\varphi/2}|\downarrow\rangle)$ . (c) The application of a  $\pi$ -pulse rotates the spin around the  $\hat{x}$ -axis by an angle of  $180^\circ$  which effectively flips the phase  $\varphi \rightarrow -\varphi$  such that the contribution of the phase previously accumulated is eliminated and phase-coherence is maintained.

spin-echo pulses is schematically shown in Fig. 8.1. For example, let us consider a single spin subject to a stationary but random magnetic field  $\vec{B} = (0, 0, B_z)^T$  along the  $\hat{z}$ -direction of the Bloch sphere. The spin will precess with a frequency  $B_z$  and dephasing is due to the random precession angle  $\varphi(t) = B_z t$ . After the time  $t' = t/2$  the random precession angle in the  $\hat{x}\hat{y}$ -plane is equal to  $\varphi(t/2) = B_z t/2$ . If it would be possible to flip the precession angle such that  $\varphi \rightarrow -\varphi$  during the following time-interval  $[t/2, t]$  then the subsequent precession would completely eliminate the phase accumulated during the first time-interval  $[0, t/2]$ , regardless of the random magnetic field  $B_z$ . At the end of the time-interval  $[0, t]$  both phase contributions cancel each other and one ends up with the total phase  $\varphi(t) = 0$ . Thus we have achieved a decoupling from the noisy environment and revived the qubit.

In the general case, for a randomly fluctuating magnetic field, only fluctuations with  $\omega t \ll 1$  will be eliminated by this procedure, because they can be regarded as quasi-static. A  $180^\circ$ -rotation of the spin around the  $\hat{x}$ -axis has exactly the effect of flipping the precession angle  $\varphi$ . This can be accomplished by applying a strong magnetic field in the  $\hat{x}$ -direction for a short time. Therefore, pulses of this kind are termed as  $\pi$ -pulses.

Various schemes of pulse-sequences have been proposed in order to fight decoherence. Recently [64], an optimized  $\pi$ -pulse sequence extending the *Carr-Purcell-Meiboom-Gill* (CPMG) cycle well known in the NMR community has been suggested. The central idea of this approach was to optimize the duration between pulses in a sequence of  $\pi$ -pulses such that the decoherence is minimized. In contrast to the CPMG-cycle, the duration between consecutive pulses is no longer equal for all pulses but can vary depending on the number of preceding pulses. For a qubit subject to an Ohmic bath it has been shown that the efficiency of the optimized sequence is

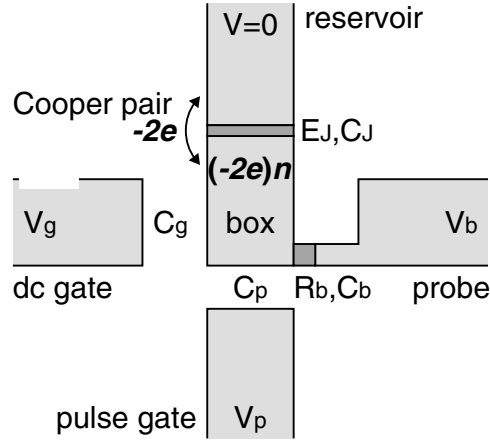


**Figure 8.2:** Schematic experimental setup of Nakamura's charge-echo experiment [69]. A small superconducting island is coupled by a Josephson-junction (with capacity  $C_J$  and Josephson coupling energy  $E_J$ ) to a reservoir. Additional voltage biased gate-electrodes (with capacity  $C_g$ , bias voltage  $V_g$ ) allow for qubit manipulations by adjusting the voltage  $V_p$  of the pulse-gate (with capacity  $C_p$ ). A dc current is detected at the probe electrode (capacitance  $C_b$ , bias voltage  $V_b$ ) via a highly resistive tunnel-junction (Resistance  $R_b$ ). (With courtesy of Y. Nakamura.)

by a factor of 40 better than the equidistant pulse-sequence for strong qubit-bath coupling and for weak coupling the improvement is still about a factor of 4. Although the pulse-sequence has been optimized for a Gaussian Ohmic bath we employ the same sequence for non-Gaussian quantum telegraph noise in our numerical simulation and compare it against a sequence of equidistant pulses [see Sec. 8.3.4].

Echo protocols are now standard in qubit experiments, particularly in the solid state. NAKAMURA *et al.* [69] have studied the charge echo in a Cooper pair box subject to a sequence of gate voltage pulses [see Fig. 8.2]. The Cooper-pair box consists of a small superconducting island (made of Al) coupled by a Josephson junction to a reservoir. The box is capacitively coupled to two gate electrodes. Adjusting the dc-gate voltage  $V_g$  allows to transfer an excess number of Cooper-pairs onto the island, while the modulation of the pulse-gate  $V_p$  allows for qubit manipulation. The total induced charge on the box is  $Q(t) = Q_0 + C_p V_p(t)$  and  $Q_0 = C_g V_g + C_b V_b$ . The Cooper-pair box operates as a qubit when the induced charge on the island is close to 1, i.e.  $Q = 1$ . Then, due to the charging effect the Cooper-pair box is effectively described by its two lowest lying eigenstates which differ by just a single Cooper pair.

The evolution of the qubit may be effectively mapped onto a fictitious spin-1/2 in a magnetic field  $\vec{B} = (E_J, 0, \delta E(Q))^T$  and the effective Hamiltonian has the familiar form

$$\hat{H} = \frac{\delta E(Q)}{2} \hat{\sigma}_z - \frac{E_J}{2} \hat{\sigma}_x, \quad (8.1)$$

where  $\delta E(Q) = 4E_C(Q/|e| - 1)$  and  $E_C = e^2/2C_\Sigma$  is the single-particle charging energy,  $C_\Sigma$  is the total capacitance. Pulses are generated by modulating  $Q(t)$  which correspond to a rotation of the magnetic field  $\vec{B}$  in the  $\hat{x}\hat{z}$ -plane of the Bloch-sphere.

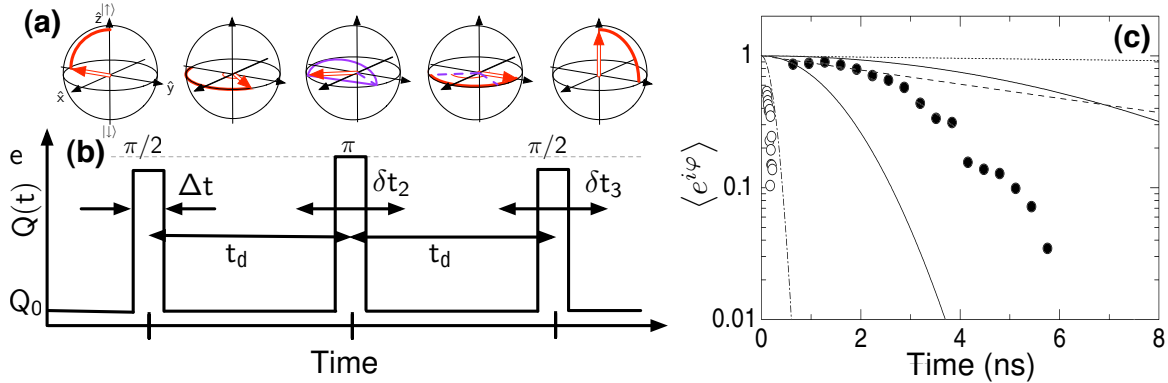


**Figure 8.3:** Charge-echo experiment: (a) Sequence of qubit manipulations in Nakamura's charge-echo experiment. (b) Sequence of charge pulses. (c) Decay of the coherence in the charge echo experiment (filled circles) in comparison with the free induction signal (open circles) when no  $\pi$ -pulses have been applied on the qubit. Estimated coherence  $\langle e^{i\varphi} \rangle$  due to the electromagnetic environment (dotted line), the readout-process (dashed line) and  $1/\omega$ -noise (dashed-dotted line). (Figure (c) with courtesy of Y. Nakamura)

The sequence of pulse-operations applied on the qubit is shown in Fig. 8.3(a) and (b). The first  $\pi/2$ -pulse initializes a superposition  $|\psi(0)\rangle = 1/\sqrt{2}(|\uparrow\rangle + |\downarrow\rangle)$  and the quantum state accumulates a phase  $\varphi = \Delta E(Q_0)t_d$ , where  $\Delta E(Q_0) = (\delta E(Q_0)^2 + E_J^2)^{1/2}$  is the energy difference of the qubit's eigenstates. The second  $\pi$ -pulse flips the spin of the qubit, thereby “filtering out” the effect of the low frequency fluctuations due to the coupling to the intrinsic background fluctuators. The third pulse projects the qubit to the measurement basis. It is widely accepted that decoherence is mainly caused by an ensemble of bistable fluctuators such that the noise-spectrum is  $\langle \delta \hat{Q} \delta \hat{Q} \rangle_\omega \propto 1/\omega$ . However if the qubit couples to only a few bistable fluctuators non-Gaussian effects may become important [see Chap. 7].

Figure 8.3(c) shows the spin-echo signal (filled circles) after the elapsed time  $2t_d$  in comparison with the free-induction signal (open circles) and estimated coherence factors  $\langle e^{i\varphi} \rangle$  due to different sources of noise for comparison.

In the preceding chapter we investigated the time evolution of the density matrix of the charge qubit subject to quantum telegraph noise. We start with a brief review of spin-echo experiments in the semi-classical model introduced in Chap. 6 which is indeed the high-temperature limit of the full quantum mechanical model. An exact derivation of the spin-echo signal for the full quantum mechanical model including all backaction and memory effects for a single  $\pi$ -pulse is shown as well as an extension to arbitrary pulse sequences. The time evolution of the spin-echo signal is calculated numerically for different regimes and parameters.

## 8.2 Spin-echo for classical telegraph noise

Here we present the time evolution of the density matrix for a qubit subject to classical telegraph noise in a spin-echo experiment. We neglect the backaction of the qubit on the heat-bath and as a consequence the bath can be regarded as a stochastic process whose dynamics is governed by the Markoff rate equations [see Eq. (6.22)]. We consider the effect of a single  $\pi$ -pulse applied on the qubit at time  $t' = t/2$  when the qubit is initially prepared in a superposition of its eigenstates at  $t' = 0$ ,  $|\psi(0)\rangle = 1/\sqrt{2}(|\uparrow\rangle + |\downarrow\rangle)$ , and then let the qubit further progress up to time  $t' = t$ . During the first half of the time-interval the qubit evolves according to the Hamiltonian  $\hat{\mathcal{H}} = (\Delta/2)\hat{\sigma}_z + (v/2)Q(t)\hat{\sigma}_z$  and accumulates a random phase  $\varphi(t') = -v \int_0^{t'} dt'' Q(t'')$  after their elapsed time  $t' \in [0, t/2]$ . The state of the qubit is equal to

$$|\psi(t')\rangle = \frac{1}{\sqrt{2}} \left( e^{-i\Delta t'/2} e^{i\varphi(t')/2} |\uparrow\rangle + e^{i\Delta t'/2} e^{-i\varphi(t')/2} |\downarrow\rangle \right). \quad (8.2)$$

The application of the  $\pi$ -pulse  $\hat{\mathcal{W}}$  at the intermediate time  $t/2$

$$\begin{aligned} \hat{\mathcal{W}} &= \exp\left(\frac{i\pi}{2}\hat{\sigma}_x\right), \\ &= i\hat{\sigma}_x, \end{aligned} \quad (8.3)$$

interchanges the qubit's eigenstates such that at  $t' = t/2$  the interaction changes its sign, i.e.

$$(v/2)Q\hat{\sigma}_z \rightarrow -(v/2)Q\hat{\sigma}_z, \quad (8.4)$$

and the evolution of the qubit is subsequently determined by the Hamiltonian  $\hat{\mathcal{H}} = (\Delta/2)\hat{\sigma}_z - (v/2)Q(t)\hat{\sigma}_z$ . Thus for  $t' > t/2$  the qubit will acquire a random phase  $\varphi(t') = v \int_{t/2}^{t'} dt'' Q(t'')$ , with a reversed sign of the coupling strength  $v$ . The qubit's state at time  $t$  is equal to

$$|\psi(t)\rangle = \frac{i}{\sqrt{2}} \left( e^{i\tilde{\varphi}(t)/2} |\uparrow\rangle + e^{-i\tilde{\varphi}(t)/2} |\downarrow\rangle \right), \quad (8.5)$$

where the acquired phase during the time-interval  $[0, t]$  is equal to

$$\tilde{\varphi}(t) = -v \int_0^{t/2} dt' Q(t') + v \int_{t/2}^t dt' Q(t'). \quad (8.6)$$

Equation (8.6) can be written as a convolution over the kernel  $\beta(t')$  used to encode the  $\pi$ -pulse or sequences of pulses

$$\tilde{\varphi}(t) = -v \int_0^t dt' \beta(t-t') Q(t'), \quad (8.7)$$

with the kernel

$$\beta(t-t') = \begin{cases} 0, & \text{for } t' < 0 \\ +1, & \text{for } 0 \leq t' < t/2 \\ -1, & \text{for } t' \geq t/2 \end{cases} \quad (8.8)$$

As a result the density matrix of the qubit at time  $t$  after the application of a  $\pi$ -pulse at  $t' = t/2$  can be written in a similar way as in Chap. 6,

$$\hat{\rho}^{\text{red}}(t) = \begin{pmatrix} \rho_{\uparrow\uparrow}(0) & \rho_{\uparrow\downarrow}(0)D_{\text{Echo}}(t) \\ \rho_{\downarrow\uparrow}(0)D_{\text{Echo}}^*(t) & \rho_{\downarrow\downarrow}(0) \end{pmatrix}, \quad (8.9)$$

with the *spin-echo signal*  $D_{\text{Echo}}(t)$  at time  $t$  which describes the decay of the off-diagonal elements of the density-matrix in a spin-echo experiment,

$$D_{\text{Echo}}(t) = \left\langle \exp \left[ -iv \int_0^t dt' \beta(t-t') Q(t') \right] \right\rangle, \quad (8.10)$$

where  $\langle \dots \rangle = \int d\varphi(\dots)p(\varphi, t)$  denotes an average over the phase distribution function  $p(\varphi, t)$  for classical telegraph noise [see. Eq.(6.32)].

### 8.2.1 Time evolution of the echo according to the Gaussian approximation

As in the preceding chapters we begin with the Gaussian approximation of the spin-echo signal  $D_{\text{Echo}}(t)$  for the semi-classical model [see Chap. 6] which is indeed the weak-coupling limit  $v/\gamma \ll 1$  of the exact result. The Gaussian approximation is equal to

$$\left\langle e^{i\tilde{\varphi}(t)} \right\rangle = e^{i\langle \tilde{\varphi}(t) \rangle - \frac{1}{2} \langle \delta\tilde{\varphi}^2(t) \rangle}, \quad (8.11)$$

but now with vanishing mean  $\langle \tilde{\varphi}(t) \rangle = 0$  and variance  $\langle \delta\tilde{\varphi}^2(t) \rangle$

$$\langle \delta\tilde{\varphi}^2(t) \rangle = v^2 \int_0^t dt' \int_0^t dt'' \beta(t-t') \beta(t-t'') \langle \delta Q(t') \delta Q(t'') \rangle. \quad (8.12)$$

Inserting the correlation function Eq. (6.4) into the expression above and carrying out the integrals we obtain the Gaussian approximation for the spin-echo signal to be equal to

$$D_{\text{Echo}}^{\text{Gauss}}(t) = \exp \left[ - \left( \frac{v}{2\gamma} \right)^2 \left( \gamma t - 3 + 4e^{-\gamma/2} - e^{-\gamma} \right) \right]. \quad (8.13)$$

At long times  $\gamma t \gg 1$  the spin-echo signal decays at a rate  $v^2/4\gamma$  which coincides with the decoherence rate  $\Gamma_{\varphi}^{\text{Gauss}}$  without a  $\pi$ -pulse in the Gaussian approximation. The time evolution of the spin-echo signal  $D_{\text{Echo}}^{\text{Gauss}}(t)$  compared against the exact result is shown in Fig. 8.4(a).

### 8.2.2 Time evolution of the spin-echo signal

We derive the exact time evolution of the spin-echo signal  $D_{\text{Echo}}(t)$  [see Eq. (8.10)] employing the equation of motion approach which permits the calculation of  $D_{\text{Echo}}(t)$  without knowing the probability distribution of the phase  $p(\varphi, t)$ . Other methods to calculate the spin-echo signal for classical telegraph noise make use of stochastic differential equations and get the same result [39, 34].

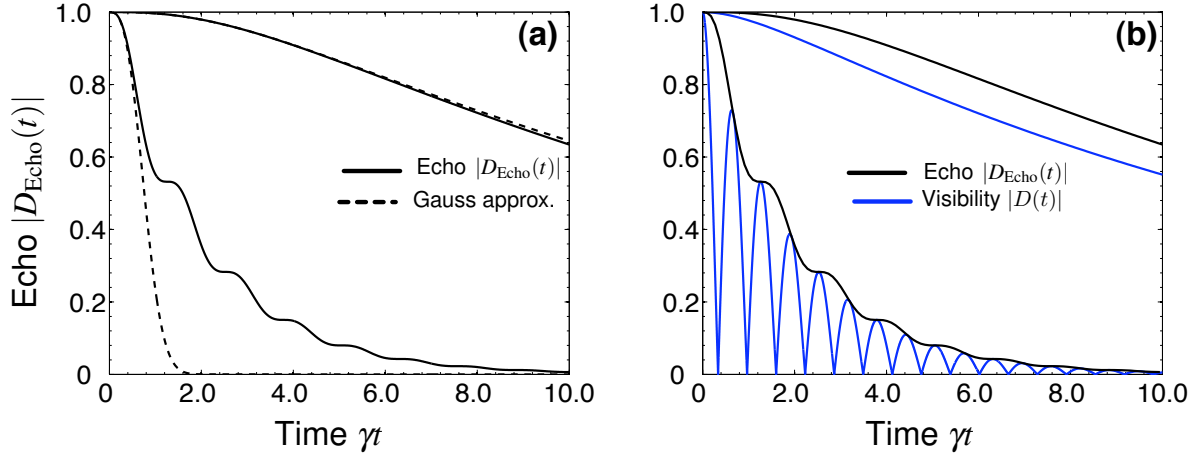


**Figure 8.4:** Time evolution of the spin-echo signal  $|D_{\text{Echo}}(t)|$  for classical telegraph noise when a  $\pi$ -pulse is applied at time  $t/2$ . (a) Spin-echo signal  $|D_{\text{Echo}}(t)|$  (solid line) in comparison to the Gaussian approximation (dashed line) for different coupling strengths  $v/\gamma = 0.5$  and  $v/\gamma = 10.0$ . For weak coupling  $v \ll \gamma$  the Gaussian result is a good approximation to the exact spin-echo signal whereas for strong-coupling  $v \gg \gamma$  the Gaussian approximation strongly underestimates the exact result. (b) Spin-echo signal in comparison with the visibility for (from top to bottom)  $v/\gamma = 0.5, 10.0$ . In the strong-coupling regime the spin-echo signal  $D_{\text{Echo}}(t)$  has plateaux at every second top of the visibility. The occurrence of plateaux in the time evolution of the echo reflects again the non-Gaussian properties of telegraph noise.

The idea of this approach is to calculate the coherence  $D(t)$  right before the  $\pi$ -pulse at  $t' = t/2 - \delta t$  with coupling  $v$  and right after the application of the pulse at  $t' = t/2 + \delta t$ , with a coupling whose sign is reversed  $v \rightarrow -v$ . Then both solutions match at  $t' = t/2$ :  $D(t/2 - \delta t; v) = D(t/2 + \delta t; -v)$ , the solution which fulfills this condition gives the spin-echo signal  $D_{\text{Echo}}(t)$  ( $\delta t$  is an infinitesimal time-interval). Details of the derivation can be found in App. C and we just present the results here. The spin-echo signal of a qubit subject to classical telegraph noise is equal to

$$D_{\text{Echo}}(t) = \frac{1}{2} e^{-\gamma/2} \left( \frac{\gamma}{2\delta} \right) \left[ \left( 1 + \frac{\gamma}{2\delta} \right) e^{\delta t} - \left( 1 - \frac{\gamma}{2\delta} \right) e^{-\delta t} - \frac{v^2}{\gamma\delta} \right], \quad (8.14)$$

where  $\delta = \frac{1}{2} \sqrt{\gamma^2 - v^2}$ . Figure 8.4(a) shows the spin-echo signal in comparison with the Gaussian approximation. In the weak-coupling limit ( $v \ll \gamma$ ) the Gaussian result is in good agreement with the exact spin-echo signal. However, for increasing coupling strength the Gaussian approximation fails even qualitatively. The most prominent feature in the time evolution of the spin-echo signal  $D_{\text{Echo}}(t)$  due to non-Gaussian telegraph noise is the occurrence of plateaux for  $v > \gamma$ . The heights of these plateaux are decaying exponentially with their position. A similar feature was observed in the charge echo experiments in qubits by NAKAMURA *et al.* in [69], [see Fig. 8.3(b)]. For  $v \gg \gamma$ ,  $\sqrt{\gamma/t}$  the spin-echo signal has the simple form

$$D_{\text{Echo}}(t) \approx e^{-\gamma/2} \left( 1 + \frac{\gamma}{v} \sin \frac{vt}{2} \right). \quad (8.15)$$

The plateaux arise when  $\frac{d}{dt}D_{\text{Echo}}(t) = 0$ , i.e.

$$v \cos \frac{vt}{2} - \gamma \sin \frac{vt}{2} = 1. \quad (8.16)$$

The positions of the plateaux are located at  $t^* \approx 4\pi k/v$ ,  $k$  is an integer number and indicates the position of the plateaux, and the heights of the plateaux decay exponentially with  $k$  like  $e^{-2\pi k\gamma/v}$ .

The comparison of the spin-echo signal  $D_{\text{Echo}}(t)$  and the visibility  $v(t)$  is presented in Fig. 8.4(b). At strong coupling the spin-echo signal has a plateau at every second top in the time evolution of the visibility. The short-time behaviour  $\gamma t \ll 1$  of  $D_{\text{Echo}}(t)$  can be approximated as

$$D_{\text{Echo}}(t) \approx 1 - \frac{1}{48}v^2\gamma^3 t^3, \quad (8.17)$$

irrespective of the ratio  $v/\gamma$ . The Gaussian approximation [see Eq. (8.12)] gives the same result. However, the long-time limit depends on the ratio  $v/\gamma$ . For  $\gamma t \gg 1$  we obtain

$$-\log D_{\text{Echo}}(t) \approx \begin{cases} v^2 t / 4\gamma, & v \ll \gamma \\ \gamma t / 2, & v > \gamma \end{cases} \quad (8.18)$$

Comparing  $D_{\text{Echo}}(t)$  with Eq. (8.13) one notices that the Gaussian result is the weak-coupling limit ( $v \ll \gamma$ ) of Eq. (8.14). Figure 8.4(a) shows that in the strong coupling case  $v \geq \gamma$  the Gaussian approximation strongly underestimates the exact result for the spin-echo signal for  $t > 2\pi/v$ . The origin of this discrepancy in the strong coupling regime  $v \gg \gamma$  is similar to the well-known *motional narrowing* of spectral lines, [70]. In that case the energy levels of the qubit are splitted rather than broadened. The fluctuator dynamics can be considered as slow and the qubit experiences rare hops between these levels. The splitting is of the order of  $v$  and the typical switching rate is  $\gamma$ . However, in the weak-coupling limit  $v \ll \gamma$  the levels are broadened and the typical decay rate of the echo signal is approximately  $v^2/4\gamma$ .

Knowing the position and height of the first plateau of the spin-echo signal permits one to determine both the coupling strength  $v$  and the switching rate  $\gamma$  from experimental data. In NAKAMURA'S charge echo experiment the first plateau arises at  $t^* = 3.5$  ns at a height of  $|D_{\text{Echo}}| = 0.3$  [see Fig. 8.3(c)]. This yields for the coupling-strength  $v \approx 570$  MHz and  $\gamma = 110$  MHz for the switching rate. If the fluctuator is a charge trap near the gate then the fluctuator interacts via a fluctuating dipole field with the qubit with a coupling strength  $v = e^2(\vec{a} \cdot \vec{r})/r^3$ . We estimate the qubit-gate distance by  $r = 0.5 \mu\text{m}$ , and we get an estimate for the tunneling distance between the charge trap and the gate of  $a \approx 80 \text{ \AA}$ , which seems to be reasonable.

Finally, Fig. 8.5 displays the effect of the offset  $\Delta\gamma/\gamma$  on the time evolution of the spin-echo signal  $|D_{\text{Echo}}(t)|$ . At strong coupling (b) the height of the plateaux are increased but the steps in-between are lifted for increasing  $\Delta\gamma/\gamma$ .

## 8.3 Quantum spin-echo

The dynamical decoupling of a qubit subject to non-Gaussian quantum noise due to intrinsic background fluctuators is considered. We present an exact derivation of the spin-echo signal based on a trace-formula for a single idealized instantaneous  $\pi$ -pulse as well as the generalization for arbitrary pulse sequences.

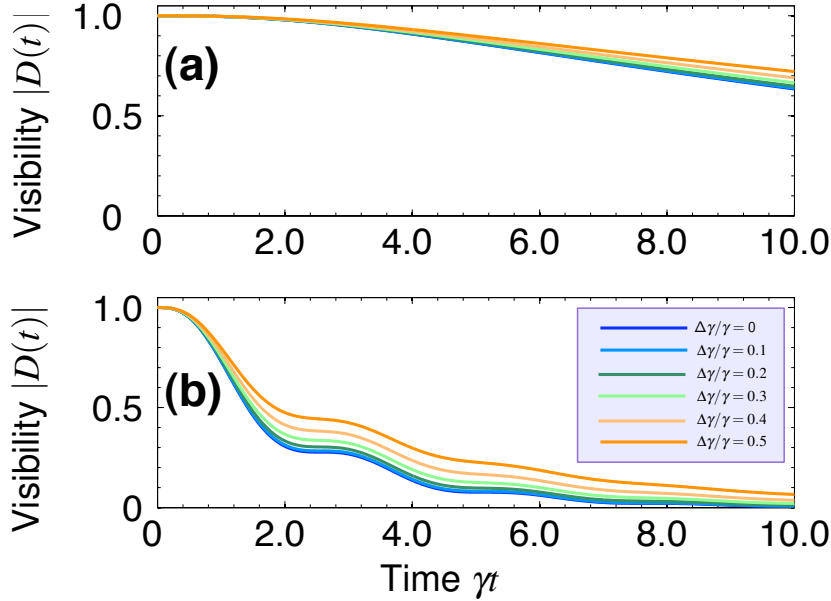


**Figure 8.5:** Time evolution of the spin-echo signal  $D_{\text{Echo}}(t)$  for (a)  $v/\gamma = 0.5$  and (b)  $v/\gamma = 5.0$  for different offsets  $\Delta\gamma/\gamma = 0, 0.1, 0.2, 0.3, 0.4, 0.5$ .

### 8.3.1 Time evolution of the spin-echo signal: General exact solution

Let's derive the spin-echo signal when a  $\pi$ -pulse is applied at  $t' = t/2$  and the signal is observed after the elapsed time  $t$ . We assume that the system is initially prepared in the product state  $|\psi(0)\rangle = 1/\sqrt{2}(|\uparrow\rangle + |\downarrow\rangle) \otimes |\chi\rangle$  and the interaction between qubit and environment is switched on for  $t' > 0$ . The Hamiltonian of the system is equal to

$$\hat{\mathcal{H}} = \frac{\Delta}{2} \hat{\sigma}_z + \frac{v}{2} \hat{Q} \hat{\sigma}_z + \hat{\mathcal{H}}_B. \quad (8.19)$$

During its time evolution qubit and heat-bath get entangled and the state at  $t' < t/2$  is described by

$$|\psi(t')\rangle = \frac{1}{\sqrt{2}} \left( e^{-i\Delta t'/2} e^{-i(\hat{\mathcal{H}}_B + v\hat{Q}/2)t'} |\uparrow\rangle \otimes |\chi\rangle + e^{i\Delta t'/2} e^{i(\hat{\mathcal{H}}_B - v\hat{Q}/2)t'} |\downarrow\rangle \otimes |\chi\rangle \right), \quad (8.20)$$

where  $|\chi\rangle$  is a thermal state of the heat-bath. The effect of the  $\pi$ -pulse  $e^{i\pi\hat{\sigma}_x/2}$  at  $t' = t/2$  on the qubit flips the eigenstates, i.e.  $|\uparrow\rangle \rightarrow |\downarrow\rangle$  and  $|\downarrow\rangle \rightarrow |\uparrow\rangle$ . The heat-bath state  $|\chi\rangle$  will then evolve according to the Hamiltonian  $\hat{\mathcal{H}}_B \mp (v/2)\hat{Q}$  which effectively corresponds to a reversed sign of the coupling  $v$ . For times  $t > t/2$  the state of the system can be written as

$$|\psi(t')\rangle = \frac{i}{\sqrt{2}} \left( e^{-i(\hat{\mathcal{H}}_B - v\hat{Q}/2)t/2} e^{-i(\hat{\mathcal{H}}_B + v\hat{Q}/2)t/2} |\uparrow\rangle \otimes |\chi\rangle + e^{-i(\hat{\mathcal{H}}_B + v\hat{Q}/2)t/2} e^{-i(\hat{\mathcal{H}}_B - v\hat{Q}/2)t/2} |\downarrow\rangle \otimes |\chi\rangle \right), \quad (8.21)$$

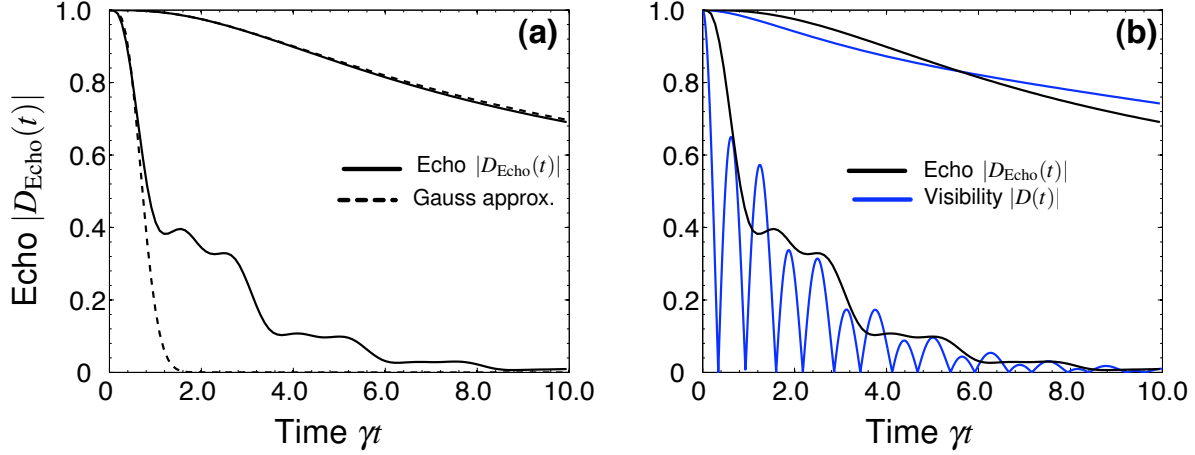


**Figure 8.6:** Time evolution of the spin-echo signal  $|D_{\text{Echo}}(t)|$  for quantum telegraph noise when a  $\pi$ -pulse is applied at  $t/2$  and the echo is observed after the time  $t$ . (a) Spin-echo signal  $|D_{\text{Echo}}(t)|$  (solid line) in comparison to the Gaussian approximation (dashed line) for different coupling strengths  $v/\gamma = 0.5$  and  $v/\gamma = 10.0$  at low temperature  $T/\gamma = 0.1$ . (b) Spin-echo signal in comparison with the visibility for (from top to bottom)  $v/\gamma = 0.5, 10.0$  at low temperature  $T/\gamma = 0.1$ .

The reduced density matrix  $\hat{\rho}^{\text{red}}(t)$  can then be written in the same way as in Eq. (8.9) but with the spin-echo signal  $D_{\text{Echo}}(t)$

$$D_{\text{Echo}}(t) = \left\langle e^{i(\hat{\mathcal{H}}_B - v\hat{Q}/2)t/2} e^{i(\hat{\mathcal{H}}_B + v\hat{Q}/2)t/2} e^{-i(\hat{\mathcal{H}}_B - v\hat{Q}/2)t/2} e^{-i(\hat{\mathcal{H}}_B + v\hat{Q}/2)t/2} \right\rangle. \quad (8.22)$$

We have already encountered expectation values of the form above and we now apply the same trace-formula which leads to a determinant for the coherence. Identifying the time evolution operator  $\hat{U}_{\pm,t} = e^{-i(\hat{\mathcal{H}}_B \pm v\hat{Q}/2)t}$  we can apply Eq. (7.10) to Eq. (8.22), and we recast the result for  $D_{\text{Echo}}(t)$  as a determinant

$$D_{\text{Echo}}(t) = \det \left[ 1 - \hat{n} + \hat{U}_{-\frac{t}{2}}^\dagger \hat{U}_{+\frac{t}{2}}^\dagger \hat{U}_{-\frac{t}{2}} \hat{U}_{+\frac{t}{2}} \hat{n} \right], \quad (8.23)$$

where  $\hat{U}_{\pm,t} = e^{-i(\hat{\mathcal{H}}_B \pm v\hat{Q}/2)t}$  is the time evolution operator in the single particle basis and  $\hat{n}_{\alpha\beta} = f_T(\epsilon_\alpha) \delta_{\alpha\beta}$  is the occupation number operator,  $f_T(\epsilon)$  is the Fermi-Dirac distribution. The Hamiltonian of the heat-bath is assumed to diagonal in this basis, i.e.  $\hat{H}_{B,\alpha\beta} = \epsilon_\alpha \delta_{\alpha\beta}$  and the charge operator is given by

$$\hat{Q}_{\alpha\beta} = \frac{1}{\pi v_0} \sqrt{\text{Im}G^R(\omega = \epsilon_\alpha) \text{Im}G^R(\omega = \epsilon_\beta)}, \quad (8.24)$$

where  $v_0$  is the density of states in the conduction band and  $G^R(\omega) = (\omega - \epsilon + i\gamma/2)^{-1}$  is the retarded Green's function of the fluctuator and  $\gamma$  is the switching rate.

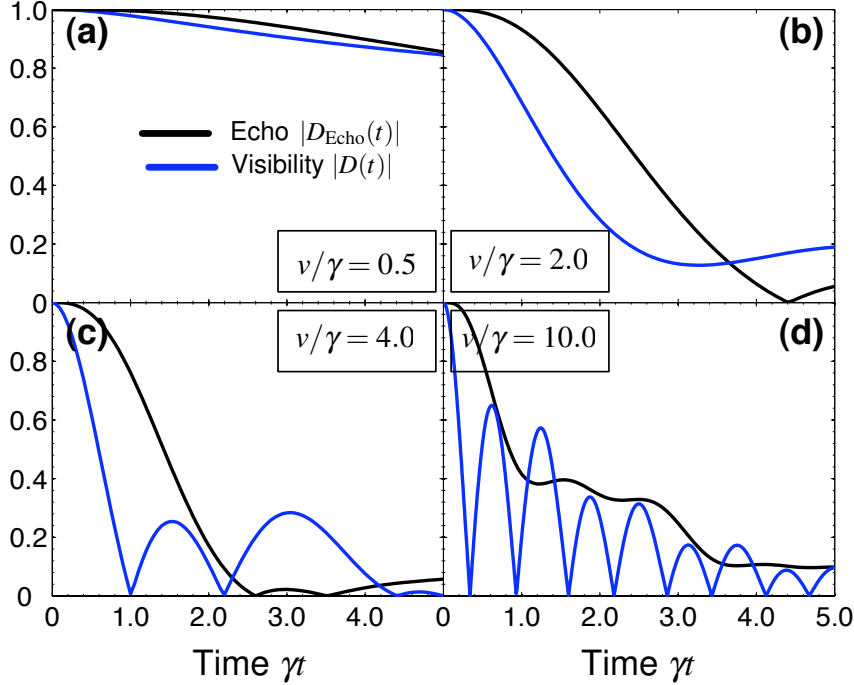


**Figure 8.7:** Time evolution of the spin-echo signal  $|D_{\text{Echo}}(t)|$  and the corresponding visibility  $v(t)$  for different couplings  $v$ . From (a)-(d)  $v/\gamma = 0.5, 2.0, 4.0, 10.0$ ,  $T/\gamma = 0.1$  and  $\varepsilon = 0$ . This figure shows the transition from weak- to strong-coupling [from (a)-(d)] for the visibility and the corresponding echo according to the phase diagram of the fluctuator.

### 8.3.2 Time evolution of the echo according to the Gaussian approximation

We derive the expression for the spin-echo signal in the Gaussian approximation. As in Sec. 7.3 we assume  $\hat{Q}$  to be a linear superposition of harmonic oscillator coordinates which are in thermal equilibrium. Then the Gaussian approximation of the spin-echo signal is equal to

$$D_{\text{Gauss}}^{\text{Echo}}(t) = \exp \left[ -\frac{v^2}{2} \int_0^t dt_1 \int_0^t dt_2 \beta(t-t') \beta(t-t'') \langle \hat{X} \delta \hat{Q}(t') \delta \hat{Q}(t'') \rangle \right], \quad (8.25)$$

and the modulus of the spin-echo signal  $|D_{\text{Gauss}}(t)|$  may be expressed as

$$|D_{\text{Gauss}}^{\text{Echo}}(t)| = \exp \left[ -\frac{v^2}{2} \int_0^t dt_1 \int_0^t dt_2 \beta(t-t') \beta(t-t'') \frac{1}{2} \langle [\delta \hat{Q}(t'), \delta \hat{Q}(t'')]_+ \rangle \right]. \quad (8.26)$$

The Gaussian approximation for the spin-echo signal is equal to

$$|D_{\text{Gauss}}^{\text{Echo}}(t)| = \exp \left[ -\frac{v^2}{2} \int \frac{d\omega}{2\pi} \langle \delta \hat{Q} \delta \hat{Q} \rangle_{\omega} \frac{\sin^4(\omega t/4)}{(\omega/4)^2} \right], \quad (8.27)$$

and the noise-power  $\langle \delta \hat{Q} \delta \hat{Q} \rangle_{\omega}$  is given by Eq. (7.26). Figure 8.6(a) shows the time evolution of the exact spin-echo signal  $|D_{\text{Echo}}(t)|$  compared against the Gaussian approximation  $D_{\text{Echo}}^{\text{Gauss}}(t)$  in

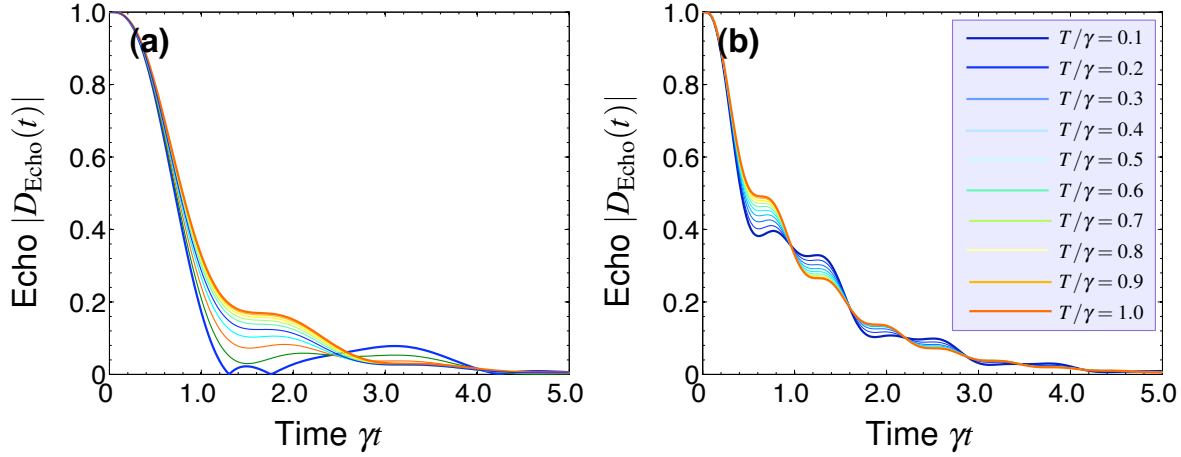


**Figure 8.8:** Time evolution of the spin-echo signal  $|D_{\text{Echo}}(t)|$  for different temperatures  $T$ , and coupling strengths (a)  $v/\gamma = 4.0$ , (b)  $v/\gamma = 10.0$ , (Other parameters  $\varepsilon = 0$ ).

the strong- and weak-coupling regime. For weak-coupling the Gaussian result is a good approximation to the exact spin-echo signal whereas for strong-coupling the Gaussian approximation strongly underestimates the exact result.

### 8.3.3 Exact numerical results and discussion

Here we discuss the time evolution of the spin-echo signal  $D_{\text{Echo}}(t)$  which has been obtained by direct numerical evaluation of the determinant in Eq. (8.23) that yield the exact time evolution of the spin-echo signal of a qubit subject to charge fluctuations of intrinsic background fluctuators. We employ a discretization of  $N$  equally spaced energy levels  $\varepsilon_n = n\delta$  within an energy band of width  $2W$ ,  $\varepsilon_n \in [-W, W]$  such that the density of states in the conduction band is constant  $\nu_0 = N/2W$ . Convergence has been already achieved for  $W = 20$  and  $N = 400$ .

Figure 8.7 shows the time evolution of the spin-echo signal compared against the visibility in the low-temperature regime  $T \ll \gamma$  for increasing coupling strength  $\nu$ . This figure shows the transition from the weak-coupling to the strong-coupling regime according to the phase diagram [see Fig. 7.8]. For weak-coupling the spin-echo signal is always larger than the corresponding visibility at least in the observed time-interval. However, for increasing coupling-strength one encounters regions of larger visibility, which means that spin-echo pulses become insufficient to maintain phase-coherence. Beyond a certain threshold one observes zeros in the time evolution of the spin-echo signal with complete loss of echo and revivals in-between. At strong-coupling [see Fig. 8.7(d)] plateaux occur in the time evolution of  $|D_{\text{Echo}}(t)|$ .

Finally, Fig. 8.8 displays the time evolution of the spin-echo signal  $|D_{\text{Echo}}(t)|$  in the strong coupling regime for different temperatures. At high temperature the spin-echo signal corresponds to the classical result and its time evolution shows a steplike behaviour. If temperature is decreased the height of the first plateau is lowered and the height of the second plateau is increased [see Fig. 8.8(a)] until  $|D_{\text{Echo}}(t)|$  reaches the time-axis and zeros in the time evolution of

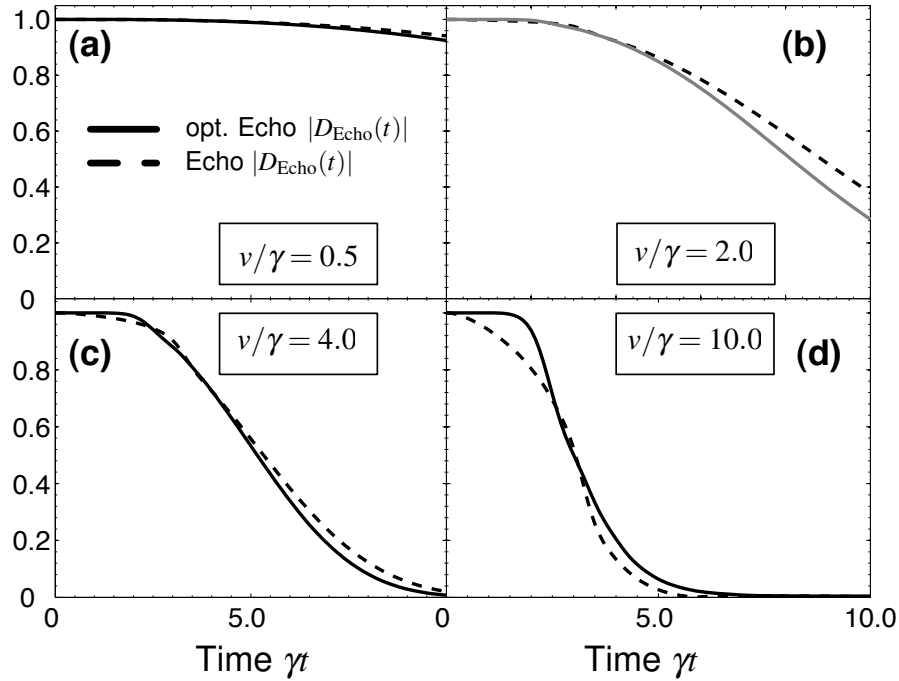


**Figure 8.9:** Time evolution of the spin-echo signal for a sequence of 10 instantaneous  $\pi$ -pulses. The dashed line shows the spin-echo signal for a sequence of 10 instantaneous equidistant pulses. Comparison with the "optimized" sequence (solid line) in the low-temperature regime  $T/\gamma = 0.1$  for different coupling strengths  $v/\gamma = 0.5, 2.0, 4.0, 10.0$ ,  $\varepsilon = 0$ .

the spin-echo signal occur. In Fig. 8.8(b) the height of the first plateau is lowered when temperature is decreased but does not reach the horizontal axis. Subsequent plateaux show the opposite behavior in an alternating pattern.

### 8.3.4 Arbitrary pulse-sequences

It is possible to maintain phase coherence of the qubit even more efficiently than for a single  $\pi$ -pulse by applying sequences of repeated  $\pi$ -pulses on the qubit. Several pulse-sequences have been proposed e.g. a sequence of equidistant  $\pi$ -pulses CPMG-cycle, Bang-Bang protocols [71] or optimized versions of the CPMG-cycle where the duration between consecutive pulses may vary in order to optimize the phase coherence of the qubit [64].

We show the generalization of the approach introduced in Sec. 8.3 to sequences of  $N$   $\pi$ -pulses at arbitrary times of arbitrary duration between consecutive pulses. Let us split the time-interval  $[0, t]$  into  $N$  subintervals  $\delta_i t$ :  $0 \rightarrow \delta_1 \rightarrow \delta_2 \rightarrow \dots \rightarrow \delta_N < 1$  such that at each instance of time  $\delta_i t$  a  $\pi$ -pulse is applied on the qubit. The spin-echo signal can then be written as

$$D_{\text{Echo}}(t) = \left\langle \hat{u}_{-, \delta_1 t}^\dagger \hat{u}_{+, (\delta_2 - \delta_1) t}^\dagger \cdots \hat{u}_{\mp, (\delta_N - \delta_{N-1}) t}^\dagger \hat{u}_{\pm, (\delta_N - \delta_{N-1}) t} \cdots \hat{u}_{-, (\delta_2 - \delta_1) t} \hat{u}_{+, \delta_1 t} \right\rangle, \quad (8.28)$$

where  $\hat{U}_{\pm,(\delta_i-\delta_j)t} = e^{-i(\hat{H}_B \pm v\hat{Q}/2)(\delta_i-\delta_j)t}$  is the time evolution operator during the time-interval  $(\delta_i - \delta_j)t$ . Using Eq. (8.23) we can express the above expectation value as

$$D_{\text{Echo}}(t) = \det \left[ 1 - \hat{n} + \hat{U}_{-, \delta_1 t}^\dagger \hat{U}_{+, (\delta_2 - \delta_1)t}^\dagger \cdots \hat{U}_{\mp, (\delta_N - \delta_{N-1})t}^\dagger \cdots \hat{U}_{\pm, (\delta_N - \delta_{N-1})t} \cdots \hat{U}_{-, (\delta_2 - \delta_1)t} \hat{U}_{+, \delta_1 t} \hat{n} \right], \quad (8.29)$$

where  $\hat{U}_{\pm,(\delta_i-\delta_j)t}$  is the time evolution operator during the time-interval  $(\delta_i - \delta_j)t$  written in the single-particle basis. Although the optimized sequence of  $N$   $\pi$ -pulse was found for a spin-boson model with an Ohmic noise-power, we employ here the same sequence and check whether it is more efficient than the CPMG-cycle for the same number of pulses in the case of quantum telegraph noise. The instance of time  $\delta_j t$  at which the  $j$ -th  $\pi$ -pulse is applied is equal to

$$\delta_j = \sin^2 \left( \frac{\pi j}{2N+2} \right). \quad (8.30)$$

In Fig. 8.9 we display the spin-echo signal for the optimized sequence of  $N = 10$  instantaneous  $\pi$ -pulses compared against the CPMG-cycle for equidistant pulses for different coupling strengths at low temperature. Only for short times and at large coupling [see [Fig. 8.9(d)] a significant enhancement of the ‘‘optimized’’ pulse sequence is observed.

## 8.4 Summary

In this chapter we discussed spin-echo experiments of a qubit subject to non-Gaussian quantum telegraph noise. We analyzed the high-temperature limit (classical) and showed that plateaux arise in the time evolution of  $|D_{\text{Echo}}(t)|$  in the strong-coupling regime. Furthermore, we have shown an exact quantum mechanical solution of the spin-echo signal for single instantaneous  $\pi$ -pulse as well as for generalizations to arbitrary sequences of pulses. A numerical simulation of  $D_{\text{Echo}}(t)$  was performed for various regimes and parameters.

*An expert is a man who has made all the mistakes which can be made in a very narrow field.*

NIELS BOHR

# Chapter 9

## Open questions

THE extension of the model of a single localized impurity level to many background fluctuators coupled to a charge qubit is straightforward and is of great interest in current research. In that case the fluctuating charge  $\hat{Q} = \sum_{i=1}^N v_i \hat{d}_i^\dagger \hat{d}_i$  contains the contributions from many defect levels inside the metal, where  $v_i$  is the coupling to the  $i$ -th impurity. One may introduce a distribution such as  $P(v) \propto 1/v^2$ . As a consequence all results need to be averaged over the distribution of couplings. However, the time evolution of the density matrix of the full quantum mechanical model has not been achieved so far and calculations for the dynamics of the coherence remained in the classical limit [39, 36].

Another interesting system is a disordered metallic quantum dot which is tunnel-coupled to some electron reservoir [see Fig. 9.1]. A qubit placed nearby the quantum dot experiences the charge fluctuations  $\delta\hat{Q}$  inside the dot. Charge-correlations inside disordered quantum dots are usually described by Random Matrix Theory (or supersymmetric non-linear  $\sigma$ -models), which assumes a random hermitean Hamiltonian for the dot with Gaussian-distributed entries. As a result the energy-levels of the system are correlated with mean density according to WIGNER'S semi-circle and the level-spacing follows a WIGNER-DYSON distribution. We expect the charge fluctuations inside the dot to be non-Gaussian and it is challenging to calculate the coherence.

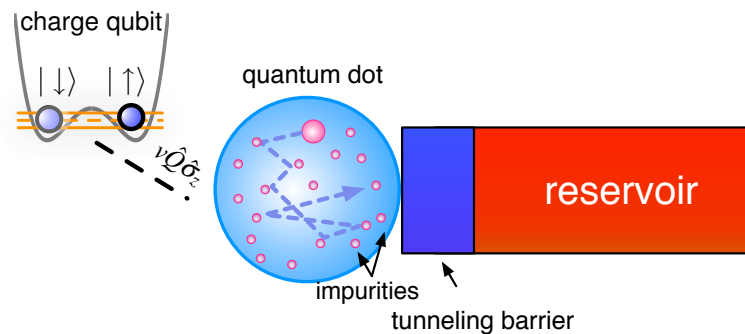


**Figure 9.1:** *Open disordered quantum dot coupled to an electronic reservoir. A qubit longitudinally coupled to the charge fluctuations inside the QD will experience non-Gaussian fluctuations.*



## Hamiltonian of the three-junction flux qubit

### A.1 Calculation of the Hamiltonian

IN this appendix we calculate the Hamiltonian of the three-junction flux qubit [see Fig. A.1]. Three superconducting islands are connected by tunnel junctions with capacitance  $C$  and Josephson coupling  $E_J$ , the top junction is by a factor  $\alpha$  smaller and has capacitance  $\alpha C$  and Josephson coupling  $\alpha E_J$ . We derive the classical equation of motion for the phase-difference  $\Delta\varphi_i$  across the junction. The current along the left (L), right (R) and top (T) edges of the circuit are given by,

$$I_L = I_0 \sin(\Delta\varphi_1) + C\dot{V} = I_0 \sin(\Delta\varphi_1) + C \frac{\phi_0}{2\pi} \Delta\ddot{\varphi}_1, \quad (\text{A.1})$$

$$I_R = I_0 \sin(\Delta\varphi_3) + C \frac{\phi_0}{2\pi} \Delta\ddot{\varphi}_3, \quad (\text{A.2})$$

$$I_T = \alpha I_0 \sin(\Delta\varphi_1 - \Delta\varphi_3 + 2\pi f) + \alpha C \frac{\phi_0}{2\pi} (\Delta\ddot{\varphi}_1 - \Delta\ddot{\varphi}_3), \quad (\text{A.3})$$

where  $I_0 = I_c \Phi_0 / (2\pi)$  and  $I_c$  is the critical current that the junction can carry without dissipation. We have defined the phase differences across the junctions as  $\Delta\varphi_1 = \varphi_1 - \varphi_2$  and  $\Delta\varphi_3 = \varphi_3 - \varphi_2$ . Current conservation imposes the following condition on the currents

$$I_L = -I_R = I_T. \quad (\text{A.4})$$

The Lagrangian  $L(\{\Delta\varphi_i, \Delta\dot{\varphi}_i\})$  is equal to

$$\begin{aligned} L(\{\Delta\varphi_i, \Delta\dot{\varphi}_i\}) = & \frac{C}{2} \left( \frac{\phi_0}{2\pi} \right)^2 \Delta\dot{\varphi}_1^2 + \frac{C}{2} \left( \frac{\phi_0}{2\pi} \right)^2 \Delta\dot{\varphi}_3^2 + \frac{\alpha C}{2} \left( \frac{\phi_0}{2\pi} \right)^2 (\Delta\dot{\varphi}_1 - \Delta\dot{\varphi}_3)^2 \\ & + E_J \cos(\Delta\varphi_1) + E_J \cos(\Delta\varphi_3) + \alpha E_J \cos(\Delta\varphi_1 - \Delta\varphi_3 + 2\pi f). \end{aligned} \quad (\text{A.5})$$

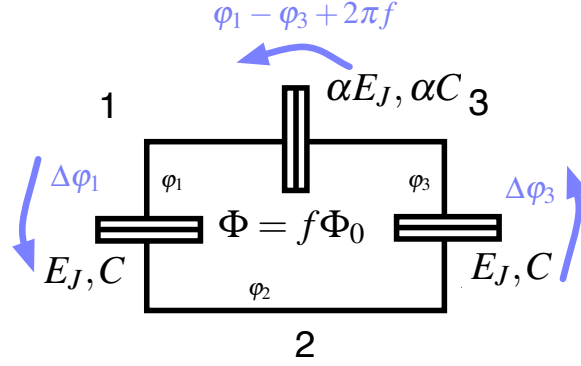


**Figure A.1:** Circuit diagram of the three junction flux qubit. Three superconducting islands are connected by Josephson junctions. Left and right junctions have capacitance  $C$  and Josephson coupling energy  $E_J$ , the top junction has capacitance  $\alpha C$  and Josephson coupling  $\alpha E_J$ . The three junction flux qubit encloses a magnetic flux  $\Phi = f\Phi_0$ .

The canonical conjugated variables  $q_i = \frac{\partial L}{\partial \Delta\phi_i}$  are given by

$$q_1 = C \left( \frac{\phi_0}{2\pi} \right)^2 \Delta\phi_1 + \alpha C \left( \frac{\phi_0}{2\pi} \right)^2 \Delta\phi_3, \quad (\text{A.6})$$

$$q_3 = C \left( \frac{\phi_0}{2\pi} \right)^2 \Delta\phi_3 - \alpha C \left( \frac{\phi_0}{2\pi} \right)^2 (\Delta\phi_1 - \Delta\phi_3).$$

From the equations above the expression for  $\Delta\phi_i$  follows as

$$\Delta\phi_1 = \frac{1}{C(\phi_0/2\pi)^2} \frac{1+\alpha}{1+2\alpha} q_1 + \frac{1}{C(\phi_0/2\pi)^2} \frac{1}{1+2\alpha} q_3, \quad (\text{A.7})$$

$$\Delta\phi_3 = \frac{1}{C(\phi_0/2\pi)^2} \frac{\alpha}{1+2\alpha} q_1 + \frac{1}{C(\phi_0/2\pi)^2} \frac{1}{1+2\alpha} q_3.$$

The Legendre-transformation delivers the Hamiltonian  $H(\{q_i, \Delta\phi_i\}) = \sum_{i=1}^2 q_i \Delta\phi_i - L(\{\Delta\phi_i, \Delta\dot{\phi}_i\})$  which is equal to

$$H = \frac{4e^2/(2C)}{(2e(\phi_0/2\pi))^2} \left( \frac{1+\alpha}{1+2\alpha} q_1^2 + \frac{2\alpha}{1+2\alpha} q_1 q_3 + \frac{1+\alpha}{1+2\alpha} q_3^2 \right) - E_J \cos(\Delta\phi_1) - E_J \cos(\Delta\phi_3) - \alpha E_J \cos(\Delta\phi_1 - \Delta\phi_3 + 2\pi f). \quad (\text{A.8})$$

From the Hamiltonian equations  $\Delta\phi_i = \partial H / \partial q_i$  and  $\dot{q}_i = -\partial H / \partial \Delta\phi_i$  one obtains the classical equations of motion. We now write down the Hamiltonian  $H(\{q_i, \phi_i\})$  in the charge basis, using  $q_i = (\phi_0/2\pi) Q_i$ , where  $Q_i$  is the excess charge on each island, we can rewrite the Hamiltonian in the form  $H = H_C + H_T$ ,

$$H_C = \frac{1}{2C} \left( Q_1^2 + Q_3^2 - \frac{(Q_1 - Q_3)^2}{2 + 1/\alpha} \right), \quad (\text{A.9})$$

for the charging part and

$$H_T = -\frac{EJ}{2} \left( e^{i(\varphi_2 - \varphi_1)} + e^{i(\varphi_3 - \varphi_2)} + \alpha e^{i(\varphi_1 - \varphi_3 + 2\pi f)} + \text{h.c.} \right), \quad (\text{A.10})$$

for the tunneling part of the Hamiltonian. Quantum mechanically,  $Q_i$  and  $\Delta\varphi_i$  become canonically conjugated operators and one imposes the commutation relation  $[\hat{Q}_i, \Delta\hat{\varphi}_j] = 2i|e|\delta_{ij}$ .



## Coherence for classical telegraph noise

THE coherence  $D(t) = \langle e^{i\varphi(t)} \rangle$  can be derived as an average over the phase  $\varphi(t)$  which requires the explicit knowledge of the distribution function for the random phase  $p(\varphi, t)$ . However, it is easier to use an equation of motion approach which circumvents the use of the probability distribution. The system of coupled differential equations for the time evolution of  $\langle e^{i\varphi_\xi(t)} \rangle$ , derived in Sec. 6.5, is equal to

$$\frac{d}{dt} \langle e^{i\varphi_\xi(t)} \rangle = -iv \langle \xi(t) e^{i\varphi_\xi(t)} \rangle, \quad (\text{B.1})$$

$$\frac{d}{dt} \langle \xi(t) e^{i\varphi_\xi(t)} \rangle = -\gamma \langle \xi(t) e^{i\varphi_\xi(t)} \rangle + (\Delta\gamma - iv) \langle e^{i\varphi_\xi(t)} \rangle,$$

where  $\varphi_\xi(t) = -v \int_0^t dt' \xi(t')$ ,  $v$  is the coupling of the qubit to the fluctuator which switches between  $\xi = \pm 1$  at the rate  $\gamma$  and  $\Delta\gamma = \gamma^+ - \gamma^-$ . The coherence for classical telegraph noise (i.e. for a fluctuator with  $Q = 0/1$ ) and the solution of Eq. (B.1) are related by  $D(t) = e^{-ivt/2} \langle e^{i\varphi_\xi(t)} \rangle|_{v/2}$ . We will first show the solution for  $\langle e^{i\varphi_\xi(t)} \rangle$  and then relate that result to the coherence  $D(t)$  for classical telegraph noise.

We make the following ansatz for the solution (spezializing to  $\Delta\gamma = 0$ ):

$$\begin{pmatrix} \langle e^{i\varphi_\xi(t)} \rangle \\ \langle \xi(t) e^{i\varphi_\xi(t)} \rangle \end{pmatrix} = \vec{a} e^{\lambda t}. \quad (\text{B.2})$$

Inserting the ansatz into Eq. (B.1) reduces the system of differential equations to a system of linear equations,

$$\begin{pmatrix} \lambda & iv \\ iv & \lambda + \gamma \end{pmatrix} \vec{a} e^{\lambda t} = 0. \quad (\text{B.3})$$

The system of linear equations has only a solution for certain eigenfrequencies  $\lambda$  and eigenvectors  $\vec{a}$  if the determinant of the matrix of coefficients vanishes, i.e.

$$\det \begin{pmatrix} \lambda & iv \\ iv & \lambda + \gamma \end{pmatrix} = 0. \quad (\text{B.4})$$

- *Eigenfrequencies:* We obtain the eigenfrequencies  $\lambda_{1,2}$  as the solution of the characteristic equation  $\lambda^2 + \lambda\gamma + v^2 = 0$  to be equal to

$$\lambda_{1,2} = -\frac{\gamma}{2} \pm \sqrt{\left(\frac{\gamma}{2}\right)^2 - v^2} \quad (\text{B.5})$$

- *Eigenvectors*

$$\vec{a}_{\lambda_1} = \frac{1}{iv} \begin{pmatrix} -\gamma/2 - \delta \\ iv \end{pmatrix}, \quad (\text{B.6})$$

$$\vec{a}_{\lambda_2} = \frac{1}{iv} \begin{pmatrix} -\gamma/2 + \delta \\ iv \end{pmatrix} \quad (\text{B.7})$$

$$(\text{B.8})$$

- *Solution:* An arbitrary solution of Eq. (B.1) can be written as:

$$\begin{pmatrix} \langle e^{i\varphi_\xi(t)} \rangle \\ \langle \xi(t) e^{i\varphi_\xi(t)} \rangle \end{pmatrix} = \frac{C_1}{iv} \begin{pmatrix} -\gamma/2 - \delta \\ iv \end{pmatrix} e^{(-\gamma/2 + \delta)t} + \frac{C_2}{iv} \begin{pmatrix} -\gamma/2 + \delta \\ iv \end{pmatrix} e^{(-\gamma/2 - \delta)t}, \quad (\text{B.9})$$

where we have defined  $\delta = \sqrt{(\gamma/2)^2 - v^2}$ , and  $\lambda_{1,2} = -\gamma/2 \pm \delta$ .

- *Initial conditions:* The constants  $C_{1,2}$  follow from the initial conditions at  $t = 0$

$$\begin{pmatrix} \langle e^{i\varphi_\xi(t)} \rangle \\ \langle \xi(t) e^{i\varphi_\xi(t)} \rangle \end{pmatrix} \Big|_{t=0} = \begin{pmatrix} 1 \\ 0 \end{pmatrix} \quad (\text{B.10})$$

The coefficients  $C_{1,2}$  are equal to

$$C_1 = -\frac{iv}{2\delta}, \quad (\text{B.11})$$

$$C_2 = -C_1 = \frac{iv}{2\delta}. \quad (\text{B.12})$$

Finally, the solution for the coherence  $D(t) = e^{-ivt/2} \langle e^{i\varphi_\xi(t)} \rangle|_{v/2}$  of a qubit subject to classical telegraph noise is equal to

$$D(t) = \frac{1}{2} e^{-i(v-i\gamma)t/2} \left[ \left(1 + \frac{\gamma}{2\delta}\right) e^{\delta t} + \left(1 - \frac{\gamma}{2\delta}\right) e^{-\delta t} \right], \quad (\text{B.13})$$

where  $\delta = \frac{1}{2} \sqrt{\gamma^2 - v^2}$ , when ‘‘up’’- and ‘‘down’’-jumps are equally likely. The calculation for  $\Delta\gamma \neq 0$  follows the same steps which lead to Eq. (B.13) but now with  $\lambda_{1,2} = -\gamma/2 \pm \delta$ , where  $\delta = \sqrt{(\gamma/2)^2 - iv(\Delta\gamma - iv)}$ . An arbitrary solution is then given by

$$\begin{pmatrix} \langle e^{i\varphi_\xi(t)} \rangle \\ \langle \xi(t) e^{i\varphi_\xi(t)} \rangle \end{pmatrix} = \frac{C_1}{\Delta\gamma - iv} \begin{pmatrix} \gamma/2 + \delta \\ \Delta\gamma - iv \end{pmatrix} e^{(-\gamma/2 + \delta)t} + \frac{C_2}{\Delta\gamma - iv} \begin{pmatrix} \gamma/2 - \delta \\ \Delta\gamma - iv \end{pmatrix} e^{(-\gamma/2 - \delta)t}, \quad (\text{B.14})$$

and the coefficients  $C_{1,2}$  follow from the initial conditions<sup>1</sup> at  $t = 0$ :

$$\left( \begin{array}{c} \langle e^{i\varphi_{\xi}(t)} \rangle \\ \langle \xi(t) e^{i\varphi_{\xi}(t)} \rangle \end{array} \right) \Big|_{t=0} = \left( \begin{array}{c} 1 \\ \Delta\gamma/\gamma \end{array} \right), \quad (\text{B.15})$$

We obtain for the coefficients  $C_{1,2}$

$$C_1 = \frac{1}{2\delta} \left[ \Delta\gamma - iv - \frac{\Delta\gamma}{\gamma}(\gamma/2 - \delta) \right], \quad (\text{B.16})$$

$$C_2 = \frac{1}{2\delta} \left[ -(\Delta\gamma - iv) + \frac{\Delta\gamma}{\gamma}(\gamma/2 + \delta) \right]. \quad (\text{B.17})$$

The final solution for the coherence  $D(t)$  is then equal to

$$D(t) = \frac{1}{2} e^{-i(v-i\gamma)t/2} \left[ \left( 1 + \frac{\gamma - (iv/2)(\Delta\gamma/\gamma)}{2\delta} \right) e^{\delta t} + \left( 1 - \frac{\gamma - (iv/2)(\Delta\gamma/\gamma)}{2\delta} \right) e^{-\delta t} \right], \quad (\text{B.18})$$

here  $\delta = \sqrt{(\gamma/2)^2 - (iv/2)[\Delta\gamma - (iv/2)]}$ .

---

<sup>1</sup>At  $t = 0$ ,  $\langle \xi(t) e^{i\varphi_{\xi}(t)} \rangle = p_+(0) - p_-(0)$ , where  $p_{\pm}$  is the probability for the fluctuator to be  $\pm 1$ . With the detailed balance condition,  $\gamma_- p_+ - \gamma_+ p_- = 0$  we obtain  $\langle \xi(t) e^{i\varphi_{\xi}(t)} \rangle = \Delta\gamma/\gamma$ .



## Spin-echo signal for classical telegraph noise

WE present the calculation of the spin-echo signal  $D_{\text{Echo}}(t) = \langle e^{i\tilde{\varphi}(t)} \rangle$  with the random phase  $\tilde{\varphi}(t) = -v \int_0^t dt' \text{sign}(t/2 - t') Q(t')$ , for classical telegraph noise when a  $\pi$ -pulse is applied at  $t' = t/2$  on the qubit and the echo is observed after the time-interval  $[0, t]$ . We will use the equation of motion approach for the time evolution of  $\langle e^{i\tilde{\varphi}_\xi(t)} \rangle$  and relate its solution to the spin-echo signal for classical telegraph noise by  $D_{\text{Echo}}(t) = \langle e^{i\tilde{\varphi}_\xi(t)} \rangle|_{v/2}$ , with the random phase  $\tilde{\varphi}_\xi(t) = -v \int_0^t dt' \text{sign}(t/2 - t') \xi(t')$  for a fluctuator with  $\xi = \pm 1$ .

For times  $t' < t/2$  the system evolves “freely” and its time evolution is determined by Eq. (B.1) and its solution is equal to,

$$\langle e^{i\varphi_\xi(t)} \rangle = \frac{1}{2} e^{-\gamma t/2} \left[ \left(1 + \frac{\gamma}{2\delta}\right) e^{\delta t} + \left(1 - \frac{\gamma}{2\delta}\right) e^{-\delta t} \right], \quad (\text{C.1})$$

At the time  $t' = t/2$  we perform a  $\pi$ -pulse on the qubit which results in a reversed sign of the fluctuator,  $\xi(t') \rightarrow -\xi(t')$ , for  $t' \geq t/2$ . This effectively switches the sign of the coupling and the system will subsequently evolve under the influence of Eq. (B.1) but with a reversed sign of the coupling  $v$ . Thus, for times  $t' > t/2$  the system evolves according to

$$\begin{aligned} \frac{d}{dt} \langle e^{i\varphi_\xi(t)} \rangle &= iv \langle \xi(t) e^{i\varphi_\xi(t)} \rangle, \\ \frac{d}{dt} \langle \xi(t) e^{i\varphi_\xi(t)} \rangle &= -\gamma \langle \xi(t) e^{i\varphi_\xi(t)} \rangle + (\Delta\gamma + iv) \langle e^{i\varphi_\xi(t)} \rangle. \end{aligned} \quad (\text{C.2})$$

We are calculating  $\langle e^{i\varphi_\xi(t)} \rangle$  for  $t' < t/2$  and for  $t' \geq t/2$  and match both solutions at  $t' = t/2$ . The solution for  $t' < t/2$  is already known from App. B. The solution of Eq. (C.2) follows the same lines as in App. B and an arbitrary solution can be written as (specializing to  $\Delta\gamma = 0$ ):

$$\begin{pmatrix} \langle e^{i\varphi_\xi(t)} \rangle \\ \langle \xi(t) e^{i\varphi_\xi(t)} \rangle \end{pmatrix} = \frac{C_1}{iv} \begin{pmatrix} \gamma/2 + \delta \\ iv \end{pmatrix} e^{(-\gamma/2 - \delta)t} + \frac{C_2}{iv} \begin{pmatrix} \gamma/2 - \delta \\ iv \end{pmatrix} e^{-(\gamma/2 + \delta)t}, \quad (\text{C.3})$$

where  $\delta = \sqrt{(\gamma/2)^2 - v^2}$ . At the time  $t' = t/2$  the solutions of Eq. (C.1) and Eq. (C.3) should match and this condition determines the constants  $C_{1,2}$  at  $t' = t/2$

$$\begin{pmatrix} \frac{\gamma/2+\delta}{iv} e^{\delta t/2} & \frac{\gamma/2-\delta}{iv} e^{-\delta t/2} \\ e^{\delta t/2} & e^{-\delta t/2} \end{pmatrix} \begin{pmatrix} C_1 \\ C_2 \end{pmatrix} = \begin{pmatrix} \frac{1}{2} \left[ \left(1 + \frac{\gamma}{2\delta}\right) e^{\delta t/2} + \left(1 - \frac{\gamma}{2\delta}\right) e^{-\delta t/2} \right] \\ -\frac{iv}{2\delta} \left( e^{\delta t/2} - e^{-\delta t/2} \right) \end{pmatrix}. \quad (\text{C.4})$$

By multiplication of the inverse of the matrix on the right-hand side of Eq. (C.4) we obtain the coefficients  $C_{1,2}$ . As a result

$$C_1 = \frac{iv}{2\delta} \left[ \left(1 - \frac{\gamma}{2\delta}\right) e^{-\delta t} + \frac{\gamma}{2\delta} \right], \quad (\text{C.5})$$

$$C_2 = -\frac{iv}{2\delta} \left[ \left(1 + \frac{\gamma}{2\delta}\right) e^{\delta t} - \frac{\gamma}{2\delta} \right]. \quad (\text{C.6})$$

The solution for the time evolution of the spin-echo signal  $D_{\text{Echo}}(t)$  for classical telegraph noise is related to the result of Eq. (C.3) by  $D_{\text{Echo}}(t) = \langle e^{i\varphi_\xi(t)} \rangle|_{v/2}$  and is equal to

$$D_{\text{Echo}}(t) = \frac{1}{2} e^{-\gamma t/2} \left( \frac{\gamma}{2\delta} \right) \left[ \left(1 + \frac{\gamma}{2\delta}\right) e^{\delta t} - \left(1 - \frac{\gamma}{2\delta}\right) e^{-\delta t} - \frac{v^2}{\gamma\delta} \right], \quad (\text{C.7})$$

here  $\delta = \frac{1}{2} \sqrt{\gamma^2 - v^2}$ . The solution for  $\Delta\gamma \neq 0$  follows the same steps which leads to the result Eq. (C.7) but now with the complex frequency  $\lambda_{1,2} = -\gamma/2 \pm \delta'$ , where  $\delta' = \sqrt{(\gamma/2)^2 + iv(\Delta\gamma + iv)}$  for the solution of Eq. (C.2). Note that  $\delta$  changes after applying the  $\pi$ -pulse, due to the sign change of the coupling  $v$ , and the frequency after the  $\pi$ -pulse is related to  $\delta$  by  $\delta' = \delta^*$ . Then an arbitrary solution after the  $\pi$ -pulse is given by

$$\begin{pmatrix} \langle e^{i\varphi_\xi(t)} \rangle \\ \langle \xi(t) e^{i\varphi_\xi(t)} \rangle \end{pmatrix} = \frac{C_1}{\Delta\gamma + iv} \begin{pmatrix} \gamma/2 + \delta^* \\ \Delta\gamma + iv \end{pmatrix} e^{(-\gamma/2 + \delta^*)t} + \frac{C_2}{\Delta\gamma + iv} \begin{pmatrix} \gamma/2 - \delta^* \\ \Delta\gamma + iv \end{pmatrix} e^{(-\gamma/2 - \delta^*)t}, \quad (\text{C.8})$$

and the coefficients  $C_{1,2}$  follow from the matching condition at  $t' = t/2$ . As a result we obtain for the spin-echo

$$D_{\text{Echo}}(t) = \frac{1}{2\delta^*} e^{-\gamma t/2} \left\{ \left[ (\gamma/2 + \delta^*) \langle e^{i\varphi_\xi} \rangle_{\frac{v}{2}}(t/2) e^{-\delta^* t/2} + (iv/2) \langle \xi e^{i\varphi_\xi} \rangle_{\frac{v}{2}}(t/2) e^{-\delta^* t/2} \right] e^{\delta t} - \left[ (\gamma/2 - \delta^*) \langle e^{i\varphi_\xi} \rangle_{\frac{v}{2}}(t/2) e^{\delta^* t/2} - (iv/2) \langle \xi e^{i\varphi_\xi} \rangle_{\frac{v}{2}}(t/2) e^{\delta^* t/2} \right] e^{-\delta t} \right\}, \quad (\text{C.9})$$

where  $\langle e^{i\varphi_\xi} \rangle_{\frac{v}{2}}$  and  $\langle \xi e^{i\varphi_\xi} \rangle_{\frac{v}{2}}$  are the solutions of Eq. (B.1) at  $t/2$  for the coupling  $+v/2$ .

# Appendix D

## Quantum Telegraph Noise

IN this appendix we derive the Keldysh path-integral [72, 73, 74] for the coherence  $D(t)$  of a qubit coupled to the charge fluctuations on a single localized impurity level tunnel coupled to an electronic reservoir. The calculation has been used to calculate the decoherence rate  $\Gamma_\varphi$  analytically in [31, 32].

### D.1 Coherence

The Hamiltonian of the heat-bath consisting of a single fluctuator is equal to

$$\hat{\mathcal{H}}_B = \varepsilon_0 \hat{d}^\dagger \hat{d} + \sum_{\mathbf{k}} \left( T_{\mathbf{k}} \hat{c}_{\mathbf{k}}^\dagger \hat{d} + \text{h.c.} \right) + \sum_{\mathbf{k}} \varepsilon_{\mathbf{k}} \hat{c}_{\mathbf{k}}^\dagger \hat{c}_{\mathbf{k}}, \quad (\text{D.1})$$

where  $\varepsilon_0$  is the bare energy of the impurity level,  $T_{\mathbf{k}}$  is the tunneling amplitude for hopping of an electron from the impurity level to a state with momentum  $\mathbf{k}$  inside the fermionic reservoir. The operators  $\hat{d}^\dagger / \hat{d}$  create / annihilate an electron with energy  $\varepsilon_0$  on the impurity and  $\hat{c}_{\mathbf{k}}^\dagger / \hat{c}_{\mathbf{k}}$  create / annihilate an electron with momentum  $\mathbf{k}$  inside the reservoir.

The coherence is equal to

$$D(t) = \frac{1}{\text{tr} \hat{\rho}} \text{tr} \left( \hat{U}_{-,t}^\dagger \hat{U}_{+,t} \hat{\rho} \right), \quad (\text{D.2})$$

where  $\hat{U}_{\pm,t} = e^{-i(\hat{\mathcal{H}}_B \pm v \hat{Q}/2)t}$ . We identify  $\hat{U}_{-,t}^\dagger \hat{U}_{+,t}$  with the time evolution operator  $\hat{U}_C$  along the closed time-contour  $C_K(t)$  which runs from 0 to  $t$  and comes ultimately back to its initial time  $t' = 0$ , but with a time dependent coupling constant  $v(t')$ , as depicted in Fig. D.1. The coherence can be expressed as a coherent state path integral over anti-commuting Grassman variables  $\psi, \chi$

$$D(t) = \frac{1}{Z} \int D[\bar{\psi}, \psi] D[\bar{\chi}, \chi] e^{iS[\psi, \chi]}, \quad (\text{D.3})$$

here the normalization  $Z$  is chosen such that  $D(t) = 1$  if the coupling constant vanishes,  $v = 0$ . The action  $S[\psi, \chi]$  is given by

$$S[\psi, \chi] = S_0[\bar{\psi}, \psi] + S_{\text{int}}[\bar{\psi}, \psi] + S_B[\psi, \chi], \quad (\text{D.4})$$

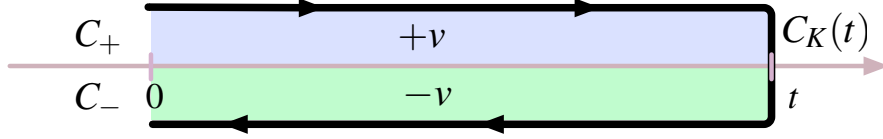


**Figure D.1:** Keldysh time-contour  $C_K(t)$  of the time-integration.  $C_+(t)$  and  $C_-(t)$  denote the forward and backward branch of the Keldysh contour. Shown is the time dependence of the potential  $v(t')$  along the Keldysh-contour.

where  $S_0[\bar{\psi}, \psi]$  is the action of the non-interacting single impurity level,  $S_{\text{int}}[\bar{\psi}, \psi]$  describes the interaction between qubit and bath, and  $S_B[\psi, \chi]$  is the action of the heat-bath. In particular,

$$S_0[\bar{\psi}, \psi] = \oint_{C_K(t)} dt' \bar{\psi}(t') (i\partial_{t'} - \varepsilon_0) \psi(t'), \quad (\text{D.5})$$

$$S_{\text{int}}[\bar{\psi}, \psi] = -\frac{i}{2} \oint_{C_K(t)} dt' v(t') \bar{\psi}(t') \psi(t'), \quad (\text{D.6})$$

$$S_B[\psi, \chi] = \sum_{\mathbf{k}} \oint_{C_K(t)} dt' \bar{\chi}_{\mathbf{k}}(t') (i\partial_{t'} - \varepsilon_{\mathbf{k}}) \chi_{\mathbf{k}}(t'), \quad (\text{D.7})$$

$$- \sum_{\mathbf{k}} \oint_{C_K(t)} dt' (T_{\mathbf{k}} \bar{\chi}_{\mathbf{k}}(t') \psi(t') + T_{\mathbf{k}}^* \bar{\psi}(t') \chi_{\mathbf{k}}(t')). \quad (\text{D.8})$$

It is important to note that due to the integration along the Keldysh contour  $C_K(t)$  the coupling  $v$  is no longer constant but it is time dependent along the contour of integration, i.e.

$$v(t') = \begin{cases} +v, & \text{if } t' \in C_+ \\ -v, & \text{if } t' \in C_- \end{cases} \quad (\text{D.9})$$

It is convenient to split the fields  $\psi, \chi$  into two components which live on the forward and backward branch of the Keldysh contour, respectively. The result of this splitting is that the time integrals along the Keldysh contour become simple integrals over the interval  $[0, t]$ . Let us denote the component that resides on the forward branch by  $\psi_+$  and the component that resides on the backward branch by  $\psi_-$ , and the same for  $\bar{\chi}, \chi$  correspondingly. As an example, the non-interacting action of the impurity level is equal to

$$S_0[\bar{\psi}, \psi] = \left[ \int_0^t dt' \bar{\psi}_+(t') (i\partial_{t'} - \varepsilon_0) \psi_+(t') - \int_0^t dt' \bar{\psi}_-(t') (i\partial_{t'} - \varepsilon_0) \psi_-(t') \right]. \quad (\text{D.10})$$

The action can be written in a compact form, by introducing the following spinor notation for the fields,

$$\hat{\bar{\psi}}(t') = \begin{pmatrix} \bar{\psi}_+(t') \\ \bar{\psi}_-(t') \end{pmatrix}^T, \quad \hat{\psi}(t') = \begin{pmatrix} \psi_+(t') \\ \psi_-(t') \end{pmatrix}, \quad (\text{D.11})$$

where the hat indicates the matrix-structure in the  $(+-)$ -space and  $\hat{\tau}_z$  is the Pauli matrix acting

onto the spinor. Finally, we get for the action  $S[\widehat{\psi}, \widehat{\chi}]$

$$\begin{aligned} S[\widehat{\psi}, \widehat{\chi}] &= \int_0^t dt' \widehat{\psi}(t') \left( i\partial_{t'} - \varepsilon_i^{(0)} \right) \hat{\tau}_z \widehat{\psi}(t') - \frac{i}{2} \int_0^t v \widehat{\psi}(t') \widehat{\psi}(t') \\ &+ \sum_{\mathbf{k}} \int_0^t dt' \widehat{\chi}_{\mathbf{k}} (i\partial_{t'} - \varepsilon_{\mathbf{k}}) \hat{\tau}_z \widehat{\chi}_{\mathbf{k}}(t') \\ &- \sum_{\mathbf{k}} \int_0^t dt' \left( T_{\mathbf{k}} \widehat{\chi}_{\mathbf{k}}(t') \hat{\tau}_z \widehat{\psi}(t') + T_{\mathbf{k}}^* \widehat{\psi}(t') \hat{\tau}_z \widehat{\chi}_{\mathbf{k}}(t') \right). \end{aligned} \quad (\text{D.12})$$

The integration over the electronic degrees of freedom of the heat-bath can be easily performed since the action is quadratic in  $\widehat{\chi}, \widehat{\chi}$ . The result for the coherence  $D(t)$  is a Gaussian integral with the effective action  $S_{\text{eff}}[\widehat{\psi}, \widehat{\psi}]$

$$D(t) = \frac{1}{Z} \int D[\widehat{\psi}, \widehat{\psi}] e^{iS_{\text{eff}}[\widehat{\psi}, \widehat{\psi}]}$$

$$S_{\text{eff}}[\widehat{\psi}, \widehat{\psi}] = \int_0^t dt' \widehat{\psi}(t') \left( i\partial_{t'} - \varepsilon_0 + \frac{v}{2} \hat{\tau}_z \right) \hat{\tau}_z \widehat{\psi}(t') \quad (\text{D.13})$$

$$- \int_0^t dt' \int_0^{t'} dt'' \widehat{\psi}(t') \widehat{\Sigma}(t' - t'') \widehat{\psi}(t''), \quad (\text{D.14})$$

where  $\widehat{\Sigma}(t' - t'')$  is the self-energy part due to the interaction with the heat-bath

$$\widehat{\Sigma}(t, t') = \sum_{\mathbf{k}} T_{\mathbf{k}}^* T_{\mathbf{k}} \widehat{g}_{\mathbf{k}}(t, t'), \quad (\text{D.15})$$

where  $\widehat{g}_{\mathbf{k}}(t, t')$  is the Green's function of the conduction-band electrons and it obeys the equation  $(i\partial_{t'} - \varepsilon_{\mathbf{k}}) \widehat{g}_{\mathbf{k}}(t, t') = \delta(t - t')$ . Performing the Keldysh-rotation on the Grassman-fields  $\overline{\psi}, \psi$  one obtains the new fields denoted by  $\check{\overline{\psi}}, \check{\psi}$ ,

$$\check{\overline{\psi}}(t) = \frac{1}{\sqrt{2}} \begin{pmatrix} 1 & -1 \\ 1 & 1 \end{pmatrix} \begin{pmatrix} \overline{\psi}_+ \\ \overline{\psi}_- \end{pmatrix}, \quad \check{\psi}(t) = \frac{1}{\sqrt{2}} \begin{pmatrix} 1 & 1 \\ 1 & -1 \end{pmatrix} \begin{pmatrix} \psi_+ \\ \psi_- \end{pmatrix}. \quad (\text{D.16})$$

As a result the Green's function then has the familiar structure in Keldysh-space and the effective action can be written as

$$S_{\text{eff}}[\check{\overline{\psi}}, \check{\psi}] = \int_0^t dt' \check{\overline{\psi}}(t') \left( \check{G}^{-1} - \check{\Sigma} + \frac{v}{2} \check{\tau}_x \right) \check{\psi}(t'), \quad (\text{D.17})$$

where  $\check{G}$  is the Green's function in Keldysh-space,

$$\check{G}(t, t') = \begin{pmatrix} G^R(t, t') & G^K(t, t') \\ 0 & G^A(t, t') \end{pmatrix}, \quad (\text{D.18})$$

with the retarded / advanced Green's functions in Fourier-space  $G^{R/A}(\omega) = (\omega - \varepsilon_0 \pm i\delta)^{-1}$  and  $G^K(\omega) = [G^R(\omega) - G^A(\omega)](1 - 2f_T(\omega))$  for the Keldysh component in thermal equilibrium, and

$f_T(\omega)$  is the Fermi-Dirac distribution,  $T$  is the temperature of the heat-bath. The self-energy part  $\check{\Sigma}$  has the same matrix structure as the Green's function  $\check{G}$  in Keldysh-space. The self-energy is equal to

$$\check{\Sigma}(t, t') = \sum_{\mathbf{k}} T_{\mathbf{k}}^* T_{\mathbf{k}} \check{g}_{\mathbf{k}}(t, t') \quad (\text{D.19})$$

and  $g_{\mathbf{k}}^{R/A}(\omega) = (\omega - \varepsilon_{\mathbf{k}} \pm i\delta)^{-1}$  is the retarded / advanced Green's function of the conduction electrons in the reservoir.

### D.1.1 Calculation of the self-energy part

The retarded / advanced components of the self-energy part are given in Fourier-space by

$$\begin{aligned} \Sigma^{R/A}(\omega) &= \sum_{\mathbf{k}} T_{\mathbf{k}i}^* T_{\mathbf{k}j} \frac{1}{\omega - \varepsilon_{\mathbf{k}} \pm i\delta} \\ &= \sum_{\mathbf{k}} T_{\mathbf{k}}^* T_{\mathbf{k}} \left[ \frac{1}{\omega - \varepsilon_{\mathbf{k}}} \mp i\pi\delta(\omega - \varepsilon_{\mathbf{k}}) \right]. \end{aligned} \quad (\text{D.20})$$

It is reasonable to assume that the position of the impurity-level is well localized on the substrate, then the tunneling amplitude can be written  $T_{\mathbf{k}} = 1/\sqrt{V} T e^{i\mathbf{k}\mathbf{r}}$ , where  $\mathbf{r}$  is the position of the impurity-level. The above expression is easily calculated as,

$$\Sigma^{R/A}(\omega) = \frac{1}{V} \sum_{\mathbf{k}} |T|^2 \left[ \frac{1}{\omega - \varepsilon_{\mathbf{k}}} \mp i\pi\delta(\omega - \varepsilon_{\mathbf{k}}) \right]. \quad (\text{D.21})$$

The real part of the self-energy is a slowly varying function of the frequency  $\omega$  and can be absorbed into the the impurity energy  $\varepsilon_0$ ,  $\varepsilon_0 \rightarrow \varepsilon_0 + \text{Re } \Sigma^{R/A}$ , the imaginary part is

$$\begin{aligned} \text{Im } \Sigma^{R/A} &= \mp \frac{\pi}{2} \sum_{\mathbf{k}} |T|^2 \delta(\omega - \varepsilon_{\mathbf{k}}), \\ &= \mp \gamma/2. \end{aligned} \quad (\text{D.22})$$

Inserting the self-energy part  $\check{\Sigma}$  into Eq. D.17 and integrating over the anticommuting Grassman variables  $\{\check{\psi}, \check{\psi}\}$  we finally obtain for the coherence  $D(t)$

$$D(t) = \frac{1}{Z} \int D[\check{\psi}, \check{\psi}] e^{iS_{\text{eff}}[\check{\psi}, \check{\psi}]} \quad (\text{D.23})$$

$$D(t) = \det \left( 1 + \frac{v}{2} \check{\tau}_x \check{G} \right),$$

where  $\check{G}$  is the full ‘‘dressed’’ Green's function with the the components

$$G^{R,A}(\omega) = \frac{1}{\omega - \varepsilon \pm i\gamma/2}, \quad (\text{D.24})$$

where  $\varepsilon$  is the renormalized energy of the fluctuator counted from the Fermi-level (we put  $\varepsilon_F = 0$ ) and  $\gamma$  is the tunneling rate,  $\gamma = 2\pi \sum_{\mathbf{k}} |T|^2 \delta(\omega - \varepsilon_{\mathbf{k}})$ . Equation (D.23) together with Eq. (D.24) give an exact expression for the coherence  $D(t)$ .

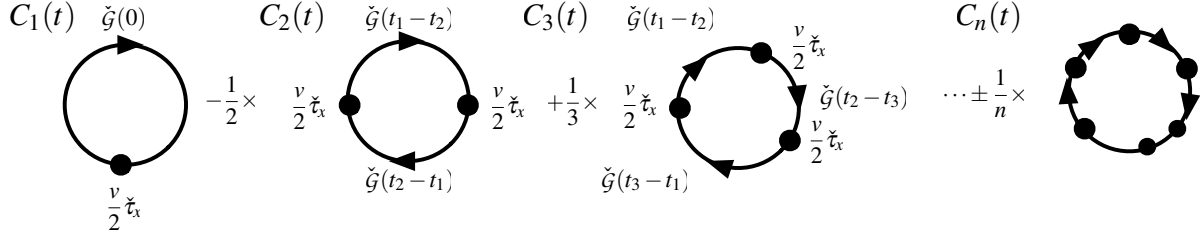


**Figure D.2:** *Linked Cluster expansion: Each diagram represents a whole class of topologically equivalent diagrams. The vertices  $v\check{\tau}_x/2$  are denoted by black dots and each line represents the Green's function  $\check{G}$  in Keldysh-space. The trace is taken with respect to time and the matrix structure in Keldysh-space. Taking into account the first two diagrams results in the Gaussian approximation of the coherence, i.e.  $D_{\text{Gauss}}(t) = e^{C_1(t)+C_2(t)}$ .*

## D.1.2 Linked Cluster Expansion

An expansion of the determinant in Eq.(D.23) in the coupling strength  $v$  results in the *linked cluster expansion*,

$$\begin{aligned}
 D(t) &= \det \left( \check{\mathbb{I}} + \frac{v}{2} \check{\tau}_x \check{G} \right) \\
 &= \exp \left[ \text{tr} \ln \left( \check{\mathbb{I}} + \frac{v}{2} \check{\tau}_x \check{G} \right) \right] \\
 &= \exp \left[ \sum_{n=0}^{\infty} C_n(t) \right],
 \end{aligned} \tag{D.25}$$

where  $C_n$  represents all connected diagrams of order  $n$  in the coupling strength  $v$ . The linked cluster series is shown in Fig. D.2 with a single cluster representing the set of all connected diagrams which emerge from permutations of the vertices. At each vertex (black dot) one has to insert a factor  $v\check{\tau}_x/2$  and a straight solid line represent the Green's function  $\check{G}$  in Keldysh-space. The trace is taken with respect to the Keldysh-space and time. The Gaussian approximation neglects contributions  $C_{n \geq 3}$  in the expansion of the determinant. The non-universal factor  $1/n$  prevents the diagrammatic series from a simple resummation, however methods have been developed to find an exact solution for the determinant for specific problems, like the X-ray edge singularity [75]. The  $n$ -th order contribution is equal to

$$C_n(t) = \frac{(-1)^{n+1}}{n} \text{tr}_K \int_0^t dt_1 \dots \int_0^t dt_n \frac{v}{2} \check{\tau}_x \check{G}(t_1 - t_2) \frac{v}{2} \check{\tau}_x \check{G}(t_2 - t_3) \dots \frac{v}{2} \check{\tau}_x \check{G}(t_n - t_1). \tag{D.26}$$

- *First order correction:*  $C_1(t)$

$$C_1(t) = \text{tr} \left( \frac{v}{2} \check{\tau}_x \check{G} \right), \tag{D.27}$$

where the trace is defined as  $\text{tr}(\dots) = \int_0^t dt' \text{tr}_K(\dots)$ . We insert the definition of  $\check{G}$  into Eq. (D.27) and note that the time-ordered  $G^T(0,0)$  and anti-time ordered Green's function

$G^{\tilde{T}}(0,0)$  have to be replaced at coinciding times as following in order to respect causality, i.e.  $G^T(0,0) \rightarrow G^T(-0,0)$  and  $G^{\tilde{T}}(0,0) \rightarrow G^{\tilde{T}}(0,0)$ , respectively. As a result, we obtain

$$C_1(t) = -iv \langle \hat{Q} \rangle t, \quad (\text{D.28})$$

as expected from the Gaussian approximation in Sec. 7.3.

- *Second order contribution:  $C_2(t)$*

$$C_2(t) = -\frac{1}{2} \text{tr} \left( \frac{v}{2} \check{\tau}_x \check{G} \right)^2, \quad (\text{D.29})$$

$$C_2(t) = -\frac{1}{2} \int_0^t dt' \int_0^t dt'' \text{tr}_K \left[ \frac{v}{2} \check{\tau}_x \check{G}(t' - t'') \frac{v}{2} \check{\tau}_x \check{G}(t'' - t') \right], \quad (\text{D.30})$$

in Fourier-space this reads as

$$C_2(t) = -\frac{v^2}{2} \int_{-\infty}^{\infty} \frac{d\omega}{2\pi} \langle \delta \hat{Q} \delta \hat{Q} \rangle_{\omega} \frac{\sin^2(\omega t/2)}{(\omega/2)^2}. \quad (\text{D.31})$$

Comparing Eq. (D.31) with Eq. (7.26) we identify the symmetrized part of the correlator as

$$\langle [\delta \hat{Q}, \delta \hat{Q}]_+ \rangle_{\omega} = \frac{1}{4} \int_{-\infty}^{\infty} \frac{d\omega'}{2\pi} \text{tr}_K [\check{\tau}_x \check{G}(\omega + \omega') \check{\tau}_x \check{G}(\omega')]. \quad (\text{D.32})$$

Inserting the Green's function  $\check{G}$  and taking the trace in Keldysh-space we obtain

$$\begin{aligned} \langle [\delta \hat{Q}, \delta \hat{Q}]_+ \rangle_{\omega} = & \\ & \frac{1}{4} \int_{-\infty}^{\infty} \frac{d\omega'}{2\pi} \left[ G^A(\omega + \omega') G^R(\omega') + G^R(\omega + \omega') G^A(\omega') + G^K(\omega + \omega') G^K(\omega') \right], \end{aligned} \quad (\text{D.33})$$

using  $G^K(\omega) = [G^R(\omega) - G^A(\omega)](1 - 2f_T(\omega))$  for the Keldysh component of the Green's function and rewriting the first two terms in Eq. (D.33) as  $[G^R(\omega') - G^A(\omega')] \cdot [G^R(\omega + \omega') - G^A(\omega + \omega')]$  since terms of the form  $G^R G^R$  and  $G^A G^A$  vanish upon integration and we obtain

$$\begin{aligned} \langle [\delta \hat{Q}, \delta \hat{Q}]_+ \rangle_{\omega} = & \\ & 2\pi \int_{-\infty}^{\infty} d\omega' \frac{1}{2} \left[ v(\omega') v(\omega + \omega') f_T(\omega') (1 - f_T(\omega + \omega')) \right. \\ & \left. + v(\omega') v(\omega' - \omega) f_T(\omega') (1 - f_T(\omega' - \omega)) \right], \end{aligned} \quad (\text{D.34})$$

where  $v(\omega) = [G^R(\omega) - G^A(\omega)]/2\pi i$  is the Lorentzian DoS of the fluctuator.

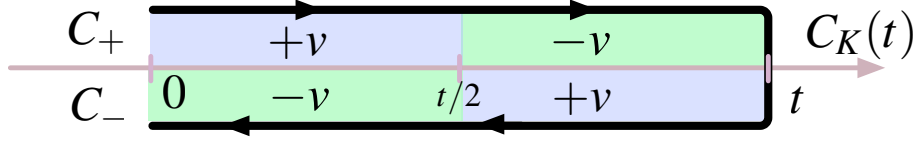


**Figure D.3:** Time dependence of the coupling  $v(t')$  along the Keldysh-contour in a spin-echo experiment when the  $\pi$ -pulse on the qubit is applied at  $t' = t/2$  and the echo is detected at  $t' = t$ .

## D.2 Spin-echo

The generalization of the Keldysh-technique to the spin-echo signal is straightforward. The spin-echo signal is equal to

$$D_{\text{Echo}}(t) = \frac{1}{\text{tr}\hat{\rho}} \text{tr} \left( \hat{U}_{-,t/2}^\dagger \hat{U}_{+,t/2}^\dagger \hat{U}_{-,t/2} \hat{U}_{+,t/2} \hat{\rho} \right), \quad (\text{D.35})$$

where  $\hat{U}_{\pm,t} = e^{-i(\hat{H}_B \pm v\hat{Q}/2)t}$ . We identify  $\hat{U}_{-,t/2}^\dagger, \hat{U}_{+,t/2}^\dagger, \hat{U}_{-,t/2}, \hat{U}_{+,t/2}$  with the time evolution operator  $\hat{U}_C$  but with a time dependent coupling constant  $v(t')$  along the Keldysh-contour  $C_K$

$$v(t') = \begin{cases} +v \text{ sign}(t/2 - t'), & \text{if } t' \in C_+ \\ -v \text{ sign}(t/2 - t'), & \text{if } t' \in C_- \end{cases} \quad (\text{D.36})$$

Repeating the same steps which lead to the expression for the coherence [see Eq. D.23] we finally obtain for  $D_{\text{Echo}}(t)$ ,

$$D_{\text{Echo}}(t) = \det \left( 1 + \frac{v}{2} (\check{\tau}_x \otimes \tau_z^{tt'}) \check{\mathcal{G}}_{tt''} \right), \quad (\text{D.37})$$

where  $\check{\mathcal{G}}_{tt'}$  is the Green's function discretized in time,  $\check{\tau}_x$  is the Pauli matrix in Keldysh-space and  $v$  is the coupling strength. The matrix  $\tau_z^{tt'} = \text{diag}(1, \dots, 1, -1, \dots, -1)$  is a matrix in the discretized time-interval  $[t_0, t_1, t_2, \dots, t_N = t]$  with  $t_N = N\delta t$ . A summation over repeated indices is implied. The generalization to arbitrary pulse-sequences is straightforward. Let's assume that a sequence of  $N$   $\pi$ -pulses are applied at times  $t_1, t_2, \dots, t_N$  onto the qubit and the spin-echo signal is observed at time  $t = 2(t_1 + t_2 + \dots + t_N)$ . Then the echo  $D_{\text{Echo}}(t)$  can be written in the same way as in Eq. (D.37) but now the matrix  $\tau_z^{tt'}$  is equal to

$$\tau_z^{tt'} = \text{diag}(+1, \dots, +1, \begin{matrix} t_1 \\ \downarrow \\ -1, \dots, -1, \end{matrix}, +1, \dots, +1, \begin{matrix} t_N \\ \downarrow \\ -1, \dots, \end{matrix}, \begin{matrix} t \\ \downarrow \\ -1 \end{matrix}) \quad (\text{D.38})$$

### D.2.1 Numerics

The determinant in Eq. (D.23) is taken with respect to continuous functions and in order to evaluate the determinant numerically it has to be approximated by a discrete matrix. For an arbitrary matrix  $W$  the determinant can be expanded into a series,

$$\det(1 + W) = \exp \left[ - \sum_{n=1}^{\infty} \frac{(-1)^n}{n} \text{tr} W^n \right]. \quad (\text{D.39})$$

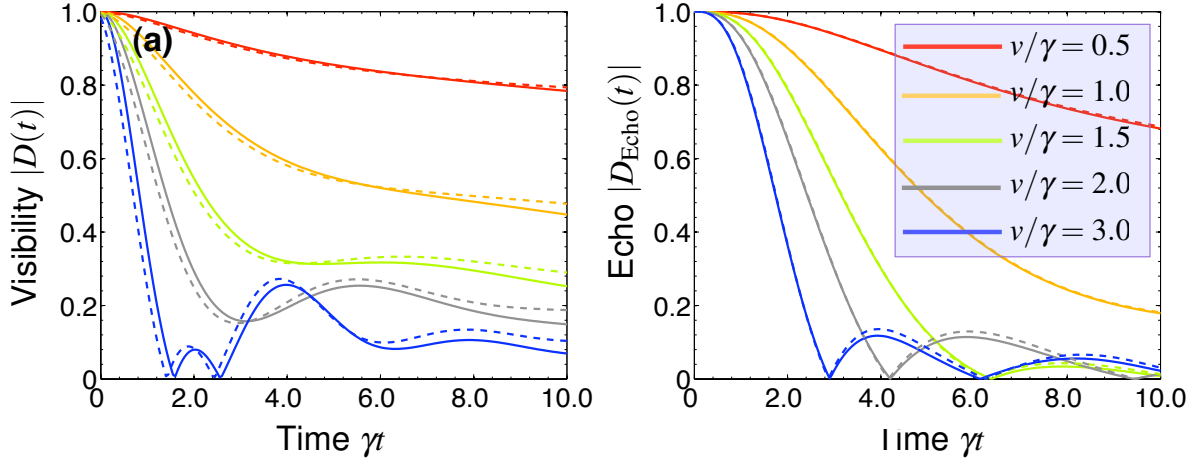


**Figure D.4:** Time evolution of the (a) visibility  $v(t) = |D(t)|$  and the (b) spin-echo signal  $|D_{\text{Echo}}(t)|$  derived by numerical evaluation of Eq. (D.23 and Eq. D.37) (dashed lines) compared to the results obtained by using the trace-formula (solid lines). (Parameters:  $T/\gamma = 0.01$ ,  $\varepsilon = 0$ ,  $\gamma = 1$ ).

Here the trace denotes a time-integration over all intermediate times from 0 to  $t$ , which can be approximated by the Riemann sum,

$$\begin{aligned} \text{tr } W^n &= \int_0^t dt_1 \dots \int_0^t dt_n W(t_1, t_2) W(t_2, t_3) \dots W(t_n, t_1) \\ &= \sum_{k_1, k_2, \dots, k_n} \delta t \dots \delta t W(t_{k_1}, t_{k_2}) W(t_{k_2}, t_{k_3}) \dots W(t_{k_n}, t_{k_1}), \end{aligned} \quad (\text{D.40})$$

where  $[t_{k_1}, t_{k_2}, \dots, t_{k_n}]$  is a discretization of the time-interval  $[0, t]$  and  $\delta t$  is the size between two time-steps. One can now define a new matrix to satisfy

$$\tilde{W}(t_{k_i}, t_{k_j}) = \delta t W(t_{k_i}, t_{k_j}). \quad (\text{D.41})$$

As a result the discrete version of Eq. (D.39) can be easily written as

$$\det(1 + W) = \det(1 + \tilde{W}). \quad (\text{D.42})$$

In particular we calculate the determinant of the discretized version of Eq. (D.23),

$$D(t) = \det \left( 1 + \frac{v}{2} \delta t \check{\chi}_x \check{\mathcal{G}}_{tt'} \right). \quad (\text{D.43})$$

Figure D.4 shows the time evolution of the visibility and the spin-echo signal obtained by direct numerical evaluation of Eq. (D.23) and Eq. (D.37) compared against the results obtained in Chaps. 7 and 8.

## Calculation of the Keldysh Green's function

### E.1 Keldysh Green's function

WE present the derivation of the Keldysh Green's function  $G^K(t, t')$  in real-time representation which appears in the derivation of the coherence, see Eq. D.23 in App. D. One can assume that  $G^K(t, t')$  depends only on the time difference  $t - t'$ , in thermal equilibrium the Keldysh Green's function is equal to

$$G^K(\omega) = [G^R(\omega) - G^A(\omega)] (1 - 2f_T(\omega)), \quad (\text{E.1})$$

where  $G^{R/A}(\omega)$  is the retarded / advanced Green's function of the fluctuator and  $f_T(\omega)$  is the Fermi-Dirac distribution function,  $f_T(\omega) = (e^{\beta\omega} + 1)^{-1}$  and  $\beta = 1/T$  is the inverse temperature of the heat-bath. Then the Keldysh Green's function in real-time representation is given by

$$G^K(t - t') = \int_{-\infty}^{\infty} \frac{d\omega}{2\pi} e^{-i\omega(t-t')} [G^R(\omega) - G^A(\omega)] (1 - 2f_T(\omega)). \quad (\text{E.2})$$

We derive the integral in Eq. (E.2) over the real axis by deforming the contour of integration from the real axis into a semicircle and let its radius grow to infinity thereby picking up all the poles which are enclosed by the contour of integration as displayed in Fig. E.1(a).

The integrand in Eq. E.2 has poles at  $\varepsilon \mp i\gamma/2$  and at  $(2n + 1)\pi Ti$  on the imaginary axis of the complex plane. One can use the following series expansion for  $f_T(\omega)$  which generates poles at the Matsubara frequencies  $\omega_n = (2n + 1)\pi Ti$ ,

$$\frac{1}{e^{\beta\omega} + 1} = \frac{1}{2} + \frac{1}{\beta} \sum_{n=-\infty}^{\infty} \frac{1}{(2n + 1)\pi Ti - \omega}. \quad (\text{E.3})$$

Then the Keldysh Green's function is equal to

$$G^K(t - t') = -\frac{1}{\beta} \sum_{n=-\infty}^{\infty} \oint_C \frac{dz}{2\pi} \frac{1}{(2n + 1)\pi Ti - z} \left[ \frac{1}{z - \varepsilon + i\gamma/2} - \frac{1}{z - \varepsilon - i\gamma/2} \right]. \quad (\text{E.4})$$

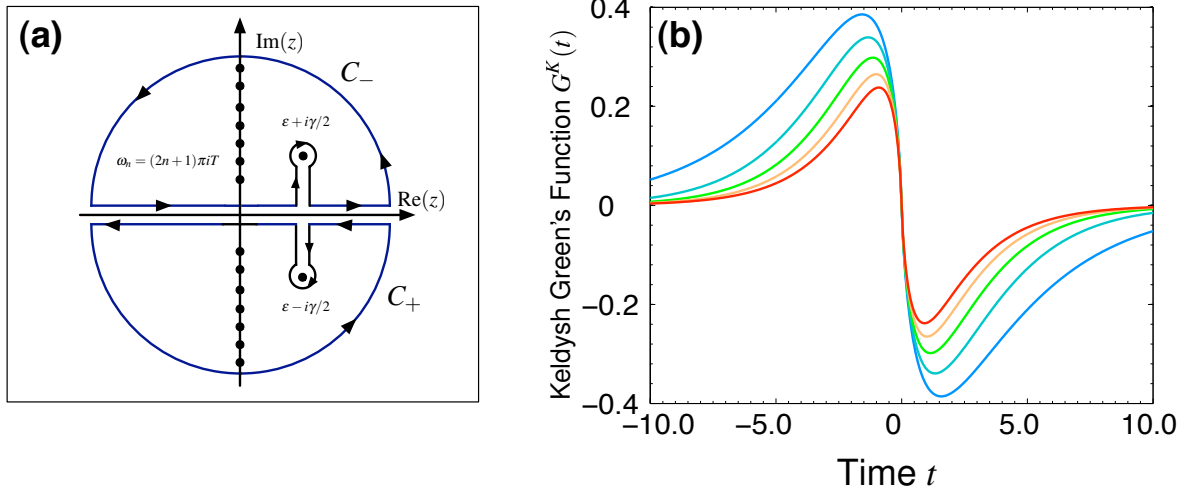


**Figure E.1:** (a) Contour of integration for calculating the Keldysh Green's function  $G^K(t)$ . For convergence reasons the contour is closed in the lower half plane for  $t > t'$ , integration along  $C_+$ , and for  $t < t'$  the integration is along  $C_-$ . (b) Keldysh Green's function  $G^K(t)$  in real-time representation for different temperatures (from top to bottom)  $T/\gamma = 0.1, 0.2, 0.3, 0.4, 0.5$ , ( $\varepsilon = 0$ ).

In order to ensure convergence of the integral above we are integrating over the contour  $C_+$  for  $t > t'$  thereby picking up the poles which are lying in the lower complex plane at  $\omega_n^* = (2n+1)\pi Ti$  with  $n = -\infty, \dots, -1$  and at  $\omega^* = \varepsilon - i\gamma/2$ . Then we obtain

$$G^K(t-t') = \frac{\gamma}{\beta} \sum_{n=-\infty}^{-1} \frac{e^{-i\omega_n(t-t')}}{(\omega_n - \varepsilon)^2 + (\gamma/2)^2} + \frac{2i}{\beta} \sum_{n=-\infty}^{\infty} \frac{e^{-i(\varepsilon - i\gamma/2)(t-t')}}{i\omega_n - \varepsilon + i\gamma/2}. \quad (\text{E.5})$$

Note that there is an overall negative factor of  $-1$  due to the reversed direction of integration along the real axis. One can perform the sum over the Matsubara frequencies  $\omega_n$  using the following relation

$$\psi(z) = \frac{d \log \Gamma(z)}{dz} = - \sum_{n=0}^{\infty} \frac{1}{n+z}, \quad (\text{E.6})$$

where  $\psi(z)$  is the logarithmic derivative of the  $\Gamma$ -function and it is termed the diGamma-function. Using the relation Eq.(E.6) we obtain for the Keldysh Green's function  $G^K(t-t')$  for  $t > t'$

$$G^K(t-t') = \frac{2\gamma}{\beta} \sum_{n=0}^{\infty} \frac{e^{-\omega_n(t-t')}}{(i\omega_n + \varepsilon)^2 + (\gamma/2)^2} + \frac{e^{-i(\varepsilon - i\gamma/2)(t-t')}}{\pi} \left\{ \psi \left[ \frac{1}{2} + \frac{1}{2\pi Ti} \left( \varepsilon - \frac{i\gamma}{2} \right) \right] - \psi \left[ \frac{1}{2} - \frac{1}{2\pi Ti} \left( \varepsilon - \frac{i\gamma}{2} \right) \right] \right\}. \quad (\text{E.7})$$

A similar derivation shows that for  $t < t'$  we have to integrate over the contour  $C_-$  thereby picking up the poles at  $\omega_n^* = (2n+1)\pi Ti$  with  $n = 0, \dots, \infty$  sitting on the imaginary axis of the complex

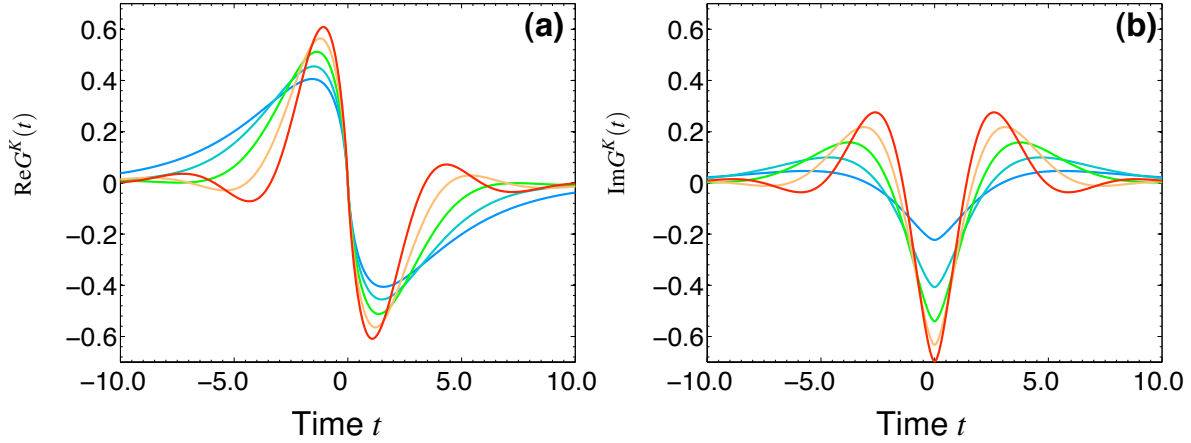


**Figure E.2:** Time evolution of (a) Real- and (b) imaginary part of  $G^K(t)$  for different  $\varepsilon/\gamma = 0.2, 0.4, 0.6, 0.8, 1.0$  (from blue to red color) and  $T/\gamma = 0.1$ .

plane and at  $\omega^* = \varepsilon + i\gamma/2$ . The result is equal to

$$\begin{aligned}
 G^K(t-t') &= -\frac{2\gamma}{\beta} \sum_{n=0}^{\infty} \frac{e^{-\omega_n(t-t')}}{(i\omega_n - \varepsilon)^2 + (\gamma/2)^2} \\
 &+ \frac{e^{-i(\varepsilon+i\gamma/2)(t-t')}}{\pi} \left\{ \psi \left[ \frac{1}{2} + \frac{1}{2\pi T i} \left( \varepsilon + \frac{i\gamma}{2} \right) \right] - \psi \left[ \frac{1}{2} - \frac{1}{2\pi T i} \left( \varepsilon + \frac{i\gamma}{2} \right) \right] \right\}.
 \end{aligned} \tag{E.8}$$

## E.2 Properties of the Keldysh Green's function

Figure E.1 shows  $G^K(t)$  as a function of time for various temperatures. The Keldysh Green's function  $G^K(t)$  decays exponentially in time on a scale set by  $\min(\gamma^{-1}, T^{-1})$ . In the zero temperature limit,  $T \rightarrow 0$ ,  $G^K(t)$  is solely determined by the second term in Eq. (E.7) and is equal to

$$G^K(t) = e^{-i(\varepsilon-i\gamma/2)(t-t')} \tan(\pi w), \tag{E.9}$$

where we have used  $\psi(1/2+w) - \psi(1/2-w) = \pi \tan(\pi w)$  and we have set  $w = (\varepsilon - i\gamma/2)/2\pi T i$ .

If  $\varepsilon \neq 0$ ,  $G^K(t)$  oscillates with frequency  $\varepsilon$  and decays exponentially on the scale  $\min(\gamma^{-1}, T^{-1})$  as displayed in Fig. E.2. Finally, the limit  $\gamma \rightarrow 0$  is reproduced by

$$\begin{aligned}
 G^K(t) &= -ie^{-i\varepsilon(t-t')} \tanh\left(\frac{\varepsilon}{2T}\right) \\
 &= -ie^{-i\varepsilon(t-t')} (1 - 2f_T(\varepsilon)).
 \end{aligned} \tag{E.10}$$



## Acknowledgement

I am especially grateful to my scientific advisor Dr. Florian Marquardt for his inspiring and stimulating collaboration. I also would like to thank Prof. Dr. Jan von Delft for suggesting the problem on “How fat is Schrödinger’s cat?” and for his fruitful collaboration on this subject.

I like to thank Sir Tony Leggett, Prof. Dr. Caspar van der Wal, Prof. Dr. Birgitta Whaley, Prof. Dr. Vinay Ambegaokar and Prof. Dr. Frank Wilhelm and Dr. Ivar Korsbakken for discussions on the Schrödinger cat.

I am thankful that I have had the opportunity to learn from such great physicists: Therefore I would like to thank Prof. Dr. Alex Kamenev, Prof. Dr. Konstantin Efetov, Prof. Dr. Leonid Glazman, Prof. Dr. Mikhael Shifman and Prof. Dr. Boris Shlokovski.

Finally, I would like to thank Prof. Dr. Yasu Nakamura for his contribution of several pictures.



## Bibliography

- [1] E. SCHRÖDINGER, Die gegenwärtige Situation in der Quantenmechanik, *Naturwissenschaften* **23**, 807, 1935.
- [2] J. E. MOOIJ, T. P. ORLANDO, L. LEVITOV, L. TIAN, C. H. VAN DER WAL, AND S. LLOYD, Josephson persistent-current qubit, *Science* **285**, 1036, 1999.
- [3] C.H. VAN DER WAL, A. C. J. TER HAAR, F. K. WILHELM, R. N. SCHOUTEN, C. J. P. M HARMANS, T. P. ORLANDO, S. LLOYD, AND J. E. MOOIJ, Quantum superposition of macroscopic persistent-current states, *Science*, **290**, 773, 2000.
- [4] J. R. FRIEDMAN, V. PATEL, W. CHEN, S. K. TOLPYGO, AND J. E. LUKENS, Quantum superposition of distinct macroscopic states, *Nature* **406**, 43, 2000.
- [5] M. ARNDT, O. NAIRZ, J. VOS-ANDREAE, C. KELLER, G. VAN DER ZOUW, AND A. ZEILINGER, Wave-particle duality of  $C_{60}$  molecules, *Nature* **401**, 680, 1999.
- [6] J. M. RAIMOND, M. BRUNE, AND S. HAROCHE, Manipulating quantum entanglement with atoms and photons in a cavity, *Reviews of Modern Physics* **73**, 565, 2001.
- [7] F. MARQUARDT AND C. BRUDER, Superposition of two mesoscopically distinct quantum states: Coupling a Cooper-pair box to a large superconducting island, *Physical Review B* **63**, 054514, 2001.
- [8] O. BUISSON AND F. HEKKING, In: *Macroscopic Quantum Coherence and Quantum Computing*, chapter Entangled states in a Josephson charge qubit coupled to a superconducting resonator, Kluwer, New York, 2001.
- [9] D. VION, A. AASSIME, A. COTTET, P. JOYEZ, H. POTHIER, C. URBINA, D. ESTEVE, AND M. H. DEVORET, Manipulating the quantum state of an electrical circuit, *Science* **296**, 886, 2002.
- [10] S. MANCINI, V. I. MANKO, AND P. TOMBESI, Ponderomotive control of quantum macroscopic coherence, *Physical Review A* **55**, 3042, 1997.

- [11] W. MARSHALL, C. SIMON, R. PENROSE, AND D. BOUWMEESTER, Towards quantum superpositions of a mirror, *Physical Review Letters* **91**, 130401, 2003.
- [12] A. D. ARMOUR, M. P. BLENCOWE, AND K. C. SCHWAB, Entanglement and decoherence of a micromechanical resonator via coupling to a Cooper-pair box, *Physical Review Letters* **88**, 148301, 2002.
- [13] D. D. AWSCHALOM, J. F. SMYTH, G. GRINSTEIN, D. P. DIVINCENZO, AND D. LOSS, Macroscopic quantum tunneling in magnetic proteins, *Physical Review Letters* **68**, 3092, 1992.
- [14] B. JULSGAARD, A. KOZHEKIN, AND E. S. POLZIK, Experimental long-lived entanglement of two macroscopic objects. *Nature* **413**, 400, 2001.
- [15] A. J. LEGGETT, Testing the limits of quantum mechanics: Motivation, state of play, prospects, *Journal of Physics: Condensed Matter* **14**, R415, 2002.
- [16] A. J. LEGGETT, *Supplement of Progress of Theoretical Physics* **69**, 80, 1980.
- [17] W. DÜR, C. SIMON, AND J. I. CIRAC, Effective size of certain macroscopic quantum superpositions, *Physical Review Letters* **89**, 210402, 2002.
- [18] J. I. KORSBAKKEN, K. B. WHALEY, J. DUBOIS, AND J. I. CIRAC, Measurement-based measure of the size of macroscopic quantum superpositions, *Physical Review A* **75**, 042106, 2007.
- [19] F. MARQUARDT, B. ABEL, AND J. VON DELFT, Measuring the size of a quantum superposition of many-body states, *Physical Review A* **78**, 12109, 2008.
- [20] Y. NAKAMURA, Y. A. PASHKIN, AND J. S. TSAI, Coherent control of macroscopic quantum states in a single-Cooper-pair box, *Nature* **398**, 786, 1999.
- [21] A. O. CALDEIRA AND A. J. LEGGETT, Influence of dissipation on quantum tunneling in macroscopic systems, *Physical Review Letters* **46**, 211, 1981.
- [22] A. J. LEGGETT, S. CHAKRAVARTY, A. T. DORSEY, M. P. A. FISHER, A. GARG, AND W. ZWERGER, Dynamics of the dissipative two-state system, *Reviews of Modern Physics* **59**, 1, 1987.
- [23] A. O. CALDEIRA AND A. J. LEGGETT, Path integral approach to quantum brownian motion, *Physica* **121A**, 587, 1983.
- [24] R. W. SIMMONDS, K. M. LANG, D. A. HITE, S. NAM, D. P. PAPPAS, AND J. M. MARTINIS, Decoherence in Josephson phase qubits from junction resonators, *Physical Review Letters* **93**, 077003, 2004.
- [25] O. ASTAFIEV, YU. A. PASHKIN, Y. NAKAMURA, T. YAMAMOTO, AND J. S. TSAI, Quantum noise in the Josephson charge qubit, *Physical Review Letters* **93**, 267007, 2004.

- 
- [26] R. H. KOCH, D. P. DIVINCENZO, AND J. CLARKE, Model for  $1/f$  flux noise in squids and qubits, *Physical Review Letters* **98**, 267003, 2007.
- [27] E. PALADINO, L. FAORO, G. FALCI, AND R. FAZIO, Decoherence and  $1/f$  noise in josephson qubits, *Physical Review Letters* **88**, 228304, 2002.
- [28] G. FALCI, A. D'ARRIGO, A. MASTELLONE, AND E. PALADINO, Dynamical suppression of telegraph and  $1/f$  noise due to quantum bistable fluctuators, *Physical Review A*, **70**, 40101, 2004.
- [29] R. DE SOUSA, K. B. WHALEY, F. K. WILHELM, AND J. VON DELFT, Ohmic and step noise from a single trapping center hybridized with a fermi sea, *Physical Review Letters* **95**, 247006, 2005.
- [30] L. FAORO, J. BERGLI, B. L. ALTSHULER, AND Y. M. GALPERIN, Models of environment and  $T_1$  relaxation in josephson charge qubits, *Physical Review Letters* **95**, 046805, 2005.
- [31] A. GRISHIN, I. V. YURKEVICH, AND I. V. LERNER, Low-temperature decoherence of qubit coupled to background charges, *Physical Review B* **72**, 060509(R), 2005.
- [32] A. GRISHIN, I. V. YURKEVICH, AND I. V. LERNER, *In: Physics of Zero- and One-Dimensional Nanoscopic Systems*, chapter Low temperature decoherence and relaxation in charge Josephson junction qubits, Springer Berlin Heidelberg, 2007.
- [33] A. SHNIRMAN, G. SCHÖN, I. MARTIN, AND Y. MAKHLIN, Low-and high-frequency noise from coherent two-level systems, *Physical Review Letters*, **94**, 127002, 2005.
- [34] Y. M. GALPERIN, B. L. ALTSHULER, J. BERGLI, AND D. V. SHANTSEV, Non-Gaussian low-frequency noise as a source of qubit decoherence, *Physical Review Letters* **96**, 097009, 2006.
- [35] J. BERGLI, Y. M. GALPERIN, AND B. L. ALTSHULER, Decoherence of a qubit by non-Gaussian noise at an arbitrary working point, *Physical Review B* **74**, 24509, 2006.
- [36] J. SCHRIEFL, Y. MAKHLIN, A. SHNIRMAN, AND G. SCHÖN, Decoherence from ensembles of two-level fluctuators, *New Journal of Physics* **8**, 1, 2006.
- [37] J. BERGLI AND L. FAORO, Exact solution for the dynamical decoupling of a qubit with telegraph noise, *Physical Review B* **75**, 54515, 2007.
- [38] Y. M. GALPERIN, B. L. ALTSHULER, J. BERGLI, D. SHANTSEV, AND V. VINOKUR, Non-Gaussian dephasing in flux qubits due to  $1/f$  noise, *Physical Review B* **76**, 64531, 2007.
- [39] Y. M. GALPERIN, B. L. ALTSHULER, AND D. V. SHANTSEV, *In: Fundamental Problems of Mesoscopic Physics*, chapter Low-Frequency Noise as a Source of Dephasing of a Qubit, Springer Netherlands, 2004.

- [40] B. ABEL AND F. MARQUARDT, Decoherence by quantum telegraph noise: A numerical evaluation, *Physical Review B* **78**, 201302, 2008.
- [41] J. L. BLACK AND B. I. HALPERIN, Spectral diffusion, phonon echoes, and saturation recovery in glasses at low temperatures, *Physical Review B* **16**, 2879, 1977.
- [42] B. D. LAIKHTMAN, General theory of spectral diffusion and echo decay in glasses, *Physical Review B* **31**, 490, 1985.
- [43] I. A. GOYCHUK, Kinetic equations for a dissipative quantum system driven by dichotomous noise: An exact result, *Physical Review E* **51**, 6267, 1995.
- [44] Y. MAKHLIN AND A. SHNIRMAN, Dephasing of solid-state qubits at optimal points, *Physical Review Letters* **92**, 178301, 2004.
- [45] L. S. LEVITOV, H. LEE, AND G. B. LESOVIK, Electron counting statistics and coherent states of electric current, *Journal of Mathematical Physics* **37**, 4845, 1996.
- [46] I. KLICH, *In: Quantum Noise in Mesoscopic Physics*, chapter Full Counting Statistics: An elementary derivation of Levitov's formula, Kluwer, Dordrecht, 2003.
- [47] I. SNYMAN AND Y. V. NAZAROV, Polarization of a charge qubit strongly coupled to a voltage-driven quantum point contact, *Physical Review Letters* **99**, 096802, 2007.
- [48] F. HASSLER, M. V. SUSLOV, G. M. GRAF, M. V. LEBEDEV, G. B. LESOVIK, AND G. BLATTER, Wave-packet formalism of full counting statistics, *preprint cond-mat/08020143*, 2008.
- [49] P. W. ANDERSON, Infrared catastrophe in fermi gases with local scattering potentials, *Physical Review Letters* **18**, 1049, 1967.
- [50] J. J. HOPFIELD, Infrared divergencies, X-ray edges, and all that, *Comments on Solid State Physics* **2**, 40, 1969.
- [51] G. D. MAHAN, *Many-particle physics*, Kluwer Academic/Plenum Publishers, New York, 2000.
- [52] E. PALADINO, M. SASSETTI, G. FALCI, AND U. WEISS, Characterization of coherent impurity effects in solid-state qubits, *Physical Review B* **77**, 41303, 2008.
- [53] I. NEDER AND F. MARQUARDT, Coherence oscillations in dephasing by non-Gaussian shot noise, *New Journal of Physics* **9**, 112, 2007.
- [54] I. NEDER, F. MARQUARDT, M. HEIBLUM, D. MAHALU, AND V. UMANSKY, Controlled dephasing of electrons by non-Gaussian shot noise, *Nature Physics* **3**, 534, 2007.

- 
- [55] P. W. SHOR, Algorithms for quantum computation: Discrete logarithms and factoring, *In: Proceedings of the 35th Annual Symposium on Foundations of Computer Science*, 124, IEEE Computer Society, Los Alamitos, 1994.
- [56] P. W. SHOR, Scheme for reducing decoherence in quantum computer memory, *Physical Review A* **52**, R2493, 1995.
- [57] A. M. STEANE, Error correcting codes in quantum theory, *Physical Review Letters* **77**, 793, 1996.
- [58] P. ZANARDI AND M. RASETTI, Noiseless quantum codes, *Physical Review Letters* **79**, 3306, 1997.
- [59] D. A. LIDAR, I. L. CHUANG, AND K. B. WHALEY, Decoherence-free subspaces for quantum computation, *Physical Review Letters* **81**, 2594, 1998.
- [60] E. KNILL, R. LAFLAMME, AND L. VIOLA, Theory of quantum error correction for general noise, *Physical Review Letters* **84**, 2525, 2000.
- [61] L. VIOLA AND S. LLOYD, Dynamical suppression of decoherence in two-state quantum systems, *Physical Review A* **58**, 2733, 1998.
- [62] L. VIOLA, S. LLOYD, AND E. KNILL, Universal control of decoupled quantum systems, *Physical Review Letters* **83**, 4888, 1999.
- [63] L. VIOLA AND E. KNILL, Robust dynamical decoupling of quantum systems with bounded controls, *Physical Review Letters* **90**, 037901, 2003.
- [64] G. S. UHRIG, Keeping a quantum bit alive by optimized  $\pi$ -pulse sequences, *Physical Review Letters* **98**, 100504, 2007.
- [65] H. M. WISEMAN, Quantum theory of continuous feedback, *Physical Review A* **49**, 2133, 1994.
- [66] H. M. WISEMAN, Erratum: Quantum theory of continuous feedback, *Physical Review A* **50**, 4428.2, 1994.
- [67] H. RABITZ, R. DE VIVIE-RIEDLE, M. MOTZKUS, AND K. KOMPA, Whither the future of controlling quantum phenomena?, *Science* **288**, 824, 2000.
- [68] J.F. POYATOS, J.I. CIRAC, AND P. ZOLLER, Quantum reservoir engineering with laser cooled trapped ions, *Physical Review Letters* **77**, 4728, 1996.
- [69] Y. NAKAMURA, Y. A. PASHKIN, T. YAMAMOTO, AND J. S. TSAI, Charge echo in a Cooper-pair box, *Physical Review Letters* **88**, 047901, 2002.
- [70] J. R. KLAUDER AND P. W. ANDERSON, Spectral diffusion decay in spin resonance experiments, *Physical Review* **125**, 912, 1962.

- [71] H. GUTMANN, F. K. WILHELM, W. M. KAMINSKY, AND S. LLOYD, Bang–bang re-focusing of a qubit exposed to telegraph noise, *Quantum Information Processing* **3**, 247, 2004.
- [72] L. V. KELDYSH, Diagram technique for nonequilibrium processes, *Zh. Eksp. Teor. Fiz* **47**, 1515, 1964.
- [73] J. RAMMER AND H. SMITH, Quantum field-theoretical methods in transport theory of metals, *Reviews of Modern Physics* **58**, 323, 1986.
- [74] A. KAMENEV, *In: Nanophysics: Coherence and Transport*, chapter Many-body theory of non-equilibrium systems, Elsevier, 2004.
- [75] P. NOZIERES, Singularities in the X-ray absorption and emission of metals, *Physical Review* **178**, 1097, 1969.